AN INVESTIGATION INTO THE EFFECTS OF LOAD MODELING ON TRANSIENT STABILITY AND ANALYSIS OF VOLTAGE COLLAPSE

BY

JOSEPH KHUMALO

GRADUATE STUDENT IN THE DEPARTMENT OF ELECTRICAL AND ELECTRONIC ENGINEERNIG AT THE UNIVERSITY OF CAPE TOWN

THESIS SUBMITTED TO

THE FACULTY OF ENGINEERING
OF THE UNIVERSITY OF CAPE TOWN
IN FULFILMENT OF THE REQUIREMENTS FOR
THE DEGREE OF MASTER OF SCIENCE

AUGUST 1992

ACKNOWLEDGEMENTS

I would like to express my deepest gratitude to my supervisor Professor A. Petroianu, for his patient advice and assistance during my graduate studies.

Heartful thanks are given to my parents for their prayers, patience and support.

I would like to thank my colleagues S.S Ahmed and E. Johnson for sharing their time and understanding through discussions.

I would also like to take this opportunity to thank SASOL for their financial support throughout my studies.

SYNOPSIS

The aim of this thesis is to investigate the effects of load modeling on transient stability studies and to analyze the phenomenon of voltage collapse. In addition, the different generator models are compared and the effects of voltage dips on induction motor performance are investigated.

The modeling of loads dates back to the late forties when network analyzers were still in use. The prohibitive computational requirements resulted in many approximations being made to the load models. In turn, this resulted in the use of simple models which did not provide sufficient information about the dynamic behavior of loads.

With the advent of digital computers, more accurate load models could be used in dynamic simulations. Despite this improvement in computational tools, the problem of load modeling for stability studies is still very complex. The load composition changes with the time of the day, the consumer's lifestyle, weather, state of the economy and other factors. The accurate load model would include amongst other things, the effects of the abovementioned factors. Since these factors are unpredictable, accurate load modeling becomes very complex indeed.

It is mainly for these reasons that the approximate models are still widely in use. Ideally, the response of these approximate models should be compared to the response of the actual loads under similar disturbances.

A further concern of the thesis is the study of voltage stability. The voltage stability problem has become a matter of growing concern amongst bulk transmission utilities worldwide over the last decade. For long, the stability of a power system was related exclusively to the synchronous stability of the generators. The power system blackouts in France, Italy, USA etc. [35], have however, added a new dimension to the stability problem. These power system blackouts resulted largely because of

a shortage of reactive power reserves due to the increase in load demand. This lack of reactive power reserves poses a serious threat to the reliability of a power system.

Having sketched the scope of the thesis, the content is presented in five sections as outlined below:

The first section gives an introduction to power system stability concepts. The different stability problems, namely: transient stability, dynamic stability and voltage stability are discussed. The various methods used to study the system stability are also discussed, namely: the equal-area criterion, the solution of the swing equation, the direct method of Lyapunov and the linearized state space method.

The second section deals with generator modeling for stability studies. Different generator models, as identified by the "IEEE task force on definition and procedures", in conjunction with the "IEEE working group on the determination and application of synchronous models for stability studies", are simulated to provide an insight into their transient behavior.

These generator models range from the simplest to the most complex generator representation. The mathematical expressions for the most complex generator model are derived in [3]. The mathematical expressions for the less complex generator models can be derived by simply neglecting the appropriate terms from the expressions of the most complex model.

The choice of a generator model for use in stability studies was found to be highly problem dependent. Before a model is chosen, it is necessary to know the needed accuracy from the study and the tools that are available. For example, in cases where the stability study involves investigating the behavior of the loads, then less complex model for the generators would suffice. However, in cases where the study involves investigating the generator behavior, then more complex models should be used.

The third section reviews the problem of load modeling for stability studies. The different types of static load models are discussed, namely: constant admittance, constant current and constant power. The different types of dynamic load models are also discussed. These are: the steady-state and transient model for the induction motors.

In addition, the characteristics of these different static and dynamic load models are discussed. Simulations are then performed to determine the effects of different load models on the transient stability results.

The modeling of local loads and remote loads is also considered. The effects of different fault locations on the transient stability results, using different load models, are also investigated.

The results of the simulation have shown that accurate load modeling is very important in transient stability studies. Different load models give completely different transient stability results.The relationship between the location of the load, the location of the fault and the load model need to be considered. If this relationship is not considered, false conclusions regarding the system stability may be drawn.

The fourth section analyzes voltage collapse in a power system with the following objectives :

(a) To review the theory of voltage collapse.
(b) To present a description of voltage stability phenomenon by using a simple example.
(c) To review the relationship between heavy loading conditions and voltage instability.

Various assumptions are made in order to separate voltage stability problem from rotor angle stability. These assumptions are oversimplifying the problem but they permit an independent analysis of voltage collapse.

The parameters that could affect voltage stability are discussed. These are: the active power, the reactive power and the transformer tap position. A brief review of the literature on voltage stability is presented and the causes of voltage instability, including the generator voltage dynamics and the load dynamics are discussed.

The simulation results showed that voltage stability is mainly caused by a relative shortage of reactive power resources. It occurs when the system is operating at or near its transmission capability and when the loading is high. Thus there is a close relationship between heavy loading conditions and voltage collapse.

The fifth section briefly reviews induction motor starting and the effects of voltage dips on the motor behavior. The effects of the following on the motor starting time was investigated :

(a) the type of load driven by the motor
(b) the MVA rating of the motor
(c) the initial load at starting
(d) the torque/slip characteristics of the motor and
(e) the motor reactance.

The effects of voltage dips with varying severities are also investigated.

The results show that the type of induction motor load affects the starting time of the motor. Induction motors driving linear loads, take longer periods to reach full load conditions. The higher the MVA rating of the machine, the longer it takes the motor to start.

The results also show that the starting period of the induction motor can be reduced by starting the motor at a fraction of the full load. The higher the reactance of the motor transformer, the longer the starting period of the motor.

All the simulation studies in the thesis were performed using the state-of-the-art industrial-grade software package "POWER SYSTEM SIMULATOR FOR ENGINEERS (PSS/E)". This software package runs on the Appollo Workstation.

TABLE OF CONTENTS

LIST OF ILLUSTRATION

FIGURES

CHAPTER 3

CHAPTER 4

CHAPTER 5

APPENDIX 1

APPENDIX 2

TABLES

CHAPTER 2

CHAPTER 3

CHAPTER 4

LIST OF THE PRINCIPAL SYMBOLS USED

δ	Rotor angle of machine
[X]	Matrix or vector, as specified
$\overline{X}$	Laplace transform of quantity X
$\dot{X}$	Derivative $\frac{d}{dt}(X)$
sub d	D-axis quantity
sub q	Q-axis quantity
ψ_{rd}	Flux linkage in the rotor, d-axis quantity
ψ_{rq}	Flux linkage in the rotor, q-axis quantity
ψ_{sd}	Flux linkage in the stator, d-axis quantity
ψ	Flux-linkage
$\Delta\psi$	Change in flux-linkage
L	Inductance of the winding
L_m	Mutual inductance between two windings
L_{1d}	First d-axis amortisseur winding inductance
L_{2d}	Second d-axis amortisseur winding inductance
L_{1q}	First q-axis amortisseur winding inductance
L_{2q}	Second q-axis amortisseur winding inductance
L_{3q}	Third q-axis amortisseur winding inductance
L_{adu}	Unsaturated value of L_{ad}
X	Reactance of the winding
X_l	Leakage reactance of the winding
X′	Transient reactance of the machine
X′′	Subtransient reactance of the machine
X_d	D-axis synchronous reactance
X_q	Q-axis synchronous reactance
V_{fd}	Field voltage
I_{fd}	Field current
R_a	Armature resistance
ω_r	Rotor angular velocity (rad/s)
ω	Instantaneous angular velocity (rad/s)
ω	Frequency of rotation
ω_e	Angular motor speed in electrical rad/s
V_s	Stator field voltage
T	Time constant
T′	Transient time constant of the machine

T''	Subtransient reactance of the machine
τ_l	Load torque
τ_e	Electrical torque
sub s	Subscript denoting the stator
sub r	Subscript denoting the rotor
sub R	Subscript denoting the outer-cage of the rotor
s	Motor slip
H	Inertia constant of the induction motor in seconds
f	Unit frequency deviation from nominal.
V	Per-unit voltage magnitude at the bus
V0	Initial voltage magnitude from load flow case
P0	Initial bus load active power, from load flow base case.
Q	Reactive power
P	Active power
V*	Complex conjugate of V
P_a	Acceleration power
P_m	Mechanical power
P_e	Electrical power

CHAPTER ONE : AN INTRODUCTION TO POWER SYSTEM STABILITY CONCEPTS AND MODELING

1.1 INTRODUCTION

This chapter provides an introduction to the power system stability concepts and the modeling requirement. Different stability problems are outlined, and their basic definitions are given. In addition, the various methods used to study the stability of the power system are discussed. Finally, a brief overview of the modeling requirements for power system analysis is given.

An interconnected power system consists of generating units (including excitation and turbine-governor systems), transmission lines, loads, transformers, static var compensators and high voltage direct current lines. A bulk transmission power system consists of many interconnected subsystems thus making the power system analysis time consuming and complex.

It has been shown in the past that although the size of interconnected power systems vary from one utility to the other, the technical problems encountered by these utilities are similar. Power system reduction methods exists, which help the operating and planning personnel to reduce the size of their respective power systems without losing the nature of the technical problems at hand.

In power system stability studies, the rotating machines which have similar oscillatory modes are identified and grouped into a single, dynamically equivalent unit. The loads which behave in a similar dynamic manner are also equivalenced into a single unit. Using this equivalencing procedure, almost every power system can be conveniently reduced to a two machine system or to a single machine connected to an infinite bus (a bus where the voltage and frequency are assumed to remain fixed).

This procedure obviously has its shortcomings because some of the details about the individual behavior of the machines are lost. This however, is not of prime importance in power system stability studies as compared to the saving in computation time achieved by this equivalencing approach. It is estimated that [1] a typical transient stability study with detailed modeling for a 500 bus 100 machine system might take up to an hour. This time requirement is largely reduced by using equivalent system models.

When defining the different stability problems, either a single machine interconnected to an infinite bus example or an example with two machines interconnected with each other, will be used. This is done in order to keep the problem as simple as possible and also because of the reasons cited above.

1.2 POWER SYSTEM STABILITY CONCEPTS AND DEFINITIONS

A power system is considered to be stable if, after a disturbance in the system, it returns to its original state or to a new stable state.

There are three types of stability problems: the steady-state (most recently known as dynamic) stability, the transient stability and the voltage stability. These stability problems are closely related to each other but for purposes of analysis, they are studied separately. These different stability problems are discussed separately.

Dynamic stability problem

A power system is considered to be dynamically stable if it returns to its original (or any stable state near the original) state, after a small disturbance. Small disturbances would include, amongst others, the gradual changes in load or generation.

Fig 1.1 shows a basic system consisting of one generator and one motor, connected through a line reactance. The power transfer between the generator (non-salient) and the motor is given by:

$$P = \frac{E_G * E_M}{X} \sin \delta \quad \ldots\ldots\ldots\ldots\ldots\ldots \quad (1.1)$$

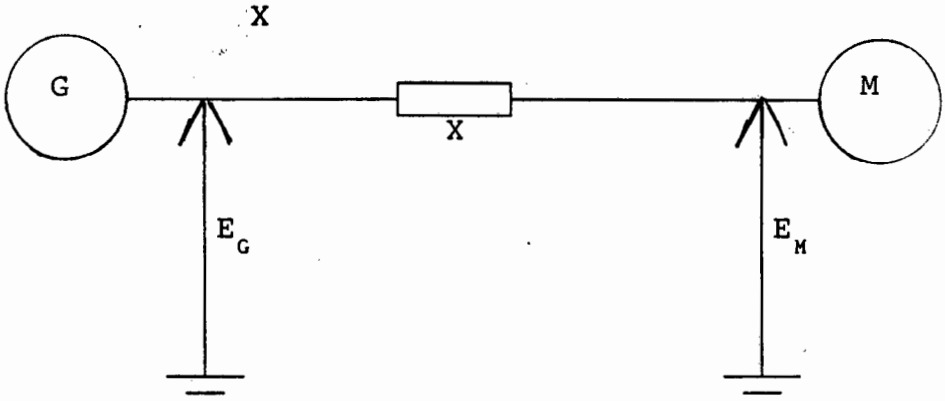

Figure 1.1: A generator and a motor connected through a line reactance

The total power transferred depends on the internal voltages of both machines, their angular difference and the reactance between them. Equation 1.1 describes what is known as the power-angle curve and is shown in figure 1.2.

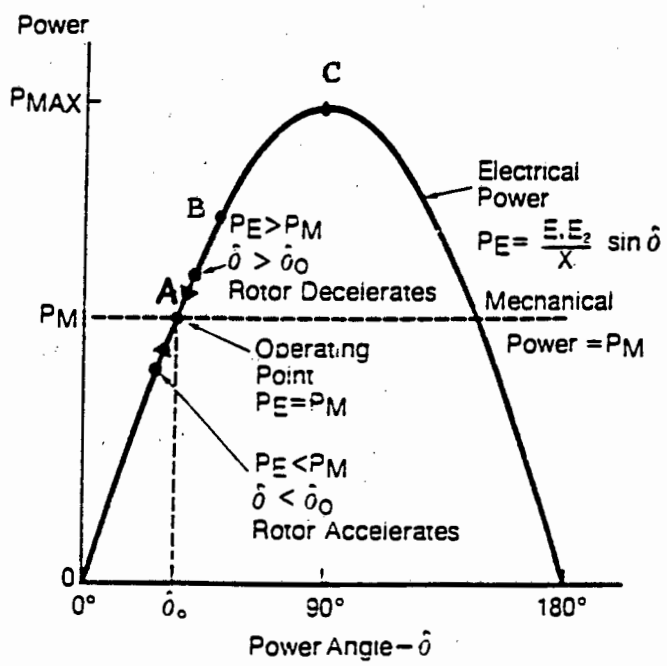

Fig 1.2 : Power angle curve

Suppose, for example, that under steady state conditions, the power system is operating at point A on the power-angle curve. At this point, the mechanical and electrical power are equal. If the motor load is increased slightly, the speed of the motor will decrease by a small amount due to the retarding torque applied.

It will take some time for the input power to change, hence a difference between input and output power will cause the motor to decelerate. The power angle will increase, which in turn will cause the input power to increase to equal the output power at point B in figure 1.2. Point B is thus a new stable state.The increase in synchronous power for a small change in δ is given by

$$\Delta P = \frac{dP}{d\delta} * \Delta\delta = P_r * \Delta\delta \qquad \text{.....} \qquad (1.2)$$

where $P_r = \frac{E_M E_G}{X} \cos\delta$ is the synchronizing power coefficient.

If the motor load is increased in small steps, a point C on the power-angle curve will be reached. An increase of δ beyond this point will be followed by a decrease in electrical power. This will increase the accelerating power and δ will increase even further. The synchronizing power coefficient will be positive when δ < 90 degrees, zero when δ = 90 and negative when δ > 90 degrees. For δ > 90 degrees, the synchronizing power indicates that synchronism between the two machines will be lost.

Point C, where the power transfer is maximum, is the steady-state stability limit. The maximum power transfer for a non-salient machine occurs when δ = 90 degrees or

$$P_{MAX} = \frac{E_M * E_G}{X} \qquad \ldots\ldots\ldots\ldots\ldots\ldots \quad (1.3)$$

Any attempt to transmit more power beyond P_{MAX} will result in steady-state instability. The power transfer for a salient pole machine with negligible resistance is given by

$$P = \frac{E_G * E_M}{X_d} \sin \delta - \frac{E_M^2}{2} \left(\frac{X_d - X_q}{X_d * X_q} \right) \sin 2\delta \quad \ldots\ldots \quad (1.4)$$

and the steady state stability limit occurs when δ < 90 degrees. If however, these generator types are fitted with automatic voltage regulators, the steady-state stability limit will occur at δ > 90 degrees.

Voltage stability problem

Voltage stability is a new type of stability problem, less understood and subject to ongoing research. In voltage stability studies, the main concern is the stability of the loads. Voltage instability is associated with a relative lack of adequate reactive power reserves, interconnection of bulk power systems operating at the limit of their transmission capacity, and the availability of generation.

Voltage stability is more difficult to analyze because it has both steady-state and dynamic aspects. The voltage at the load terminal will slide down to collapse, due to the static and dynamic behavior of the load. Voltage stability will be discussed in detail in chapter four.

1.3 METHODS USED TO STUDY STABILITY

There are various methods used to determine the stability of synchronous machines. The simplest method is the equal-area criterion although this method is limited to one machine and infinite bus, or to two machines. The more complex method which is often used for multimachine systems, is the method of solving the swing equations of the synchronous machines. This method involves solving large high order differential equations and algebraic equations and is therefore time consuming and necessitates the use of high speed digital computers.

Recently, the energy method has been used to identify region of attraction and repulsion in a power system. This method will not be covered in the research. However, the kernel of the method will be discussed briefly.

The linearized state space approach is also used to determine the stability of the system. This method is only useful in dynamic stability studies. Eigenvalues of the state matrix are calculated and these indicate whether the system is stable or not.

These different methods are discussed below separately:

1.3.1 The equal-area criterion

This method is based on the calculation of the integral of the surface between curves and is used to analyze the stability of a synchronous machine connected to an infinite bus, or the stability of two synchronous machines. The kernel of this method is the comparison of the acceleration energy of the machine, expressed as a surface and the deceleration energy of the machine, also expressed as a surface. For two machines to remain in synchronism (or one machine with respect to an infinite bus), the acceleration and deceleration surfaces must be equal.

There are some basic assumptions that are made when using this method. These are: constant input power, no damping and constant field flux linkage or constant voltage behind transient reactance. The input power is assumed constant because the action of the prime mover and the governor are so slow that, for the first swing, their effects can be neglected. In any case, when their effects become appreciable, they tend to aid stability.

Damping is neglected with the consideration that if the system is stable during the first angular swing, it is most likely to be stable when damping is introduced. The magnitude of the oscillations will die out with time.

The field flux linkage is assumed to remain constant because the flux in the field winding cannot change instantaneously. For the first cycle, it suffices to assume that the generator internal voltage is constant. If however, the generator is fitted with automatic voltage regulators, negative damping may be introduced.

Transient stability problem

Transient stability is a feature of the power system to withstand major disturbances such as three-phase faults, sudden changes in load, total loss of load or generation and tripping of transmission lines.

Suppose, the power system is operating at point A (see figure 1.2) in steady state. A sudden load is applied to the induction motor. The speed of the motor will decrease substantially causing a sudden change between input and output power. Since the mechanical power cannot change abruptly, the deceleration power will be large and will cause the rotor angle to advance faster.

The input mechanical power of the motor will increase slowly, trying to balance the electrical power. However, the acceleration of the rotor may cause δ to go beyond 90 degrees (depending on the amount of impact load applied),hence pulling the machine out of step, before the mechanical power can equal the electrical power.

The transient stability limit in this case, is determined by the maximum amount of sudden load applied to ensure that the machine remain in synchronism. If the major disturbance was a tripping of a transmission line for example, the transient stability limit would be determined by this type of disturbance. Transient stability study is thus very specific and dependent upon the type of disturbance applied. The period of concern for transient stability is usually one to two seconds after the disturbance.

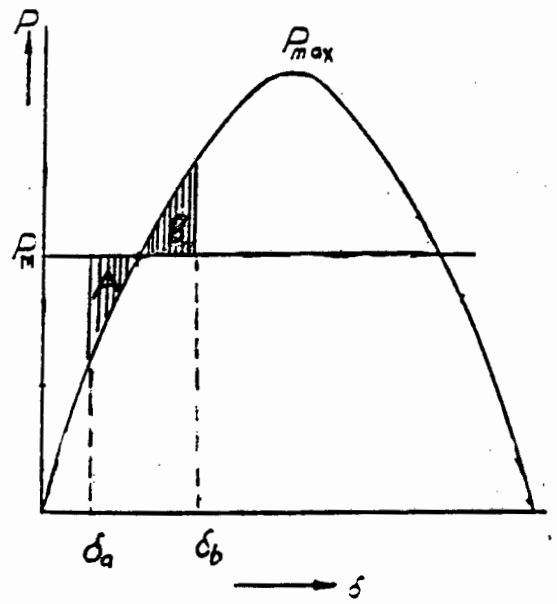

Figure 1.3 :
Equal-area criterion for change in load.

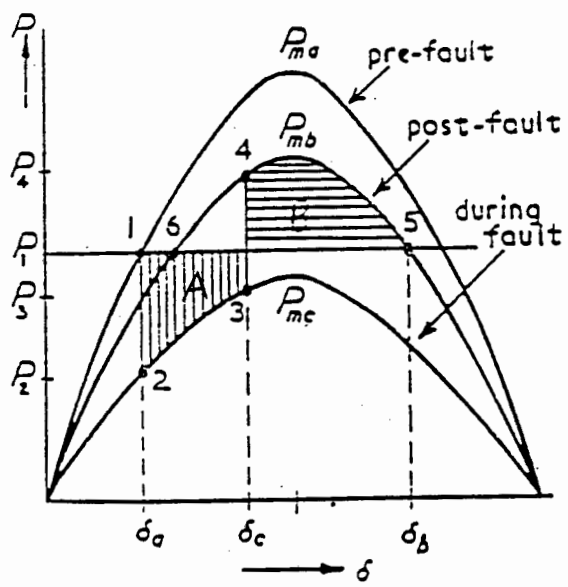

Figure 1.4:
Equal-area criterion for a branch fault,
showing critical clearing angle δ_c.

The critical clearing angle in figure 1.4 can be found from the following equation:

$$\cos \delta_c = \frac{P_1(\delta_b - \delta_a) + P_{mb}\cos \delta_b - P_{mc}\cos \delta_a}{P_{mb} - P_{mc}} \quad .. (1.9)$$

where P_{ma}, P_{mb}, P_{mc} are the maximum power transfers for the pre-fault, faulted and post-fault power/angle curves. For stability to be maintained, the shaded area "A" must be less or equal to shaded area "B" (see figures 1.3 and 1.4).

1.3.2 The solution of the swing equation

The swing equation describes the motion of the machine rotor. It gives the relationship between the inertia torque and the resultant of the mechanical and electrical torques. In its simplest form, the swing equation is given by

$$J\,\theta = T_a \quad ..... (1.10)$$

where J is the moment of inertia of the machine, and T_a is the acceleration torque. The most common representation of the swing equation is in terms of the inertia constant H, the accelerating power P_a and the angular position δ with respect to a rotating reference rather than a stationary reference as shown below:

$$\frac{2H}{\omega_r}\frac{d^2\delta}{dt^2} = P_m - P_e = P_a \quad ..... (1.11)$$

where $H = \frac{J\omega_r}{(MVA)}$

The solution of the swing equation gives δ as a function of time. A graph of the solution is known as the swing curve. Thus, if a power system contains n number of synchronous machines, n swing equations must be solved simultaneously. The direct closed form solution is not applicable, considering that differential equations are involved. A recursive (step-by-step) approach is

used to solve this equation. Once the solution is obtained, the swing curves will show whether the system is stable or not.

This point-by-point method uses iterative techniques to solve the swing equations. Some variables are assumed constant during a time step and others are calculated. At the end of the time step, new values for the variables which were previously assumed constant, are recalculated and the process repeated.

When solving the swing equation, the accelerating power is assumed constant during the time step. The final values of ω and δ are calculated from the initial values. Once these values are obtained, a new value of the accelerating power is calculated. Since the mechanical power is constant during the first swing, the problem is reduced to calculating the electrical power. This can be obtained by solving the power flow equations of the network.

1.3.3 The direct method of Lyapunov

The Lyapunov method is a general method for solving the stability of non-linear differential equations. This method can be used to determine the stability of a power system, because it provides a qualitative behavior of the differential equations governing the power system.

The method analyzes the stability of the power system by using energy functions. Since it is difficult to derive an energy function out of differential equations, a scalar function is defined and is called a Lyapunov function. This scalar function must be positive definite and its derivative, with respect to time, must be negative.

This method is more attractive because by observing the qualitative behavior of the Liapunov function, the region of

attraction can be defined. When the power system is operating in this region, it will be stable. If not, it will be unstable. Based on this fact, the time the power system operating point exits the region of attraction can be calculated. This exit time is closely related to the critical clearing time of the breakers, for different types of faults. Knowing the exit time, the stability of the power system can be determined.

1.3.4 The linearized state space approach

It is customary to use a linearized machine models in power system dynamic studies so that linear system analysis can be conveniently applied. Non-linear models are linearized around an operating point with the assumption that the variables have small deviations from the operating point.

The dynamics of a system can be described completely by using the higher order differential equations or by using the state space approach. This approach uses a set of simultaneous first-order dynamic equations, derived from the higher-order equations. The general state space formulation is as follows:

$$\dot{[x]} = [A][x] + [B][u]$$
$$[y] = [C][x] + [D][u] \qquad \ldots\ldots\ldots\ldots \quad (1.12)$$

Since the system equations are linearized around an operating point, the system performance may be analyzed by such method as root-locus plots, Nyquist method (frequency domain analysis) and Routh's criteria. These methods (Root-locus, Nyquist) are however, restricted to the analysis of small systems such as single machine connected to an infinite bus. They are also of limited value in analysis of systems having a wide range of frequency of oscillations.

For large multimachine systems, the state space approach is ideally used in connection with linear differential equations

describing the system. The system dynamic stability may be determined by examining the eigenvalues of the system state matrix [A]. By taking the Laplace transform of the above equation and solving for the state vector $\bar{X}$, the following result is obtained:

$$\bar{X} = (SI - A)^{-1}[X(0) - B\,\bar{U}]$$

$$\bar{X} = \frac{[adj(SI - A)][X(0) + B\,U]}{\det(SI - A)}$$

Substituting into the second equation of (1.12) yields:

$$Y = C(SI-A)[X(0) + DU] + DU$$

The poles of $\bar{X}$ are the roots of the characteristic equation $\det(SI-A) = 0$ and these roots correspond to the eigenvalues of the system. If the real part of the eigenvalues are all negative, then the system is dynamically stable. If however, some eigenvalues have positive real part, then the system is dynamically unstable. The imaginary part of the eigenvalues only gives information about the oscillatory behavior of the system.

1.4 MATHEMATICAL MODELS FOR POWER SYSTEM STABILITY ANALYSIS

In order to use digital computers to simulate the power system behavior, mathematical model for all the system components are required. The detail of modeling generally determines the depth and complexity of the analysis. The different modeling concepts for power system simulations are discussed in [2].

In power system stability studies, the main system components that need accurate modeling are the synchronous machines (with their controls), the loads and the interconnecting network. The network transmission lines and transformers are usually modeled with their pi-equivalent circuits, neglecting their fast

electromagnetic transients. The generators are represented by various models ranging from the most complex model to the least complex. The loads are also represented by either voltage dependent models or frequency dependent models or both.

Various excitation and turbine-governor system models also exist. Since there are many models available for almost all power system components, the choice of a model to use will ultimately depend on the study being considered, and also the required accuracy of the study. The mathematical models for generators and load used for power system stability are discussed in chapters 2 and 3 respectively.

1.5 SUMMARY

This chapter provided some basic definitions of the different stability problems. The methods used to study the stability of the system namely, the equal-area criterion, the solution of the swing equation, the direct method of Lyapunov and the linearized state space method, were outlined and discussed.

The equal area criterion method can be used only in two cases. Firstly, when the only one machine is connected to an infinite bus and secondly, when two machines are interconnected. This method is insufficient to study the stability of multimachine systems. It is however, very useful since almost all power systems could be reduced to two equivalent machines or one machine connected to an infinite bus.

The solution of the swing equation is the most commonly used method in multimachine system studies. It uses time domain techniques to solve the differential and algebraic equations of the system, hence it is time consuming and requires the use of high speed digital computers.

The direct method of Lyapunov uses energy functions to determine the zone of attraction in the power system and hence the stability of the system can be deduced. This method is enjoying increased application in stability analysis but it still has some limitation. Much work is in progress to improve its applicability.

The linearized state space method is very useful in dynamic stability studies. The eigenvalues of the linearized state matrix can indicate whether the system is dynamically stable or not.

Finally, the modeling requirements for power system components were briefly discussed. Further details about modeling

synchronous generators and loads can be found in the forthcoming chapters.

CHAPTER 2: SYNCHRONOUS GENERATOR MODELING FOR STABILITY STUDIES

2.1 INTRODUCTION

The aim of this chapter is to analyze the different generator models used in stability studies. These generator models have been identified by the "IEEE task force on definition and procedures", as the most practical models for stability studies.

The structure of the chapter is as follows :

A historical background on the evolution of synchronous generator modeling is given. Then the literature on the subject of generator modeling is reviewed, in order to compare the response of the generator models with the field tests. Furthermore, case studies are performed to compare the transient stability results obtained by using different generator models.

A major limitation of the case studies is the fact that not all the models identified by the IEEE task force, could be simulated. This is because of the following two reasons :

1). Some models require additional data not usually supplied by the manufacturers. Such data can be obtained from various tests such as : short circuits, open circuit voltage rise, and frequency tests. These tests are very expensive to conduct.

2). Some models are not supported by the simulation package used.

Finally, a summary of the chapter and conclusions are given.

2.2 HISTORICAL BACKGROUND ON SYNCHRONOUS GENERATOR MODELING

The need for improved synchronous machine modeling for stability studies has received much attention since the early 1920's. During those times, the simplest generator model, the constant voltage behind the transient reactance was used. This model came as a result of the constant field flux linkage theory which states, in its simplest form, that " in any closed circuit the flux linkage will remain constant immediately after any change in the current, voltage or position of the circuit to which it is magnetically coupled ".

This simplest synchronous machine model was the "state-of-the-art" and was used then because of the time-consuming calculations required in performing step by step stability calculations. These calculations were done only to determine the first angular swing stability of the synchronous machine, because of the limitations imposed by the power system computational tools.

The above model was then extended to include the effects of the field circuit resistance and the damper windings of hydrogenerators, as well as the field rotor circuit of turbogenerators. As the computational tools increased in size and speed, a natural evolution of power system analysis led to the stability investigations of larger and larger systems. Also, the need to extend the time scale of time-domain stability calculations became evident.

More tests were performed to determine the additional machine parameters needed for stability studies. As data for these machines became available, the response of the more detailed machine models due to disturbances of varying severity needed to be considered. As a result, stability studies were considered for periods greater than just the first angular swing. Nowadays the stability of the system is studied for tens of seconds of real time, in order to determine the damping associated with ensuing angular swings.

The damping of angular swings is associated with machine damper circuit. For hydrogenerators, the damper circuits could be easily identified as these are usually placed in the interpole spaces. For solid iron rotor machines, eg. turbogenerators, the equivalent damper winding are not easily identifiable.

More research was subsequently channeled towards identifying the damper circuit parameters in solid iron rotor machines. Park's two axes transformation theory was applied to identify the damping due to the direct axis and due to the quadrature axis. Short circuit and open circuit voltage rise tests were performed to determine the two axes parameters.

These tests however, only yielded the direct axis parameters namely the transient and sub-transient reactances and consequently the two main time constants, the transient and sub-transient time constants of the direct axis. The quadrature axis parameters could not be determined from such tests since no identifiable damper winding existed in the q-axis.

Figure 2.1 shows the equivalent circuit of the parameters which could be derived from the above mentioned standard tests.

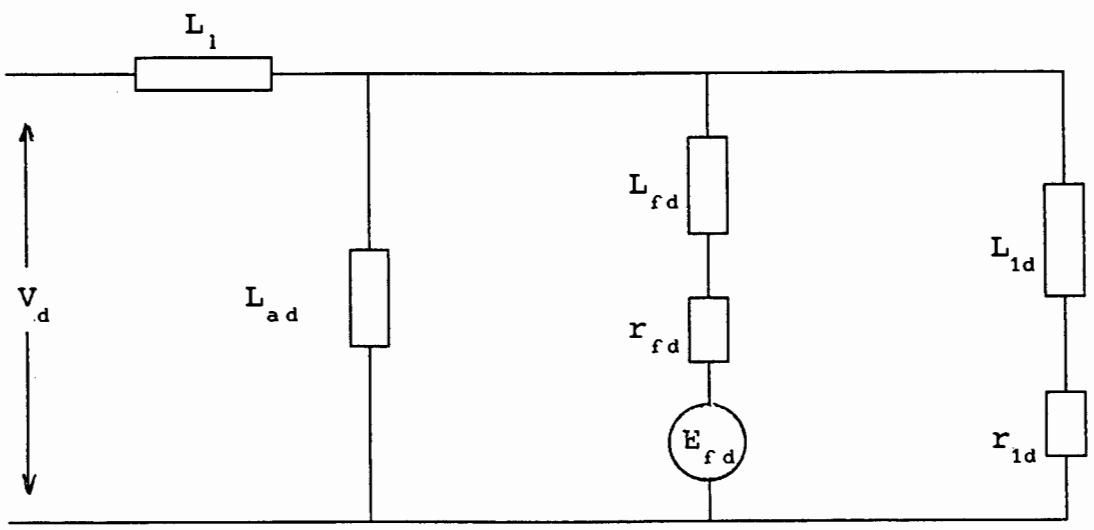

Figure 2.1: d-axis equivalent circuit

In figure 2.1, L_l is the stator leakage inductance, L_{fd} the field leakage inductance, L_{1d} the direct axis equivalent rotor inductance, L_{ad} the stator to rotor and field mutual inductance, r_{fd} the field resistance and r_{1d} the direct axis rotor equivalent resistance.

This type of direct axis representation has one major shortcoming. The mutual coupling between the rotor, the stator and the field circuit is the same. Recent studies [3], have indicated that the mutual coupling between the stator, the rotor and the field is not equal. It is thus important to account for the unequal mutual coupling between these circuits. Another shortcoming of this direct axis representation is that the level of the machine saturation is not represented fully. Finally, no suitable means were available to obtain quadrature axis parameters values and these were only provided by the manufacturer from design data.

For many years, the above model for generators was used for large disturbance stability studies and was found to be adequate for hydrogenerators. For turbogenerators however, it became apparent that the q-axis information, provided by the manufacturer was inadequate to predict the machines' damping. Questions arose because no standard procedure was available to check the validity of the q-axis parameters.

Studies after the power interruptions of 1965 which resulted in a big "blackout", showed that the q-axis parameters, especially the synchronous reactance, has a significant effect on the machines' initial rotor angle and can thus affect the trip setting of the relay for major disturbances. This realization led to the need for higher order models for transient stability studies.

Various tests were performed (called the Northfleet tests, Northeast Power Coordinating Council (NPCC) tests and the Ontario Hydro tests) [4], the objective being to obtain the machine

parameters used for stability studies and to evaluate the ability of various simulations to predict the system conditions to those tested.

It was concluded from these studies that the conventional short circuit and stator voltage rise test did not provide parameter values which could accurately predict the system performance under major disturbance. Data obtained from these tests needed to be adjusted in order to give better predictions.

It also became evident that the damping in the quadrature axis needed to be modeled accurately. As a result, various machine models, with varying degrees of complexity in the direct and quadrature axis are now available.

The "IEEE task force on definitions and procedures", in conjunction with the "IEEE working group on the determination and application of synchronous machine models for stability studies" [3] has identified the most practical generator models. These models range from the least complex, to the most complex, as listed in table 2.1. The major differences between these models is the level of modeling the damping in the direct and quadrature axes.

Table 2.1: Synchronous generator models

Complexity in q-axis →

Complexity in d axis

	No equivalent damper	One equivalent damper	2 equivalent dampers	3 equivalent dampers
const. flux linkage	MODEL(0.0)			
Field circuit only	MODEL(1.0)	MODEL(1.1)		
Field circuit + one damper circuit		MODEL(2.1)	MODEL(2.2)	
Field circuit + two dampers			MODEL(3.2)	MODEL(3.3)

Other models, which are not included in table 2.1, are available in the literature. For example, the "classical model" (the constant flux linkage model neglecting saliency), is not shown in the table. Model 0.0 is a close variation of the "classical model" and it represents saliency. Another example of a model not included in table 2.1 is a close variation of model 3.3. The model 3.3 does not account for the unequal mutual coupling between the stator, the rotor and the field circuits. The variation of model 3.3 represents the unequal mutual coupling.

The least complex of all the available practical generator model is model 0.0 in table 2.1. This model represent the constant field flux linkage and has no damper windings modeled in both axis. This is the close variation of the well known " classical " generator model, where the saliency of the generator is ignored.

There are two first order models (model 1.1 and model 1.0). Model 1.1 has a field circuit winding and one damper winding in the quadrature axis. Model 1.0 contains no damper windings in both the direct and quadrature axis and has only the field circuit in the direct axis.

Two second order models (model 2.2 and model 2.1) are also shown in table 2.1. Model 2.2 has a field circuit and one damper winding in the direct axis and two damper windings in the quadrature axis. Model 2.1 is similar to model 2.2 in the direct axis but has one less damper winding in the quadrature axis.

There are two third order models (model 3.3 and model 3.2). The most complex model in table 2.1 is the third order[1] model, model 3.3. This model has one field circuit and two damper windings in the direct axis and has three equivalent damper windings in the quadrature axis. Model 3.2 is similar to model 3.3 in the direct axis representation but has one less equivalent damper winding in the quadrature axis.

Figure 2.2 shows the equivalent circuit diagram of these models, from the least complex to the most complex. These models can only be used in large and small disturbance stability studies. They may not applicable to short circuit, fault and relay studies and are also unsuitable for sub-synchronous resonance studies. In these studies, the electromagnetic transients phenomena in the network would have to be taken into consideration.

---

[1] note that in this context, the order of the model represents only the electrical aspects of the stability model. In general, when assuming the order of the model, the electromechanical aspects of the machine (swing equation) should be considered. For example, MODEL (2.2) would be a fifth order model because it has one differential equation in the d-axis and two in the q-axis in addition to the two differential equation for the mechanical motion.

(a) model 0.0

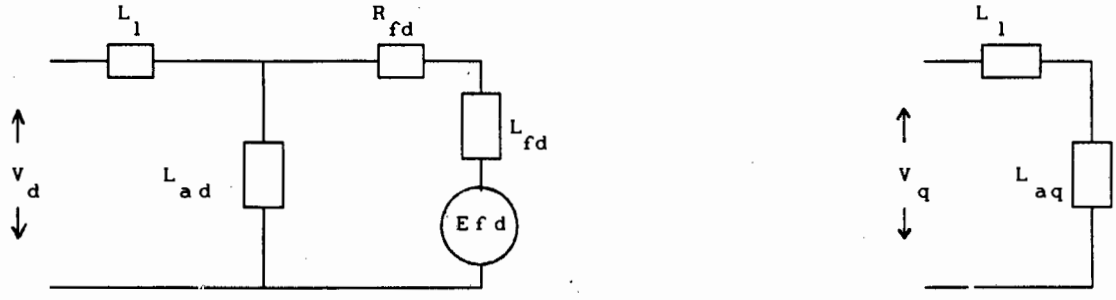

(b) model 1.0

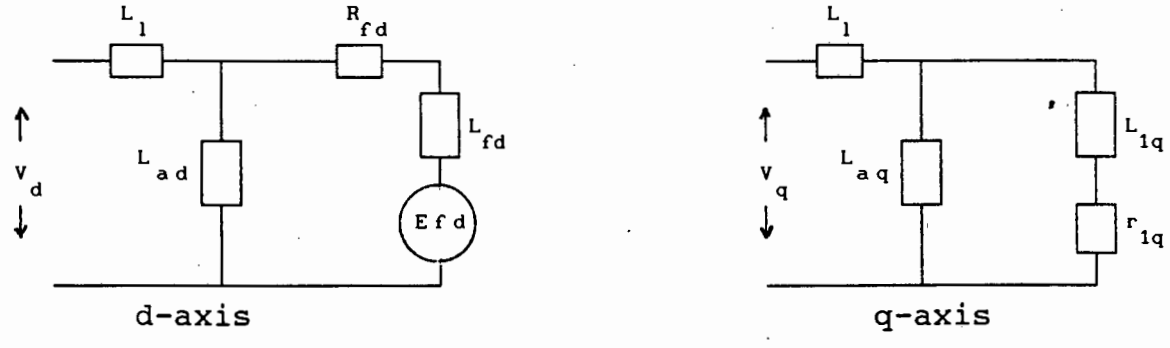

(c) model 1.1

Figure 2.2 :
Different generator models; least complex to most complex

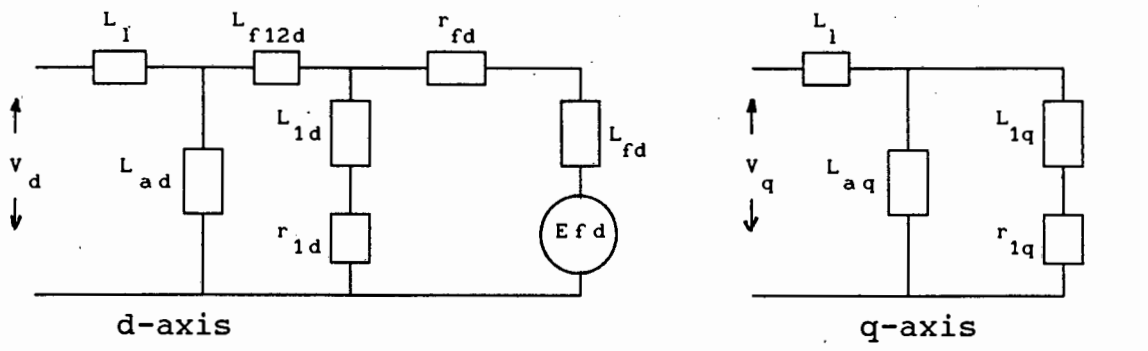

(d) model 2.1

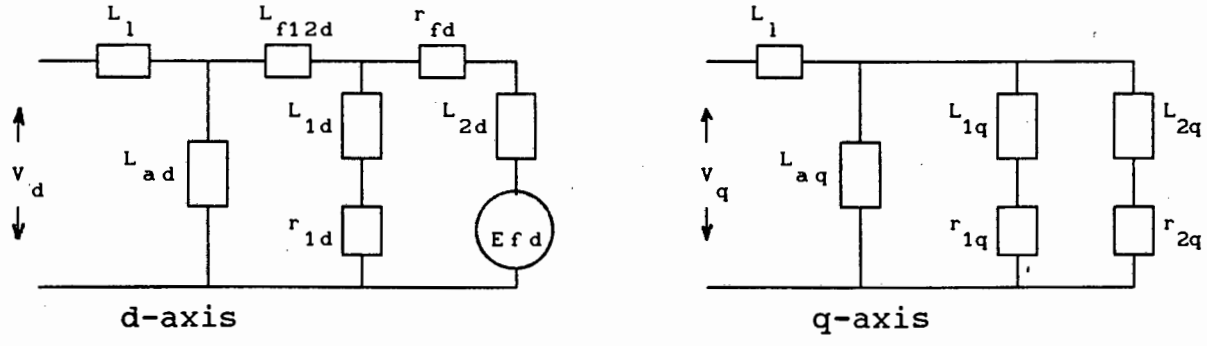

(e) model 2.2

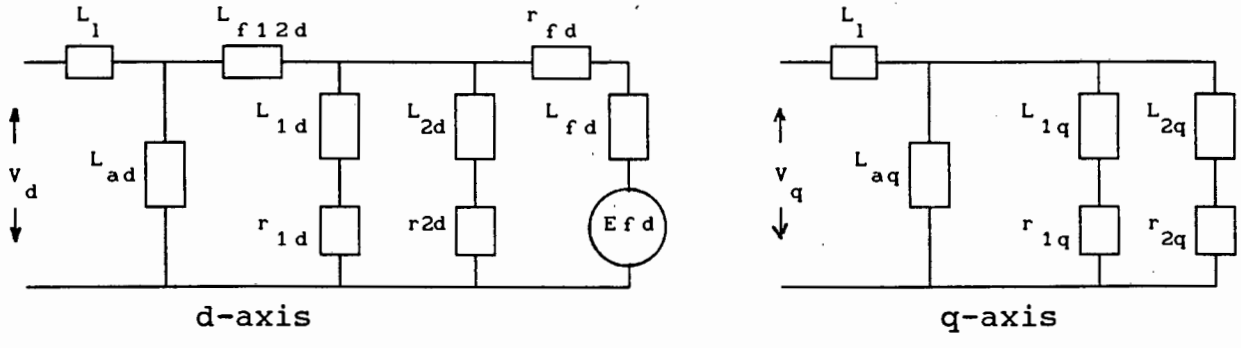

(f) model 3.2

Figure 2.2: (Continued)

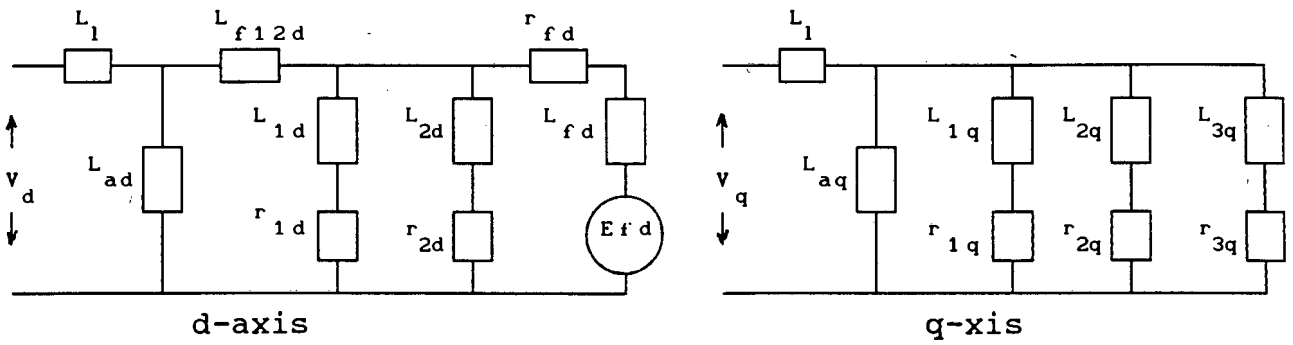

(g) model 3.3

Figure 2.2: (Continued)

The complete third order model for both axis, slightly different from model 3.3 given in figure 2.2, is shown in figure 2.3. Note that two differential leakage inductances L_{f1d} and L_{f2d} are represented in figure 2.3 in order to account for the unequal mutual coupling between the stator, the rotor and the field circuits. They represent the flux which link the field and the equivalent rotor paths but does not link the stator windings.

In practice however, it is often adequate to consider only one differential leakage path between the rotor, the stator and the field circuits. Furthermore, the inductance L_{f2d} was shown from previous model identification studies to be small enough to be neglected. Also, expensive tests need to be performed in order to obtain this parameter.

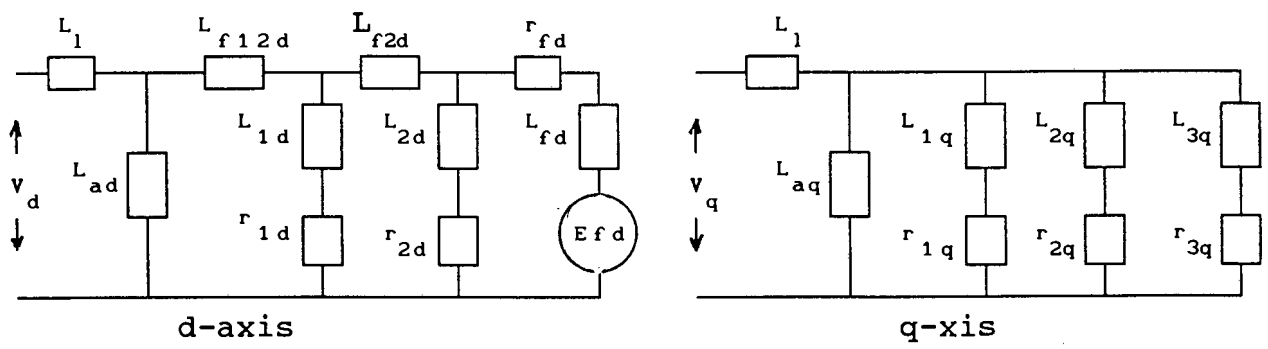

Figure 2.3 :
Close variation of model 3.3

The inductances L_{ad} and L_{aq} are represented as a function of the air gap in order to represent the effects of saturation. The effect of saturation is more pronounced in the q-axis than in the direct axis. Thus the parameter L_{aq} is very important in representing the q-axis saturation.

The mathematical expressions of model 3.3, for use in transient stability studies are derived in [3]. In this reference, the rotor circuit equations are derived first for both the direct and the quadrature axis. Thereafter, the general stator equations are derived. The stator equations are then simplified and the validity of the simplifications are discussed.

The expressions for the less complex models can be deduced form the expressions of the most complex models by simply neglecting the appropriate tems.

2.3 COMPARISON OF THE RESPONSE OF DIFFERENT GENERATOR MODELS AND FIELD TESTS: A LITERATURE REVIEW

Most of the available data for synchronous machines, in accordance with the ANSI[2] standard data, are provided by the manufacturer. This data is based either on design calculations or on actual machine tests (three-phase short circuit tests and stator open circuit voltage rise tests) [4].

New testing procedures for parameter identification have been developed. These new tests include the frequency response tests and the finite element methods. Since these tests are expensive to conduct, most of the available data is subsequently based on the ANSI standards or design information.

Various papers in the past [8],[9], have shown that such data is inadequate to accurately predict the stability performance of the turbogenerators (especially solid iron rotor constructed

[2] ANSI = American National Standards Institute

machines). The frequency response tests however, have produced more accurate data which matches the actual machines' response fairly accurately.

Previous studies have also shown that in general, the number of rotor circuits considered necessary to model, depends on the type of rotor construction. If a detailed stability study is being considered, the rotor circuits of the turbogenerators must be represented by the most complex model (model 3.3 in table 2.1), in cases where the parameters for the model are available.

Model 0.0 was compared to model 1.0 in [12]. The classical model provides optimistic results especially when the generators are equipped with slow, low response ratio exciters. If however, the generators are equipped with fast, high response ratio exciters, this model gives conservative results.

The classical constant flux linkage model corresponds to a generator fitted with a fast,high response ratio exciter only if the fault duration is very small (typically less than 42 milliseconds). For longer fault duration, the classical model corresponds to a machine with a slow, low response ratio exciter [13].

The performance of model 1.0 was analyzed in [7] and compared to model 2.1. The authors suggested that model 1.0 is the better, of the two, for stability studies and is especially useful when controlling schemes have to be included. This model was found to be fairly accurate and that there is no real advantage in using higher order models such as Model 2.1. Reference [11] also states that model 1.0 is sufficiently detailed for a synchronous machine model used in controller design purposes.

Model 1.1, when used with standard data, was found to be sufficiently accurate for use in multimachine transient stability studies [10]. Furthermore, this model requires the use of only the large time constants T'_{d0} and T'_{q0}. Thus, larger integration

time steps can be used which results in reduced computational efforts. This model is thus recommended for use in large scale stability studies.

Model 2.1 has been found to accurately represent hydrogenerators, since for these types of machines, there is only one physically identifiable circuit between the salient poles. This model does not represent the quadrature axis in detail and hence it is not recommended for use in modeling turbogenerators.

For turbogenerators without damper windings, model 2.2 was found to be adequate in predicting the system stability due to large and small disturbance. In fact, this model is the most commonly used in stability studies because data for this model is readily available. This model requires the use of larger time constants T'_{d0} and T'_{q0}, the transient time constants as well as the smaller time constants T''_{d0} and T''_{q0}, the sub-transient time constants. Smaller integration time steps are required hence the computer simulation takes longer.

2.4 CASE STUDIES

The network used to compare the transient stability results using different generator models, is shown in figure 2.4. This network is a benchmark used for comparative studies in the power system community. The parameters for the network are listed in [13] and in Appendix 1.

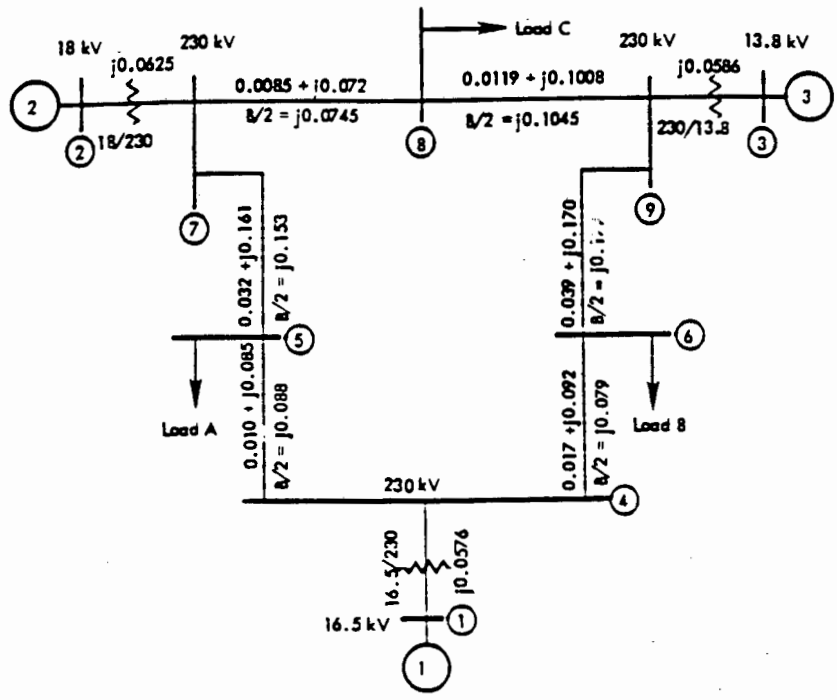

Figure 2.4 :
Ninebus benchmark model

The various generator models compared are listed in table 2.2. This table also lists the PTI[3] names of these models and the case studies in which these models are used. PTI names will ne used in

[3]Power Technologies Incorporated

the next sections.

Table 2.2 : Generator models used

MODEL NUMBER	PTI NAME	DESCRIPTION OF THE MODEL	CASE IN WHICH THE MODEL IS USED
MODEL 0.0	GENCLS	Constant flux linkage model	CASE 2.1
MODEL 1.0	GENTRA	Transient Saliency model	CASE 2.2
MODEL 2.1	GENSAL	Subtransient Saliency model	CASE 2.3
MODEL 2.2	GENROU	Solid round rotor model	CASE 2.4

The most complex model (model 3.3) is not used due to lack of adequate generator data.

CASE 2.1

In this case study, all the generators are modeled with the classical model "GENCLS". The conditions for this simulation are listed in table 2.3. The transient stability results are shown in figure 2.5.

Table 2.3: Simulation conditions - case 2.1

Generator model	all generators GENCLS
Load model	all loads constant admittance
Fault location	on transmission line between buses 5 and 7, near bus 7
Fault type	symmetrical three-phase fault
Fault duration	from t=0 to t = 0.05 seconds
Fault clearing	both breakers of the affected transmission line
Simulation time	2 seconds

The relative rotor angle plots of figure 2.5 show the angle of machines 2 and 3 with respect to machine 1. The results show a stable system, with the rotor angular swing reaching a peak value of 68 degrees at time t = 0.50 seconds. There are two angular swings in this case. Notice that the second angular swing is approximately equal in amplitude to the first swing. This is a result of small machine resistance and neglecting damping.

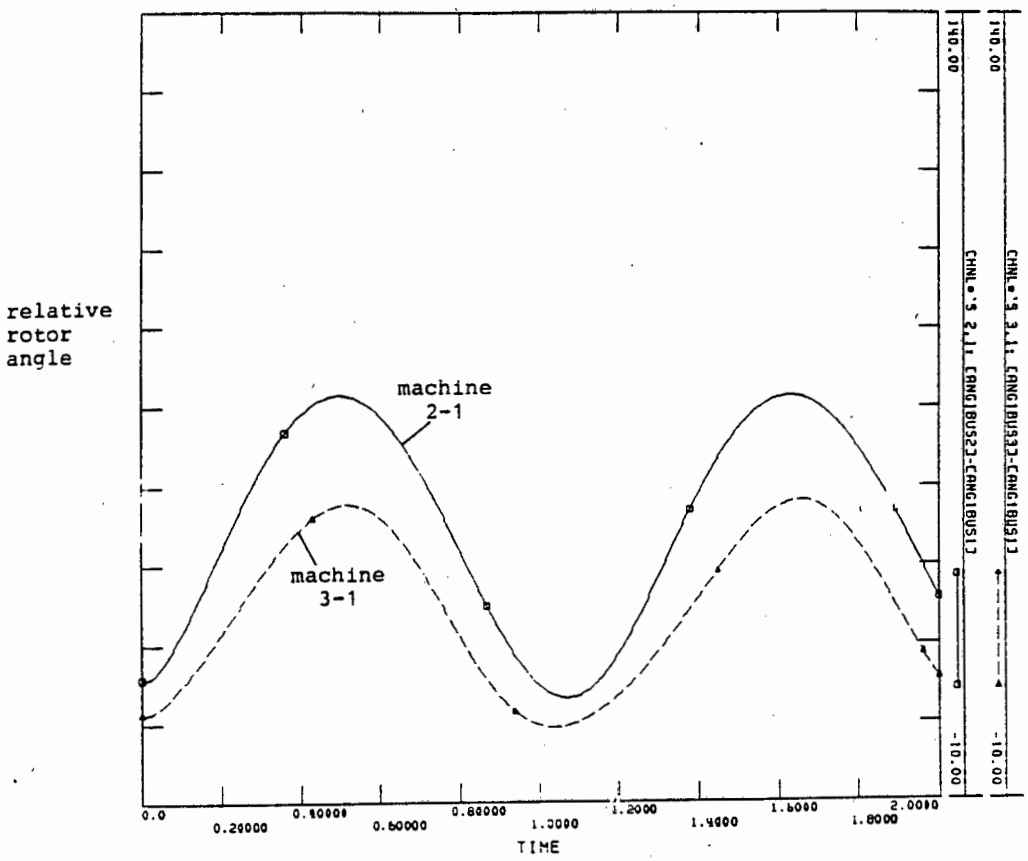

Figure 2.5:
Transient stability result; "GENCLS"

CASE 2.2

In this case study, all the generators are modeled with the transient saliency model "GENTRA". The simulation conditions are similar to those listed in table 2.3 except for the generator model. The transient stability results are shown in figure 2.6.

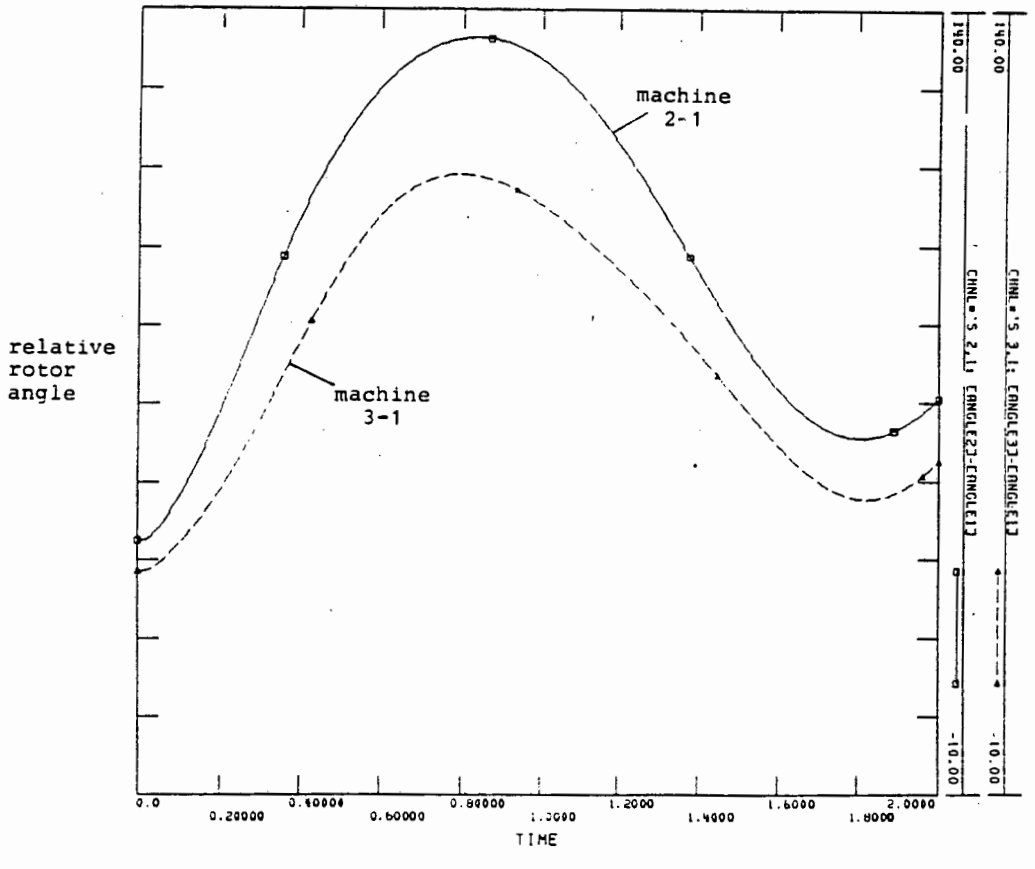

Figure 2.6:
Transient stability results; "GENTRA"

The initial relative rotor angle between machine 2 and 1 is 38.2 degrees. The initial relative rotor angle was 13 degrees when the generators were modeled as "GENCLS" (see figure 2.5). The angular difference is also evident between machine 3 and machine 1. This difference is a result of introducing additional reactances X_d and X_q. This type of generator modeling changed the initial conditions for stability calculations.

Figure 2.6 also shows that the relative angular swing increases beyond 90 degrees after 0.32 seconds and reaches a peak value of 135 degrees at time t = 0.85 seconds. The relative angle then decreases, the result showing a stable system.

Figure 2.7 shows a comparison of the two cases. The figure shows that for the same disturbance, the "GENTRA" model gives conservative/ pessimistic results as compared to "GENCLS", which gives optimistic results.

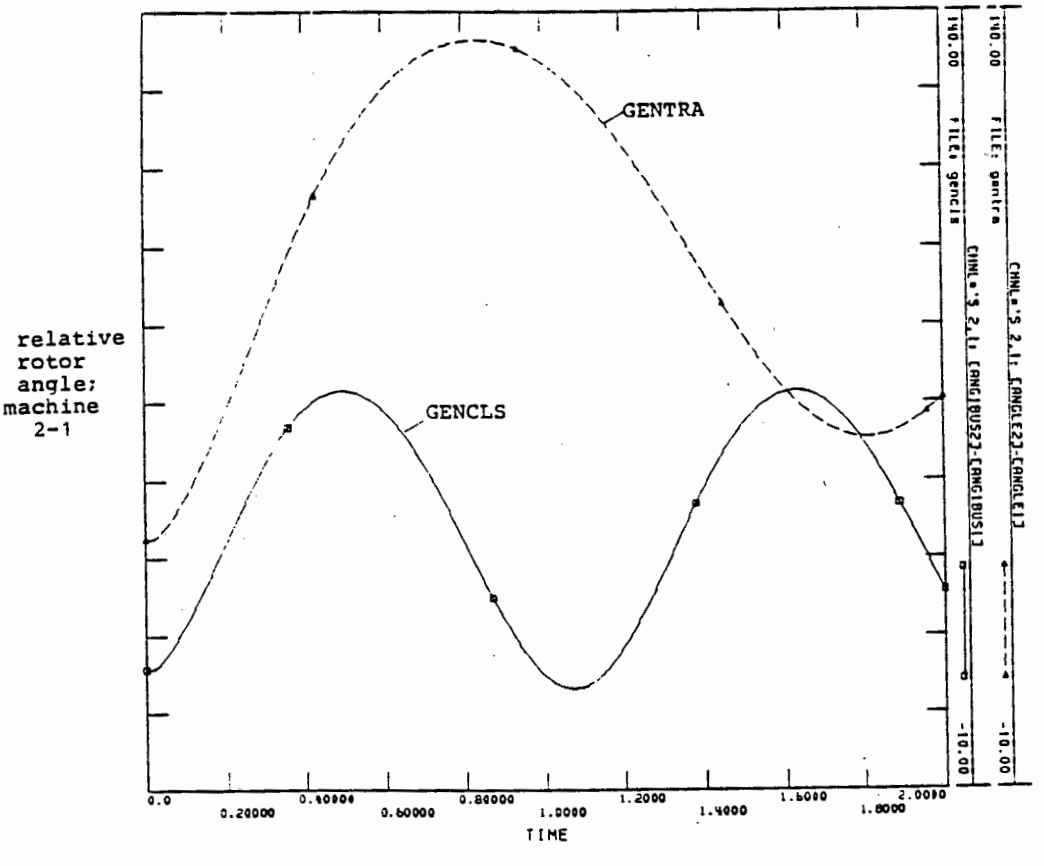

Figure 2.7:
Comparison of transient stability results;
"GENCLS" and "GENTRA"

CASE 2.3

In this case study, all the generators are modeled with the salient type generator model "GENSAL". The simulation conditions are similar to those listed in table 2.3 except for the generator model. The transient stability results are shown in figure 2.8.

The figure shows the relative rotor angle for machines 2 and 3 with respect to machine 1. The results show that the system is stable. The amplitude of the relative rotor angle for machine 2 reached a peak value of 128 degrees. The results are thus less conservative compared to those obtained in case 2.2.

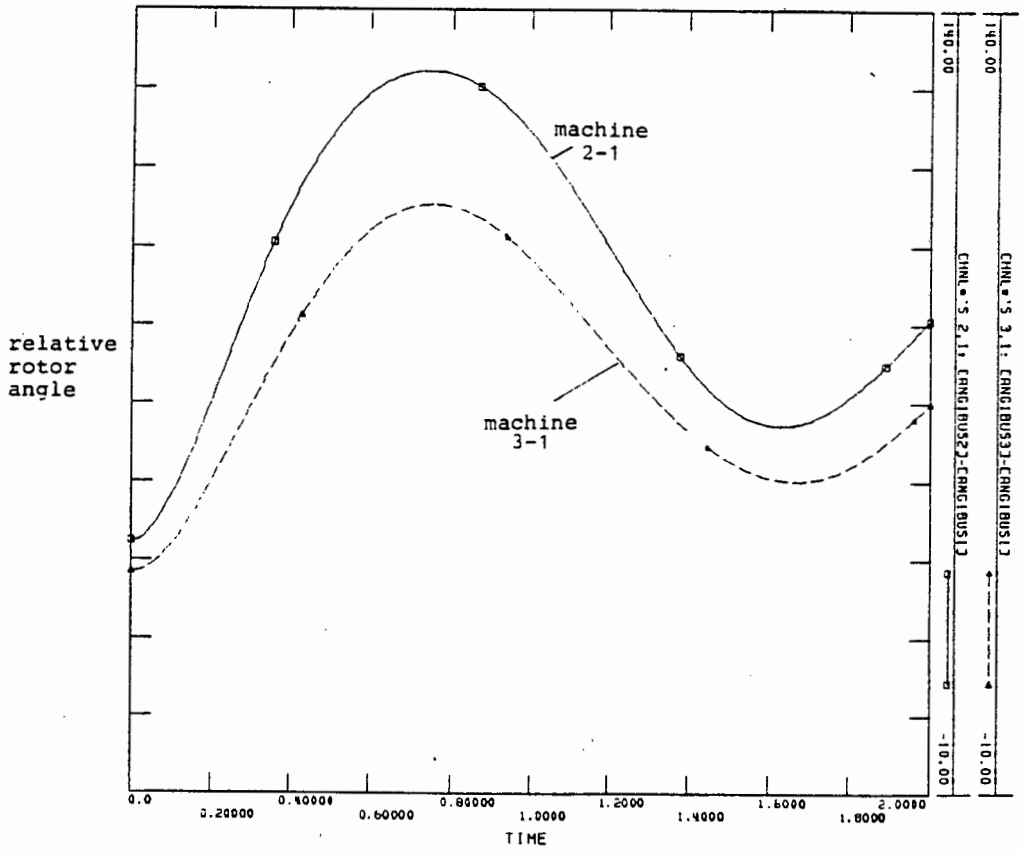

Figure 2.8:
Transient stability results; "GENSAL"

CASE 2.4

In this case study, all the generators are modeled with the solid round generator "GENROU". The simulation conditions are similar to those listed in table 2.3 except for the generator model. The transient stability results are shown in figure 2.9.

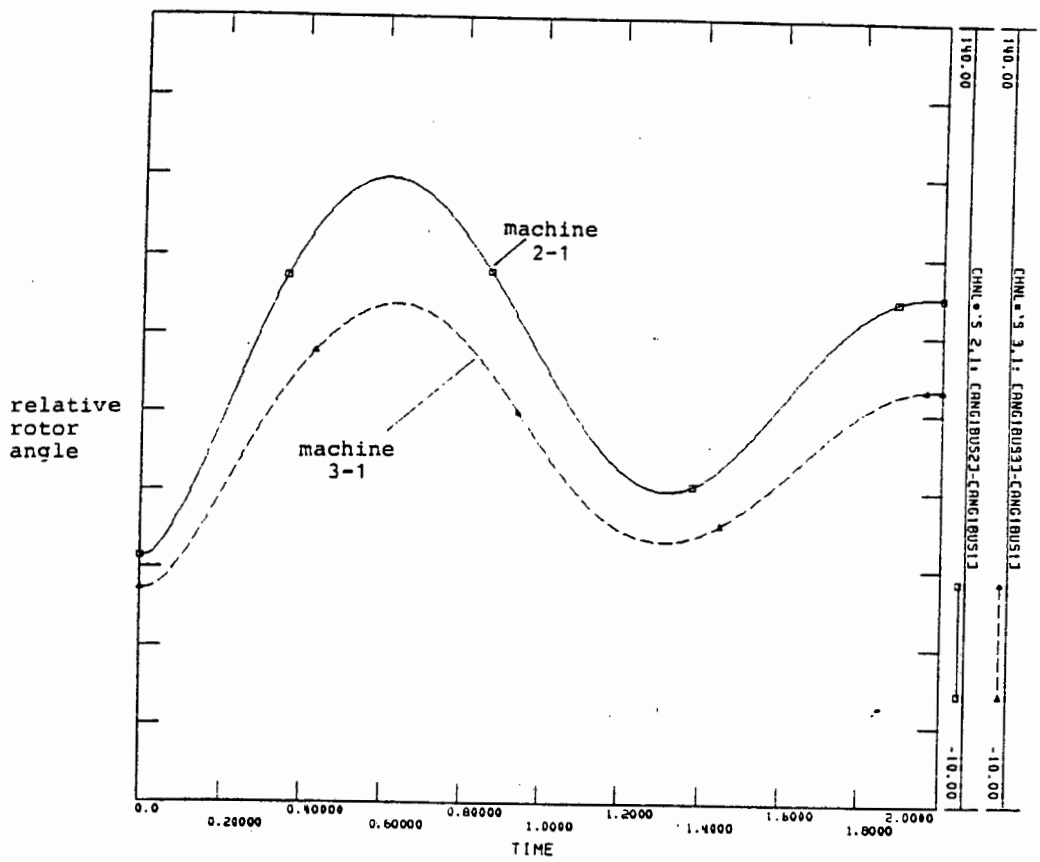

Figure 2.9:
Transient stability results; "GENROU"

The results from this figure show a stable system. The maximum relative angle between machines 2 and 1 is 110. This relative angle is less than the relative angle obtained in case 2.2 and case 2.3. The results are thus optimistic. Similar observations can be made regarding the relative rotor angle between machines 3 and 1. A comparison of the transient stability results for "GENCLS", "GENTRA", "GENSAL" are "GENROU" models is shown in figure 2.10a and 2.10b.

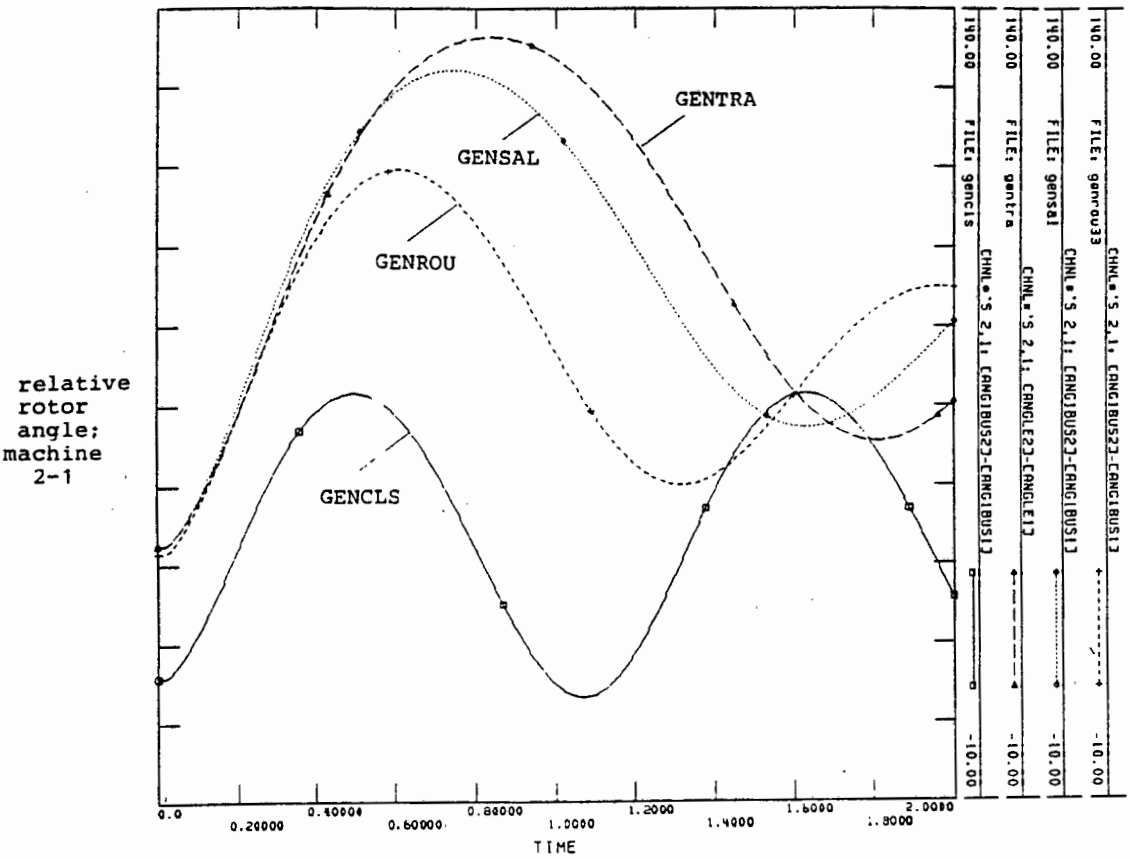

Figure 2.10a:
Comparison of the transient stability results;
"GENCLS", "GENTRA", "GENSAL" and "GENROU"
machine 2-1

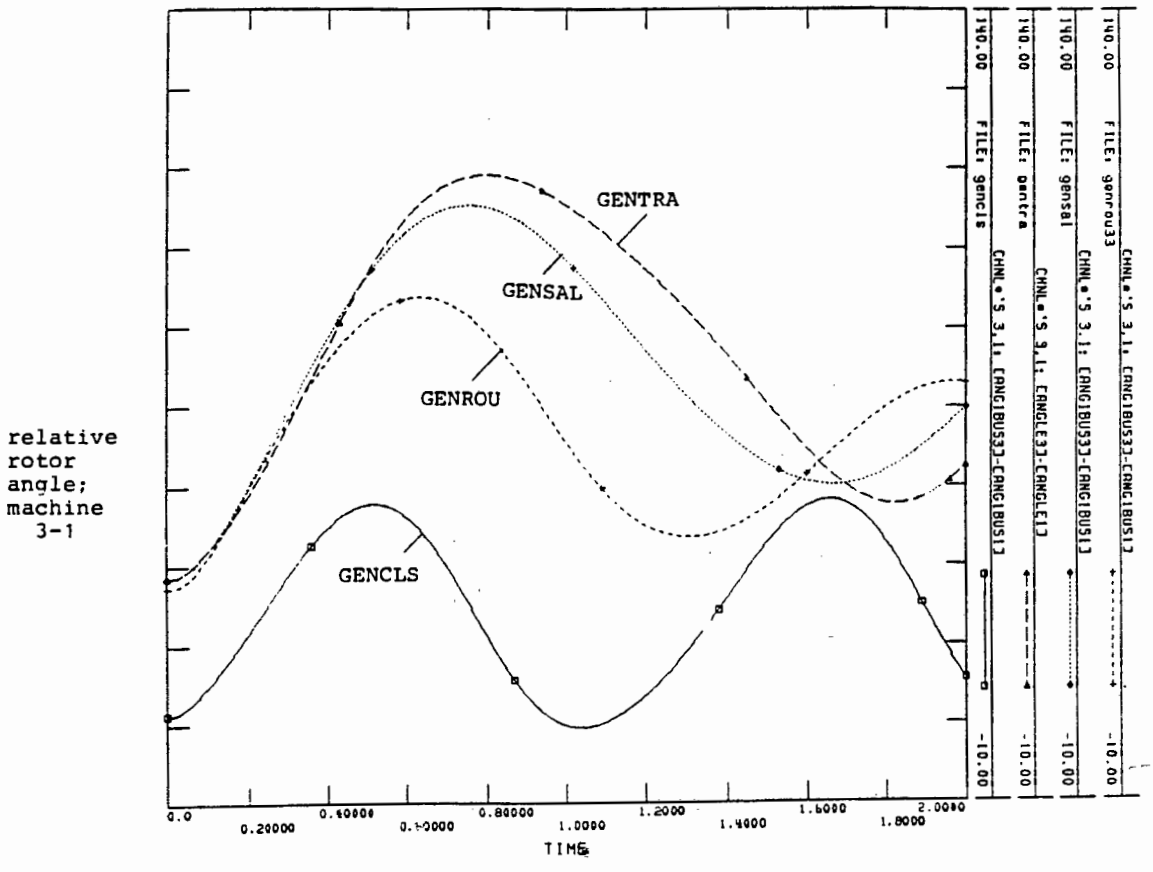

Figure 2.10b:
Comparison of the transient stability results;
"GENCLS", "GENTRA", "GENSAL" and "GENROU"
machine 3-1

Figure 2.10a and 2.10b show that "GENCLS" gives the most optimistic transient stability results, followed by "GENROU". "GENTRA" gives the most conservative transient stability results, followed by "GENSAL".

CASE 2.5

In this case the effects of the AVR[4] on the transient stability, will be investigated. It is not the purpose of this thesis to cover the functions of the AVR and its modeling in detail. However, since the AVR plays a very significant role in the transient behavior of the synchronous machines, it is only proper to briefly discuss some of its function. This case is solely for this purpose.

A voltage regulator is a generator control device that senses changes in the output voltages (and currents) and causes corrective action to take place. When there is a sudden drop in voltage at the generator terminals, due to a large disturbance, the AVR will try to keep this voltage constant or to reduce the severity of this sudden drop of voltage. This will generally have a positive effect on the transient stability.

Case 2.4 is extended in this case, by including the AVR model on all the "GENROU" modeled generators. The results can be seen in figure 2.11. The relative angle plots shows a stable system when the AVR action is included. The AVR has thus acted in a manner that improved the transient stability for the first swing.

[4] AVR = Automatic voltage regulator

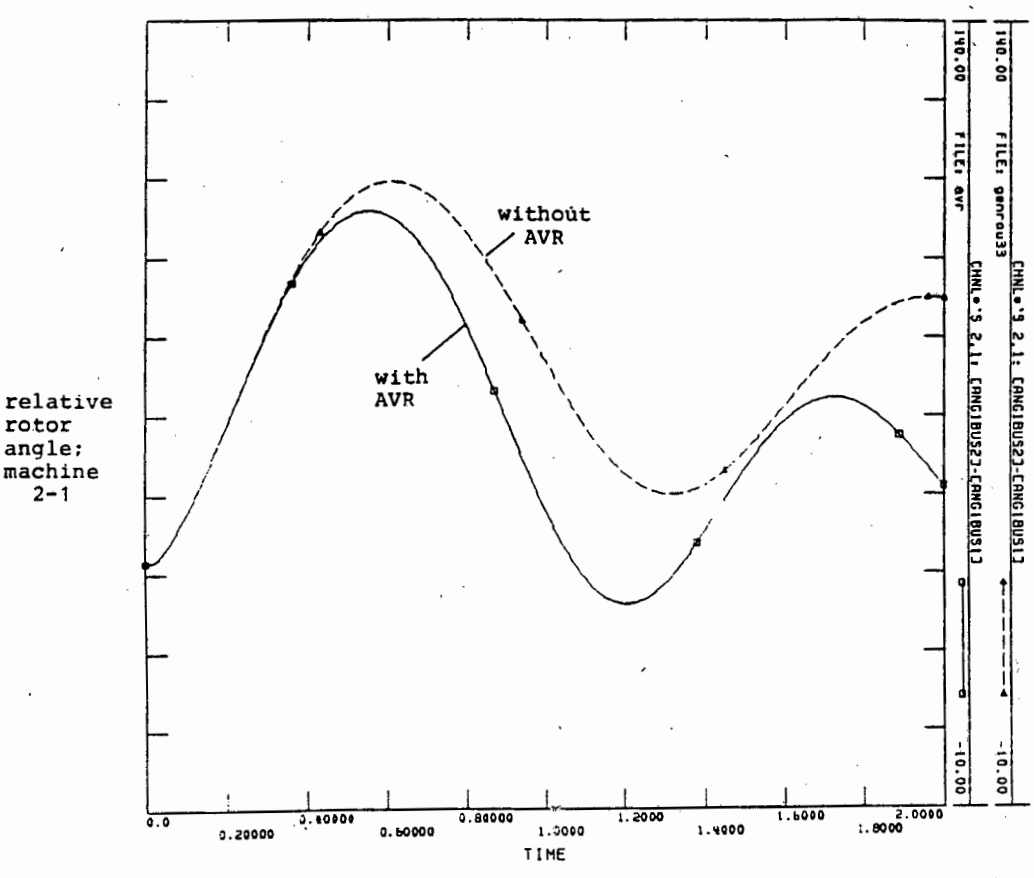

Figure 2.11 :
"GENROU" model with and without an AVR
(only machine 2 shown)

2.4 SUMMARY

This chapter focused on the mathematical modeling of synchronous generators. The different practical generator models were defined. These generator models were identified by the "IEEE Task force on definitions and procedures", in conjunction with the IEEE working group on the determination and application of synchronous machine models".

In addition, the technical literature on the subject of generator modeling was briefly reviewed and the complexity of generator modeling was highlighted. Case studies were performed to compare the transient results obtained using different generator models.

The results from the case studies are summarised in table 2.4:

Table 2.4 : Summary of the transient stability results using different generator models

MODEL NUMBER	PTI NAME	TRANSIENT STABILITY RESULT
MODEL 0.0	GENCLS	MORE OPTIMISTIC
MODEL 1.0	GENTRA	MORE CONSERVATIVE
MODEL 2.1	GENSAL	CONSERVATIVE
MODEL 2.2	GENROU	OPTIMISTIC

The following conclusions can be drawn :

Model 0.0 ("GENCLS") must be used only for the first swing transient stability studies. The transient stability results obtained using this model are more optimistic than all the other models in the table.

Model 1.0 ("GENTRA") can be used for multiswing transient stability studies. This model should only be used only if the detailed perameters of the generator are not known. The transient stability results obtained using this model are more conservative.

Model 2.1 ("GENSAL") can be used for multiswing transient stability studies. The results obtained by using this model are conservative. This model represents limited damping in the direct and quadrature axes. It is thus suitable for modeling hydraulic generators.

Model 2.2 ("GENROU") can also be used for multiswing transient stability studies. The transient stability results obtained by using this model are optimistic. The model represents more damping in the direct and quadrature axes. It is thus suitable for turbogenerators without damper windings. This model must also be used when the effects of the generator controls (such as the AVR) on the systen stability, are investigated.

CHAPTER 3 : LOAD MODELING FOR STABILITY STUDIES

3.1 INTRODUCTION

The aim of this chapter is to investigate the effects of different load models on the transient stability results. The characteristics of different types of loads, namely: static and dynamic loads are discussed.

The mathematical models used for representing the static loads are:

(i) Constant admittance
(ii) Constant current
(iii) Constant power and
(iv) Frequency and voltage sensitive

The mathematical models used for representing the dynamic loads are:

(i) "complex load model"
(ii) steady-state model
(iii) transient model

A layout of the static and dynamic loads and their mathematical models is given in Appendix 3.

The structure of this chapter is as follows :

A brief discussion on the problem of load modeling for stability studies is given. Then, different load modeling approaches are highlighted. Furthermore, the characteristics of different types of loads, namely; static loads and dynamic loads are discussed in detail.

Furthermore, methods used for aggregating power system loads are briefly discussed, namely; grouping of coherent induction motors and the equivalencing criteria for induction motors. Finally, case studies are performed to compare the transient stability results obtained by using different load models.

The contents of the case studies are as follows :

The effects of modeling the loads as constant admittance, constant current and constant power on the transient stability results, are investigated in **case 3.1.**

The effects of modeling the **local** load as constant power and constant admittance, on the transient stability results, are investigated in **case 3.2** and **case 3.3.**

The effects of modeling the load dependency of the frequency on the transient stability results are investigated in **case 3.4.**

In **case 3.5,** the loads are again modeled as constant power, constant current and constant admittance. The difference between this case and case 3.1 is the fault location.

The effects of modeling the **remote** load as constant power and constant admittance, on the transient stability results, are investigated in **case 3.6.**

The effects of modeling an industrial load with a "complex load model" on transient stability are investigated in **case 3.7.** The "complex load model" specifies different percentage composition from the total load.

The effects of modeling a large induction motor (15.3 MVA) with its steady-state, transient and static model on the transient stability results are investigated in **case 3.8.**

Finally, conclusions are drawn and a summary of the chapter is provided.

3.2 THE PROBLEM OF LOAD MODELING IN POWER SYSTEM STABILITY STUDIES

The need for power system analysis has long been recognized and the subject is well documented [14],[15],[16]. Load modeling for stability studies is part of this analysis [17].

The modeling of loads dates back to the late forties when network analyzers were still in use. The prohibitive computational requirements resulted in many approximations being made to the load models. In turn, this resulted in the use of simple models which did not provide sufficient information about the dynamic behavior of loads.

With the advent of digital computers, more accurate load models could be used in dynamic simulations. Despite this improvement in computational tools, the problem of load modeling for stability studies is still very complex. The load composition changes with the time of the day, the consumer's lifestyle, the weather, the state of the economy and other factors. The accurate model would include amongst other things, the effects of the abovementioned factors. Since these factors are unpredictable, accurate load modeling becomes very complex indeed.

It is mainly for these reasons that the approximate models are still widely in use. Ideally, the response of these approximate models should be compared to the response of the actual loads under similar disturbance.

3.3 LOAD MODELING APPROACHES

There are not enough software packages dedicated to load modeling for use in industry. The available packages like LOADSYN (load synthesis) [18] are very expensive and utility engineers are very skeptical to use them because a discrepancy still exists between results produced by these models and the field tests. The 1984 EPRI Report on "Load Modeling for Power Flow and Transient Stability Computer Studies" [18] and [55] highlighted the two

approaches of load modeling philosophy.

One approach would be to monitor the sensitivity of the active and reactive power of the load, to changes in voltage and frequency. Such a scheme requires the utilization of memory-type devices which are capable of recording the data before, during and after the disturbance. Using this monitoring approach, it is possible to obtain the correct response of the load under large disturbance conditions. The exact model of the load can then be calculated.

The shortcoming of this approach is the requirement of installing measuring equipment to monitor all loads. Since the load changes due to seasonal factors and the time of day, measurements have to be repeated and extrapolations be made.

The other approach is component based. A model is built based on the constituent parts of the load. Three sets of data are required.

3.3.1 *Load Class Mix data.*

These are the types of different classes which contribute to the total active and reactive power load. Examples would be the percentage contribution of Commercial, Industrial, and Residential loads.

3.3.2 *Load Composition data.*

This is the contribution of different load components to total power consumption. Examples for residential loads would be percentage contribution of lighting, water heating and room air conditioning amongst others.

3.3.3 *Load Characteristic data.*

The data required are the electrical characteristics of the components of the load, for example the power factor of the motors and the voltage and frequency dependency sensitivities.

Reference [18], shows the algorithm that has been developed to estimate the load representation based on the above percentage contribution of each component as inputs to the program. A schematic representation of the parts of the load is shown in figure 3.1.

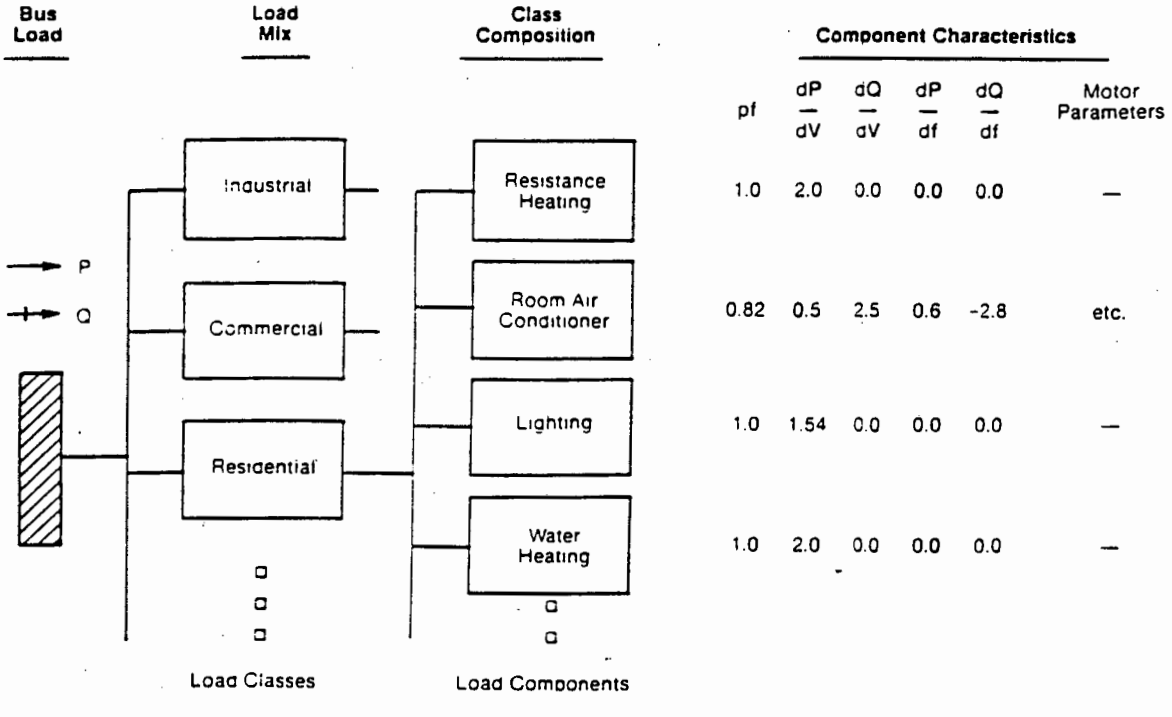

Figure 3.1
Load composition data

3.4 DIFFERENT TYPES OF LOADS

Power system loads are classified into two categories, the static load and the dynamic load. These types of loads and their effect on transient stability are discussed below.

3.4.1 Static loads

Static loads are passive or non-rotating loads. They can reasonably be expressed by polynomials or some algebraic functions like exponentials. They can either be voltage dependent, frequency dependent or both.

The frequency component contributes to the system damping. The instantaneous operating frequency and terminal voltage determine the active and reactive power components of the load. It is very difficult to determine the frequency dependency of the load because load-frequency test are rarely performed. If these test were performed, the security of the system would be threatened.

The frequency and voltage dependency are significant for large disturbances. Large disturbances would include three-phase faults, loss of generating units, loss of critical transmission line or transformer, or sudden changes in load.

There are four general ways of representing power system static loads. These are constant power representation, constant current representation, constant impedance representation and frequency and voltage sensitive load representation. Some loads are represented as a combination of these four types. Some loads e.g fluorescent lighting are inversely proportional to voltage variation. These various static load representations are discussed in detail further.

(i) Constant Power Representation

The active and reactive power are assumed to remain constant during and after the disturbance. The constant power representation is the most severe representation from the system stability point of view because of its effect in hastening the fall of voltage during a disturbance. A drop in voltage will cause an increase in current which will, in turn, cause a further drop in voltage. The results produced by this representation may indicate voltage instability even in cases where the actual system is far from collapse. Voltage collapse/instability problem is discussed in chapter 4.

The equation expressing this representation is given by

$$S = V * I^{*} = P + jQ = \text{const} \quad \ldots\ldots\ldots\ldots\ldots\ldots (3.1)$$

This representation is thus suitable for stability calculations under the assumption that the load voltage is held constant by changing transformer taps or by using other means of reactive compensation like synchronous condensers, capacitors etc.

(ii) Constant Current Representation

In this representation the complex power varies proportionally with the voltage in order to keep the load current constant. This model is used when no other information about the load is available. This model represents a compromise between constant power and constant admittance models [17]. The equation expressing this representation can be written as

$$I = (P - jQ)/ V^{*} = \text{const} \quad \ldots\ldots\ldots\ldots\ldots\ldots\ldots\ldots (3.2)$$

where I represents the load current.Constant current representation gives good results only when voltage variations are small. For large voltage variations, the error is likely to

be considerable.

(iii) Constant Admittance representation

The complex power varies as the square of the voltage to keep the impedance constant. The equation expressing this representation can be written as

$$Y = (P - jQ) / |V|^2 = \text{const} \quad \ldots\ldots\ldots\ldots\ldots (3.3)$$

where Y represents the equivalent shunt admittance of the load. The load is usually converted to constant admittance when the voltage drops below a certain percentage (about 40%) of nominal mainly to aid avoid numerical (convergence-type) problems [17],[20],[21].

(iv) Frequency and voltage sensitive representation

These types of loads vary with the change in voltage as well as the change in frequency. Gas-discharge lamps, for example, fall into this category. The power consumed by these lamps was found to decrease by 0.5 - 0.8 per cent for a frequency increase of 1 per cent [22]. The general equation governing this representation can be written as

$$\frac{S}{S_0} = A\left(\frac{V}{V_0}\right)^a (1 + k*df) + B\left(\frac{V}{V_0}\right)^b \quad \ldots\ldots\ldots (3.4)$$

where $S_0 = P_0 + jQ_0$, the initial bus active and reactive power from load flow,

V_0 = the initial bus voltage magnitude from load flow,

a = the voltage exponent for frequency dependent part of the load,

b = the voltage exponent for non-frequency dependent part of the load,

k = the frequency sensitive coefficient of the load,

df = the frequency variation and

A and B are constant coefficients.

The accurate modeling of static load is very important in power system stability studies. Concordia and Ihara [21] have shown that for loads that are remote from the generating plants, the stability limit decreases when the load is modeled as constant power as opposed to constant admittance. For loads near generating plants however, the stability limit is increased. Thus for accurate load modeling, the type and location of the load should be jointly taken into account.

3.4.2 Dynamic loads

Dynamic loads vary considerably and rapidly to changes in voltage and frequency. For example, the slip of an induction motor varies proportionally to frequency variations, if the torque is held constant. The active and reactive power consumed by the motor varies with the frequency.

The variations of voltage and frequency are not independent of each other. A variation of frequency is usually caused by an imbalance between the electrical output of the generators and the power demand by the loads. This change of frequency alters the active and reactive power taken by the load and the active and reactive power losses in the network. Consequently, the voltage at the load is changed. A decrease in frequency is generally followed by a decrease in voltage.

The large part of dynamic loads for which detailed studies have been performed is the induction motors [17-19],[22-25].This is the case since most of the loads in an industrial power system are induction motors. The dynamic behavior of large induction motors will be covered in this section but first, the techniques used in aggregating power system loads and the equivalencing methods will be discussed.

3.4.2.1 Load aggregation

A power system generally has many load areas located at different physical and electrical distances. In order to save on computing time, an aggregate load model is required. When grouping different loads, some of the characteristics of individual loads may be lost. The basis of aggregation must therefore be to retain the characteristics of individual loads in the aggregate model. Moreover, the response of the aggregate models to various system disturbances must compare favorably well to the actual system model response.

Power system loads are aggregated into two types, the static and the dynamic. When an aggregate static model is developed, the sensitivity factors of the individual loads are grouped separately into frequency dependent terms and voltage dependent terms. This representation was discussed in section 3.4.1 under static loads.

In dynamic aggregation the motor parameters are aggregated using the kVA ratings of the motors, expressed in per-unit of the total bus load as the weighting factors. The impedances of the equivalent circuit are aggregated as if each of the three branches of the equivalent circuit (shown in figure 3.2 below) were connected directly in parallel with the same branch of all the other motors, as shown in figure 3.3.

After grouping the loads, the aggregate plant model will appear as shown in figure 3.4. To validate the effectiveness of the aggregate model approach, a computer simulation study was conducted at the NPCC (Northern Power Coordinating Council) system [26]. In this study five induction motors were represented by an aggregate model. The graphical analysis of the response of the aggregate model to system disturbances compared very well to the response of individual motors.

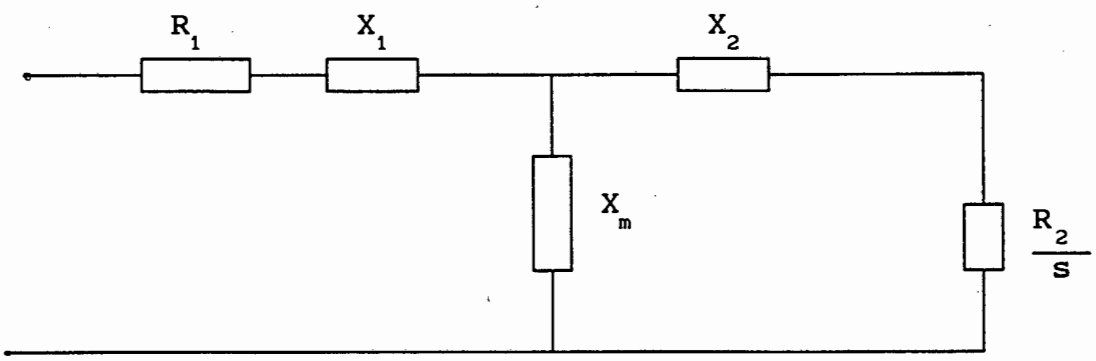

Figure 3.2 :
Induction motor equivalent circuit

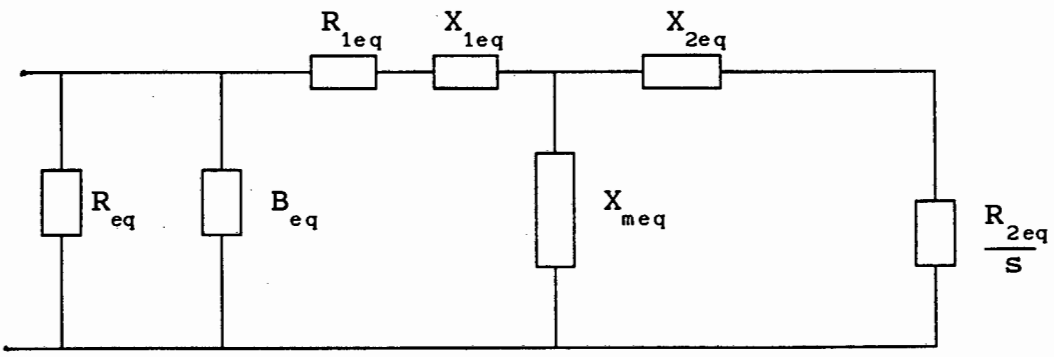

Figure 3.3 :
Aggregate induction motor equivalent circuit
with static load included (G_{eq} and B_{eq})

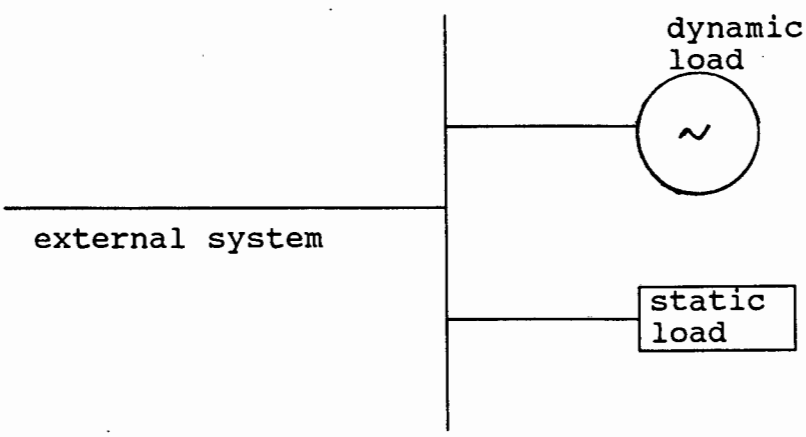

Figure 3.4 :
Aggregate plant model

Induction motor equivalencing criteria

The factors that affect the transient behavior of induction motors are the inertia constant H, the time constant of the rotor Tdo′ and the torque-speed characteristics Te(ω). The larger the inertia, the smaller the influence of Te(ω).

Hakim in [22], shows how two or more induction motors can be represented as a single dynamic unit. Computation effort is greatly reduced by grouping parallel induction motors. The general idea is that the induction motors are grouped into static and dynamic loads.

Careful consideration should be given to the following parameters when aggregating induction motor loads:

(i) Electrical parameters i.e the resistances and reactances of individual motors and of the composite motor.
(ii) Equivalent slip
(iii) Equivalent Inertia Constant
(iv) Composite load torque-speed characteristics

Several assumptions are made and the response of the aggregate model is compared to the response of separate models. The model presented in [22] is however, oversimplified because it neglects the effects of the rotor deep bar which makes large machines' rotor circuit resistances and leakage reactances to vary significantly with the slip. Also the effect of the system impedance has been neglected.

Large and low inertia motors should be differentiated. Large induction motors must be grouped separately. In fact, induction motors must be equivalenced according to their power rating. The criterion for equivalencing [10] is that the motor inertia must be greater than half the rotor time constant with the stator open circuited or

$$H > 0.5\ Tdo'$$

All induction motors that meet the above criteria can be represented as a single unit.

3.4.2.2. Models for dynamic loads

There are various ways of modeling induction motors for power system stability studies. These are listed below in order of increasing complexity.

1. By static loads such as constant power, constant current and constant admittance.

2. By a complex load model which contains a percentage composition of induction motors.

3. By representing the dynamics of the rotating load with its inertial differential equation and the motor with its steady-state equivalent model.

4. By representing the rotating load dynamics and the electromagnetic dynamics of the motor.

The first approach above is reasonable for many of the loads in a large-scale system study, because the details of individual loads, including induction motors are not known. This representation is not suitable for studies where the transient behavior of induction motor loads has a critical effect on the bus voltages and hence on the other loads on the system.

The second approach is better than the first approach because the load composition is more representative. Details of the individual motors are not represented.

The third approach takes the behavior of the dynamic induction motor load into consideration. The torque-slip characteristics of the dynamic load is modeled and thus the results are more representative than those from the first and the second

approaches.

The fourth approach provides a more detailed than all previous approaches. In this approach, the electromagnetic transients of the motor are modeled and hence the results produced by this model are more accurate.

A common problem encountered when modeling the induction motor, is the difficulty of obtaining the motor parameters. The manufacturers usually provide induction motor data in terms of the starting torque, starting current, starting power factor, the pull-out torque , rated power, rated power factor and rated slip. The induction motor circuit parameters have to be calculated from these and given in the form of the equivalent circuit as shown in figure 3.6, for a single-cage induction motor, and in figure 3.8, for a double-cage induction motor.

The steady-state model for a single-cage and a double-cage induction motor are discussed below separately.

(a) Induction motor single-cage model

Figure 3.5 shows the model of a single-cage induction motor. R_1 and X_1 represent the stator impedance, X_m the magnetizing reactance, and R_2/s and X_2 the rotor impedance. R_2/s reflect the combined effect of the shaft load and rotor resistance.

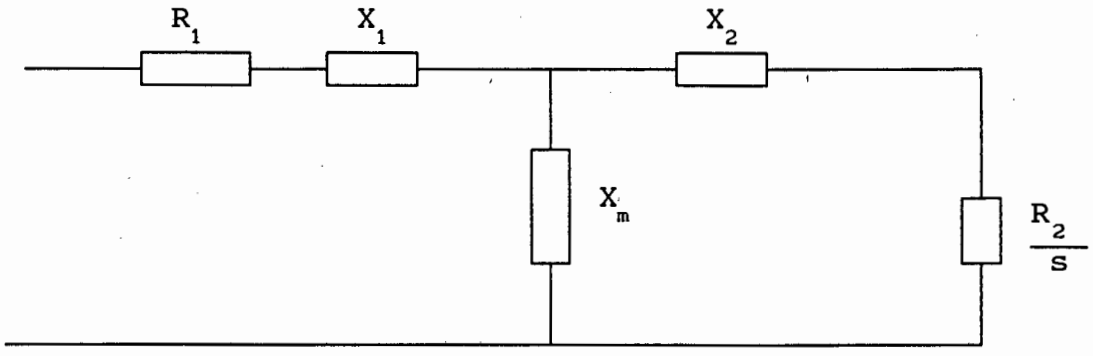

Figure 3.5 :
Steady-state model of a
single-cage induction motor

A typical torque,current and power factor versus speed curve for a single-cage induction motor is shown in figure 3.6. The motor parameters are as follows :

$$R_1 = 0.00293,\ X_1 = 0.107,\ X_m = 4.67,\ R_2 = 0.02,\ X_2 = 0.064$$

A limitation of this motor is that the rotor resistance R_2, remains constant from starting until full load conditions. Ideally, a low value of R_2 is preferred for starting purposes and a high value is preferred during running conditions. High efficiency under normal running conditions, requires a low rotor resistance, but a low rotor resistance result in a low starting torque and high current as shown in figure 3.6.

In order to achieve this ideal, the design of the represents a compromise between the starting requirements and the running requirements. The rotor is designed such that the resistance R_2 is different at low and high speeds. The single-cage induction motor model gives good results at low values of slip.

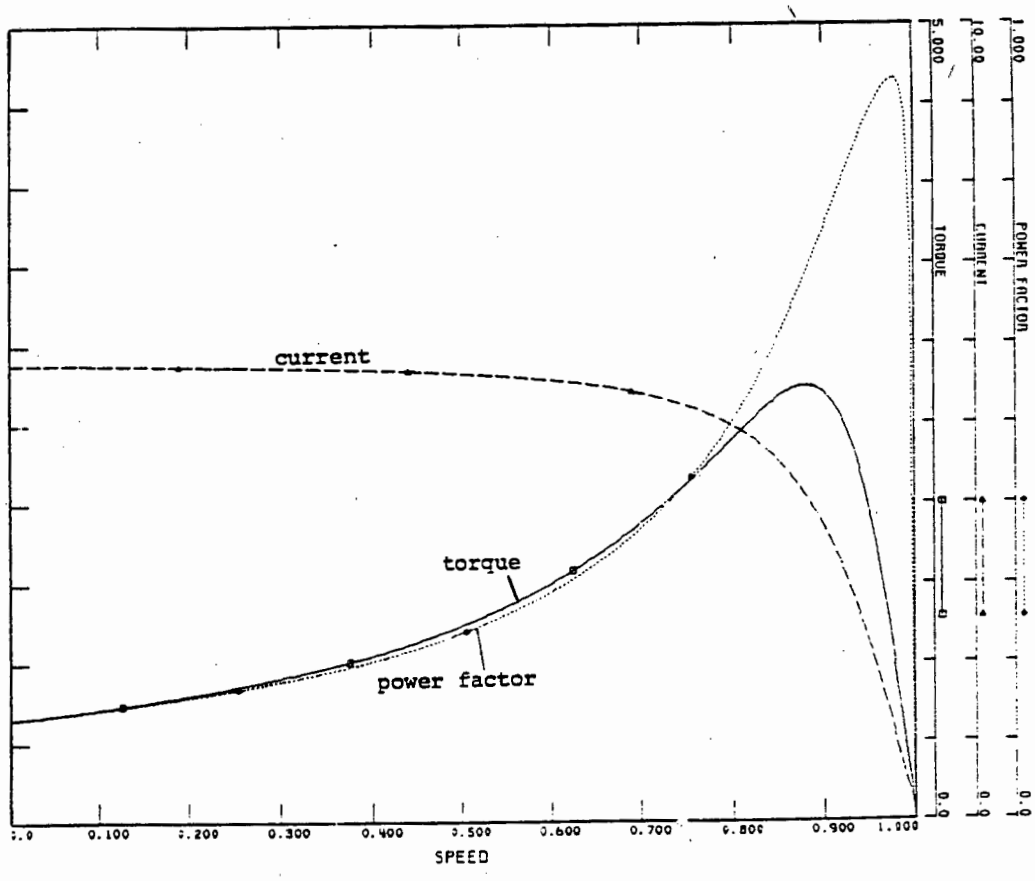

Figure 3.6:
Typical torque,current,power factor versus speed
for a single-cage induction motor

(b) Induction motor double-cage model

In order to improve the performance of a single-cage induction motor under starting and running conditions, a squirrel-cage induction motor is fitted with deep rotor bars. The effect of these deep bars is to make the rotor resistance R_2 vary automatically with speed. At starting, the effective rotor resistance is higher than when the motor is running under normal operation. Figure 3.8 shows a steady-state equivalent circuit of a double-cage induction motor.

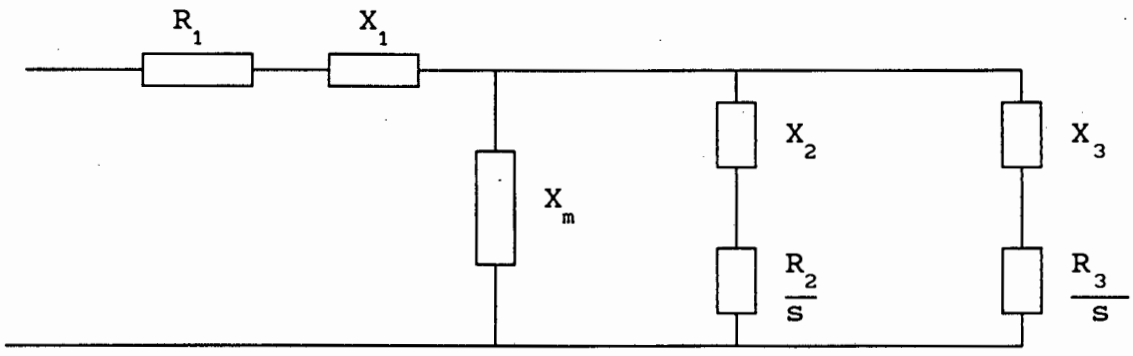

Figure 3.7 :
Steady-state model of a double-cage induction motor

A circuit similar to figure 3.6 can be obtained by substituting the two parallel rotor circuit branches by a single series circuit, where

$$R_2(s) = \frac{R_2.R_3(R_2+R_3) + s^2(R_2.X_3^2 + R_3.X_2^2)}{(R_2+R_3)^2 + (X_2+X_3)^2}$$

$$X_2(s) = \frac{R_2^2.X_3 + R_3^2.X_2 + s^2(X_2+X_3).X_2.X_3}{(R_2+R_3)^2 + s^2(X_2+X_3)^2} \quad ..(3.5)$$

At low values of slip i.e s=0, equations (3.11) reduce to

$$R_2(0) = \frac{R_2.R_3}{R_2+R_3} \quad \text{and} \quad X_2(0) = \frac{R_2^2.X_3 + R_3^2.X_2}{(R_2+R_3)^2} \quad ....(3.6)$$

Substituting $R_3$and X_3in the above equation, it can be shown that for a typical double-cage induction motor $R_3 \cong 5 * R_2$ and $X_3 \cong 2/5 * X_2$. The torque-speed curve in figure 3.8 shows that this model give torque improvement at low values of speed. The parameters of the motor are given below :

R_1= 0.00293, X_1= 0.107, X_m= 4.67, R_2= 0.02, X_2= 0.064, R_3= 0.1
X_3= 0.0256

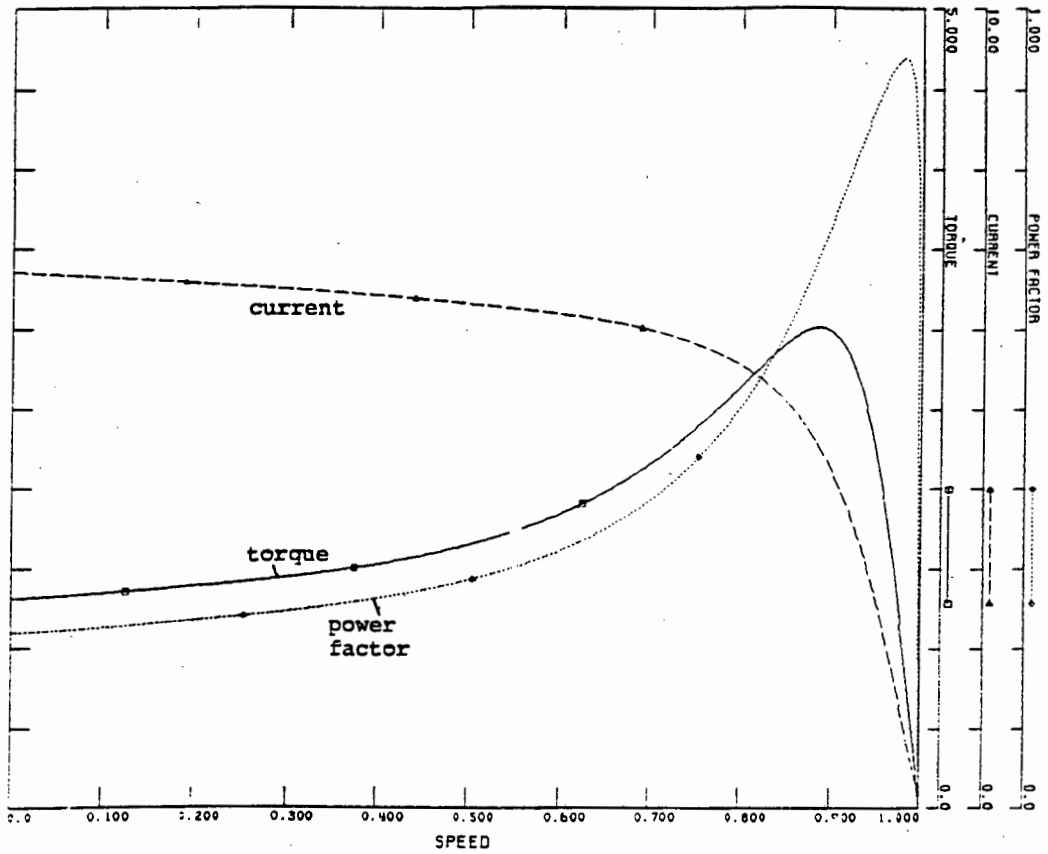

Figure 3.8 :
Typical torque,current,power factor versus speed
for a double-cage induction motor

(c) Induction motor transient model

When a short-circuit occurs at the terminals of the induction motor, the motor will feed current into the fault because of the "trapped" flux linkages with the rotor circuit. This current will have a dc component in addition to the ac component and will, in time, decay to zero.

The initial magnitude of the ac stator current can be determined in terms of the transient reactance X′ and a voltage E′ behind the transient reactance, assumed equal to the prefault value. The decay of the short-circuit current can be characterized in terms of a short circuit time constant T′. A double-cage rotor induction motor model will have an additional reactance X′′, due to the construction of the machine and a corresponding time

constant T''.

These parameters and time constants can be calculated from the steady state parameters, and are given by the following equations

$$X = X_1 + X_m$$

$$X_1 = X_1$$

$$X' = X_1 + \frac{1}{1/X_m + 1/(X_2)}$$

$$X'' = X_1 + \frac{1}{1/X_m + 1/(X_2) + 1/(X_3)}$$

$$T' = \frac{X_m + X_2}{\omega_0 R_2}$$

$$T'' = \frac{X_3 + \dfrac{X_2 . X_m}{X_m + X_2}}{\omega_0 R_3} \qquad \text{.....(3.7)}$$

Figure 3.9 shows the representation of the induction motor for transient stability studies.

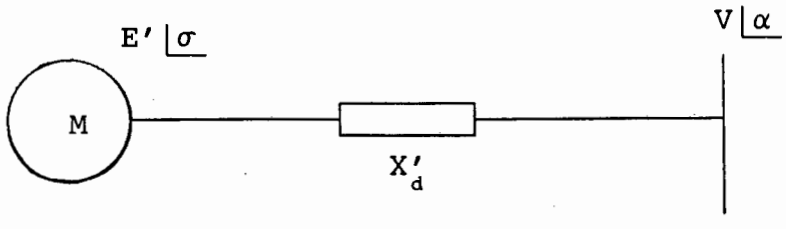

Figure 3.9:
Transient model for an induction motor

(d) Induction motor transient model including driven load dynamics

To obtain accurate results of the dynamic behavior of induction motors and their driven loads, the model must consider the whole electromechanical system.The differential equations governing the combined induction motor and load dynamic behavior are given by equation 3.12, as

$$\frac{d\omega}{dt} = \frac{1}{2H} \left[T_e - T_m - T_{loss} \right] \qquad .....(3.8)$$

where T_e is the electrical torque, T_m the mechanical torque and T_{loss} the torque loss due to friction and windage; ω and H are the speed and the combined inertia constant of the motor and load respectively. The mechanical torque is a fraction of speed and is given by

$$T_m = A\omega^2 + B\omega + C \qquad .....(3.9)$$

Different types of motor loads will thus give different mechanical torques and hence different motor acceleration. A diagram showing the complete dynamic load model is given in figure 3.10 below:

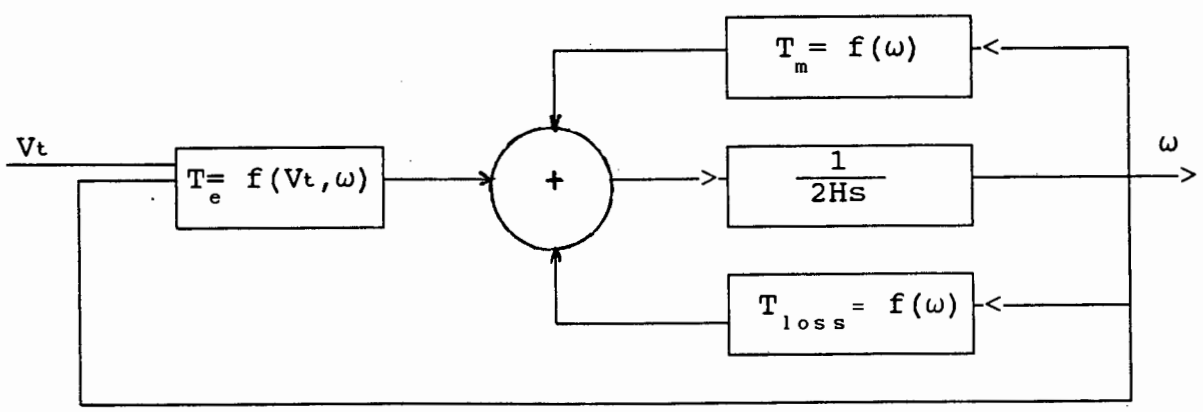

Figure 3.10:
The complete dynamic model of the induction motor

3.5 CASE STUDIES

In the following sections, case studies will be performed to determine the effects of different load models on the transient stability results. The ninebus benchmark network of figure 2.4 is used. The network parameters are listed in appendix 1.

The generators in the network are represented with the least complex model (model 0.0, see table 2.1 chapter). The least complex model is chosen in the case studies, because only the effects of the load on the transient stability will be investigated. The use of more complex generator models is not preferred because the accurate response of the generators is not of concern. The main focus of each case study is listed in table 3.1. In all case studies, the effect of the model on the transient stability results are investigated.

Table 3.1 : Main focus of each case study

CASE NUMBER	LOAD MODEL	DESCRIPTION
CASE 3.1	Y= constant I= constant P= constant	compare the transient stability results
CASE 3.2	P= constant Y= constant	local load modeled differently (other loads Y= constant)
CASE 3.3	P= constant Y= constant	local load modeled differently (other loads P= constant)
CASE 3.4	frequency & voltage	voltage and frequency dependent load models used
CASE 3.5	Y= constant I= constant P= constant	compare transient stability results. Fault location changed
CASE 3.6	P= constant Y= constant	remote load modeled differently
CASE 3.7	"complex model"	% composition of large motor in the load
CASE 3.8	steady-state and transient	compare transient stability results

CASE 3.1

In this case study, the effects of modeling all the loads as constant power, constant current and constant admittance respectively, on the transient stability results, are investigated.

Table 3.2 shows the conditions of the simulation for case 3.1. A three-phase fault is applied on the transmission line between buses 5 and 7, very close to bus 7. The fault is cleared by opening both breakers at the two ends of the transmission line.

Table 3.2: Simulation conditions - Case 3.1

generator model	model 0.0 : only H and x'_d specified
load model	all loads (1) Y = constant (2) I = constant (3) P = constant
type of fault	three-phase
position of fault	on branch 5,7 near bus 7
start time	t = 0 sec
clearing time	t = 0.11 sec
breaker operation	branch 5,7 tripped (both CB's)
simulation time	2 seconds

Figure 3.11 and 3.12 show the absolute and relative rotor angle plots respectively, for loads represented as constant admittances. In figure 3.11, the rotor angles of all three machines increases immediately after the fault was applied. The rotor angle of machine 1 however, increases at a comparatively slower rate because of the large inertia of this machine.

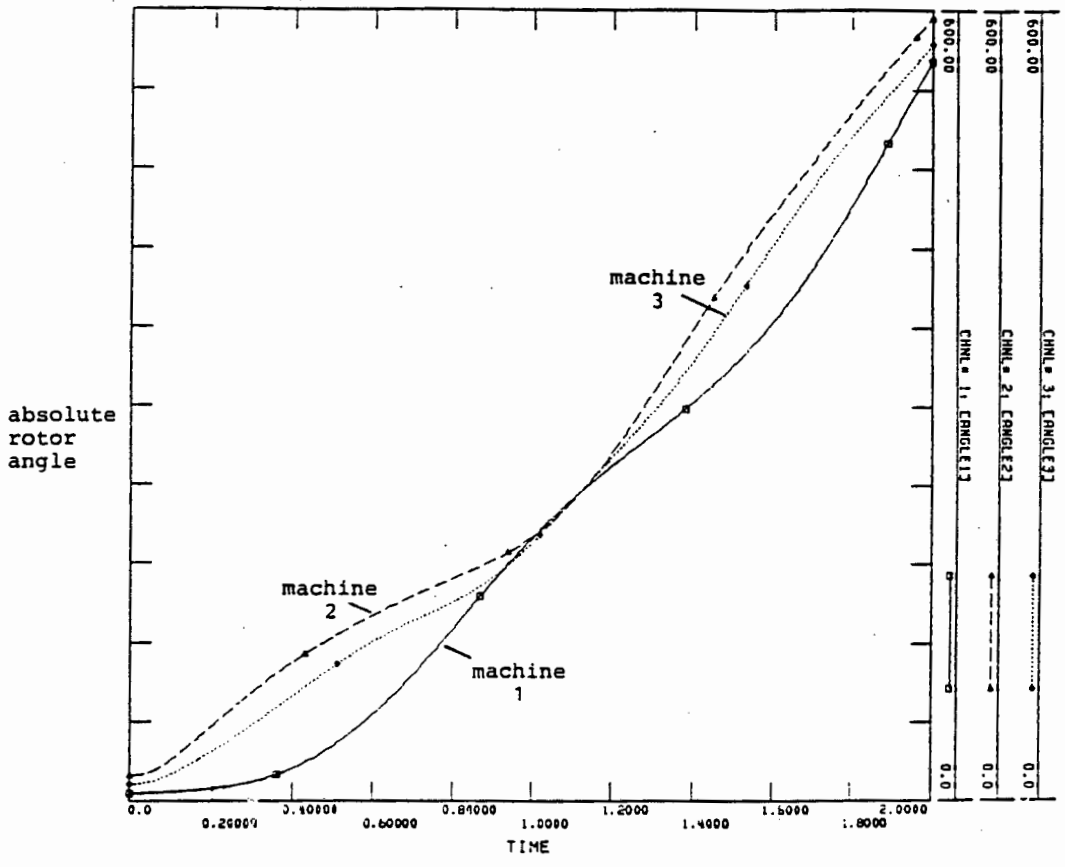

Figure 3.11 :
Absolute rotor angles; Y = constant

The machines swing together and reach approximately 600 degrees within 2 seconds. Figure 3.12 shows that there are two swings after 2 seconds. The relative rotor angle between machines 2 and 3 with respect to 1 remains below 90 degrees, thus the results indicate a transiently stable system. The relative angle between machine 2 and 1 is greater than that of machine 3 and 1 because the fault occurs very close to machine 2. There is also a larger difference between the electrical and mechanical power (for machine 2) immediately after the fault was applied, as compared to the other machines..

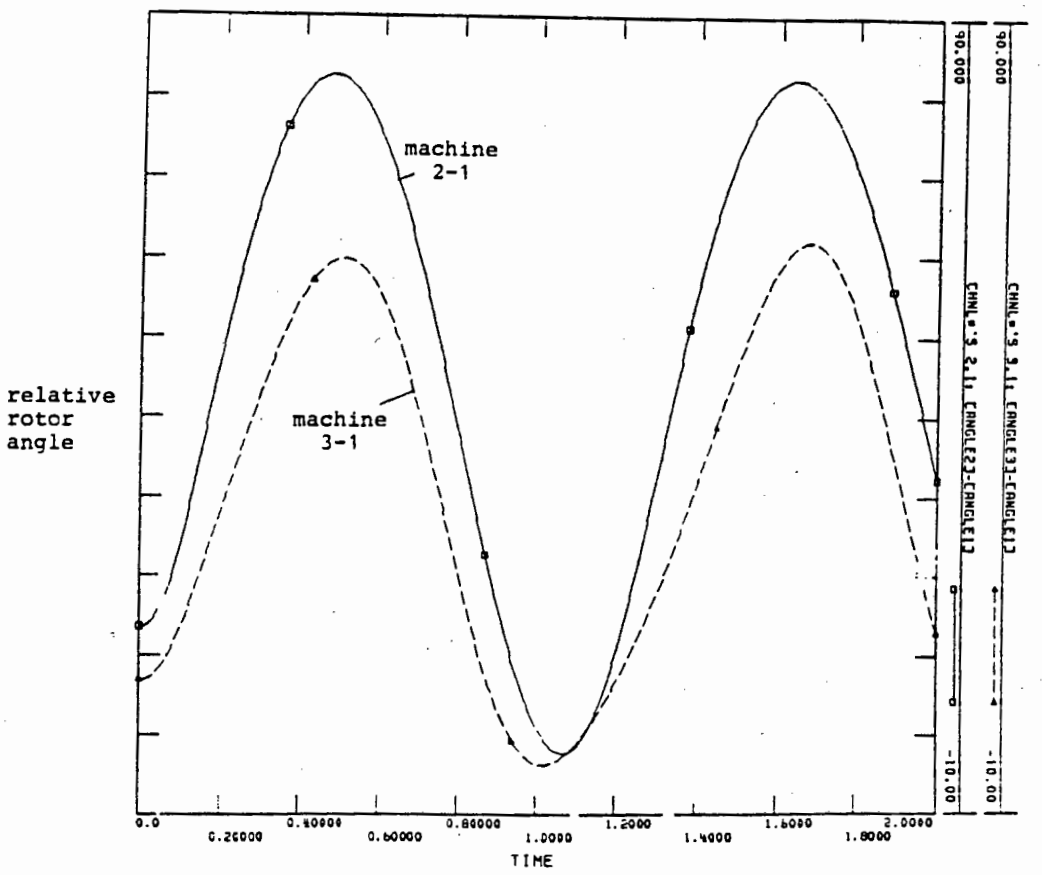

Figure 3.12 :
Relative rotor angles; Y = constant

Figures 3.13 and 3.14 show the absolute and relative rotor angle plots respectively for loads represented as constant current. In figure 3.13, the rotor angles increases up to approximately 500 degrees within 2 seconds. This is different from constant admittance modeling where the rotor angles increased up to approximately 600 degrees.

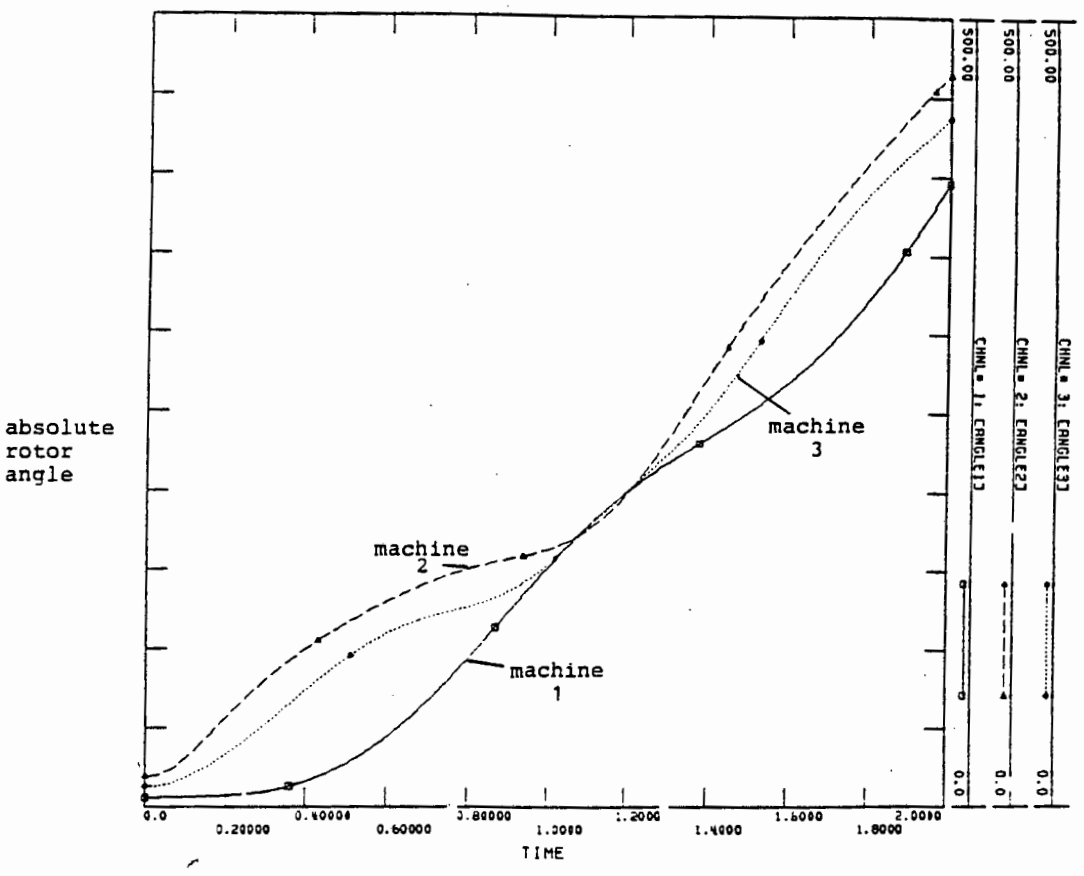

Figure 3.13 :
absolute rotor angles; I = constant

Figure 3.14 shows the relative rotor angles between machines 2 and 3 with respect to machine 1. There are also two swings within 2 seconds and the maximum angle reached is 89 degrees at t= 500 milliseconds. This result shows a marginally stable case. Comparing figure 3.14 with figure 3.12, it becomes apparent that modeling the load as constant current produces pessimistic (conservative) results as compared to those produced by modeling the load as constant admittance. This is because the relative rotor angle difference between machines 2 and 3, with respect to machine 1, is greater than when all the loads are modeled as constant current.

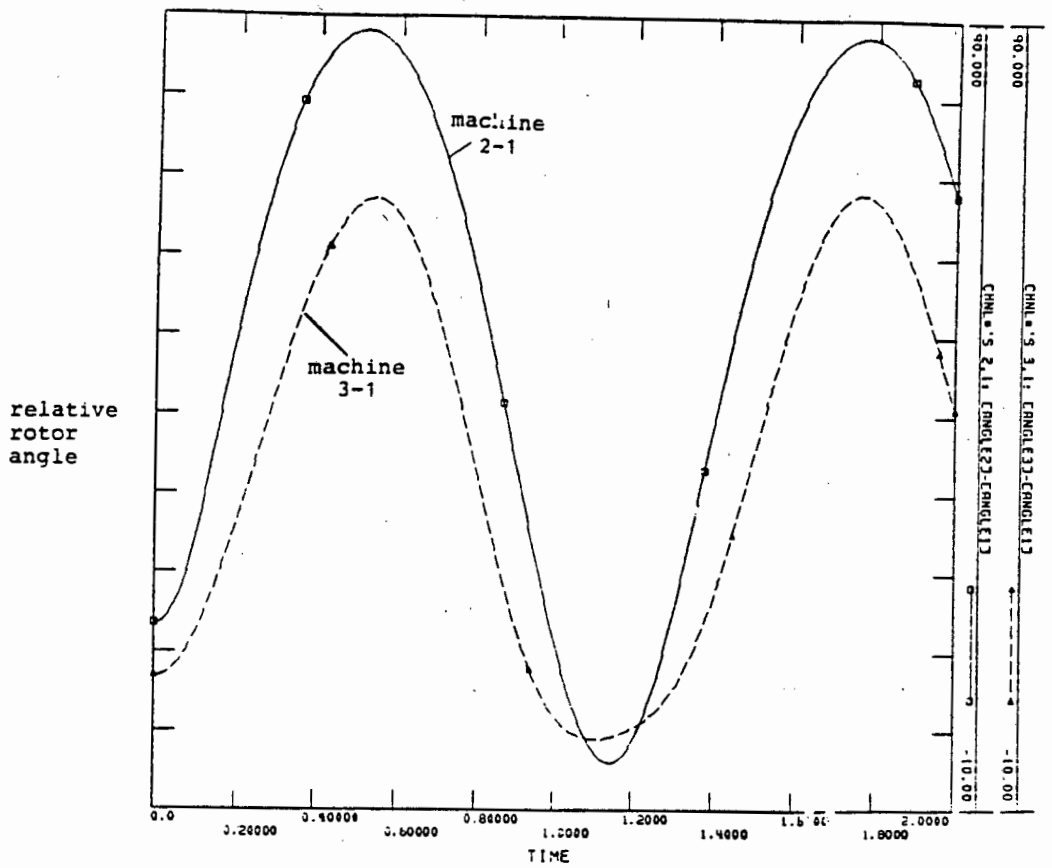

Figure 3.14 :
Relative rotor angles; I = constant

Figures 3.15 and 3.16 show the absolute and relative rotor angles when the loads are modeled as constant power respectively. In figure 3.15, machines 2 and 3 swing with each other but are out of step with machine 1. The results show that the system will be unstable when the loads are modeled as constant power. After 2 seconds, the absolute rotor angles of machines 2 and 3 are approximately 1000 degrees while for machine 1, the rotor angle is approximately 330 degrees.

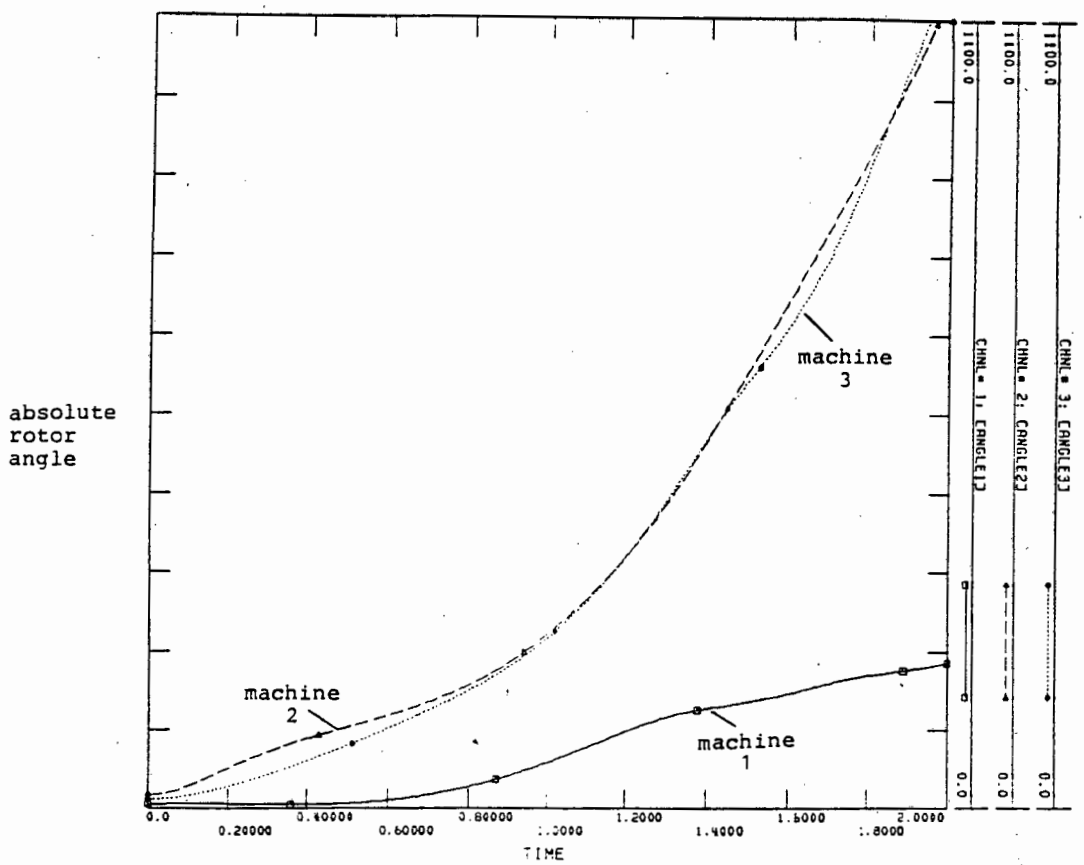

Figure 3.15 :
Absolute rotor angles; P = constant

Figure 3.16 also shows this unstable result. There are no swings of the relative rotor angles. The relative rotor angles of machines 2 and 3 with respect to machine 1 increases without bound. The results produced by modeling the loads as constant power thus are more pessimistic than when either constant current or constant admittance models are used.

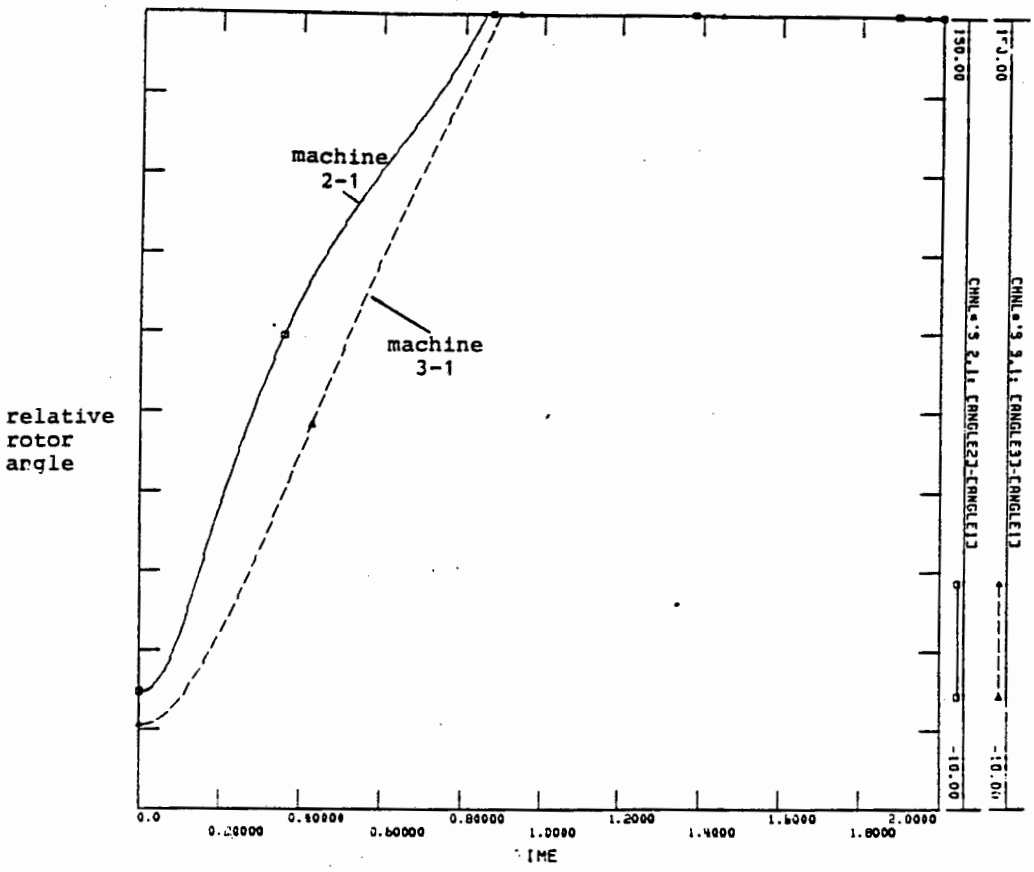

Figure 3.16 :
Relative rotor angles; P = constant

Figure 3.17 shows the effect of different load models on the transient behavior of machine 1. The rotor angle deviation of machine 1 is the largest when the loads are modeled as constant admittance. This means that this machine has the largest acceleration power, hence, it is able to swing with the machine close to the fault (machine 2). For constant power load modeling, the rotor angle of machine 1 has the least acceleration power hence, it goes out-of-step with machine 2.

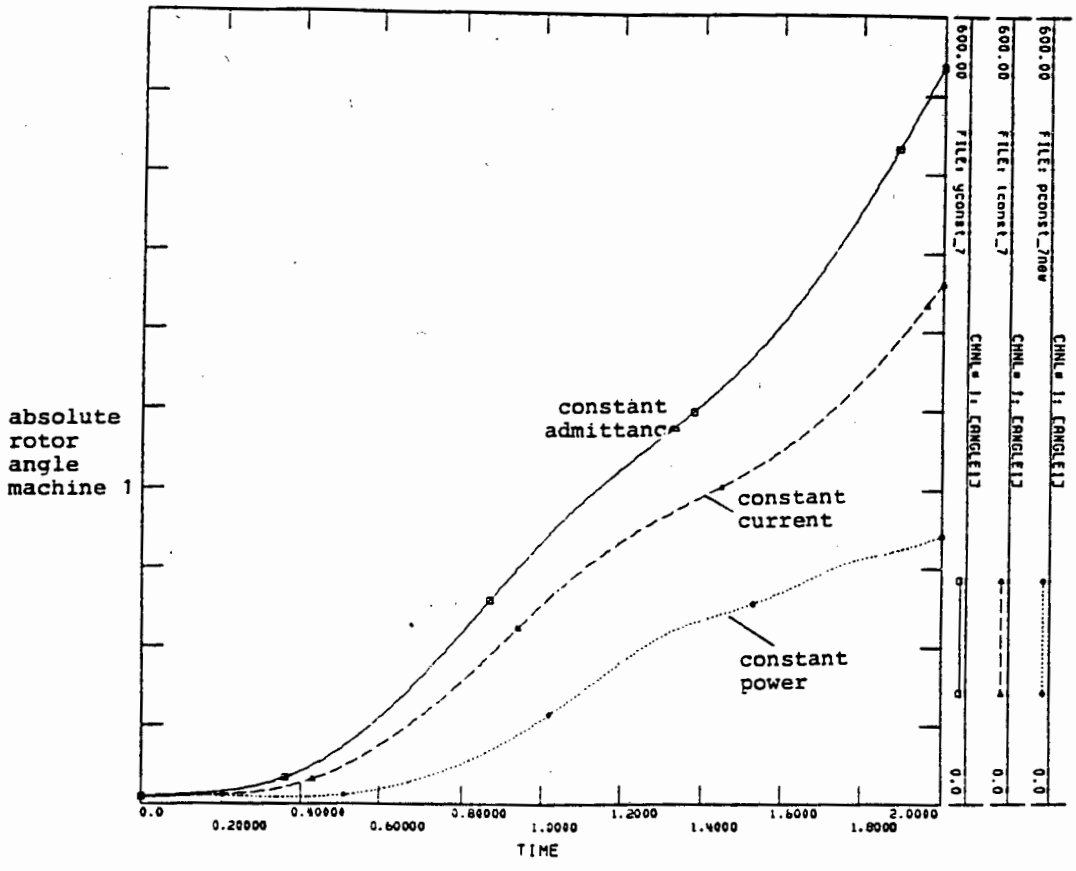

Figure 3.17 :
Effects of different load model on machine 1's behavior

A comparison of the transient stability results produced by these three different load models is shown in figure 3.18. From this figure, it is apparent that modeling the load as constant power , produces pessimistic transient stability results, while modeling the same loads as constant admittance produces optimistic results. The results produced by modeling the load as constant current lie between the results obtained by modeling the load as constant power and constant admittance.

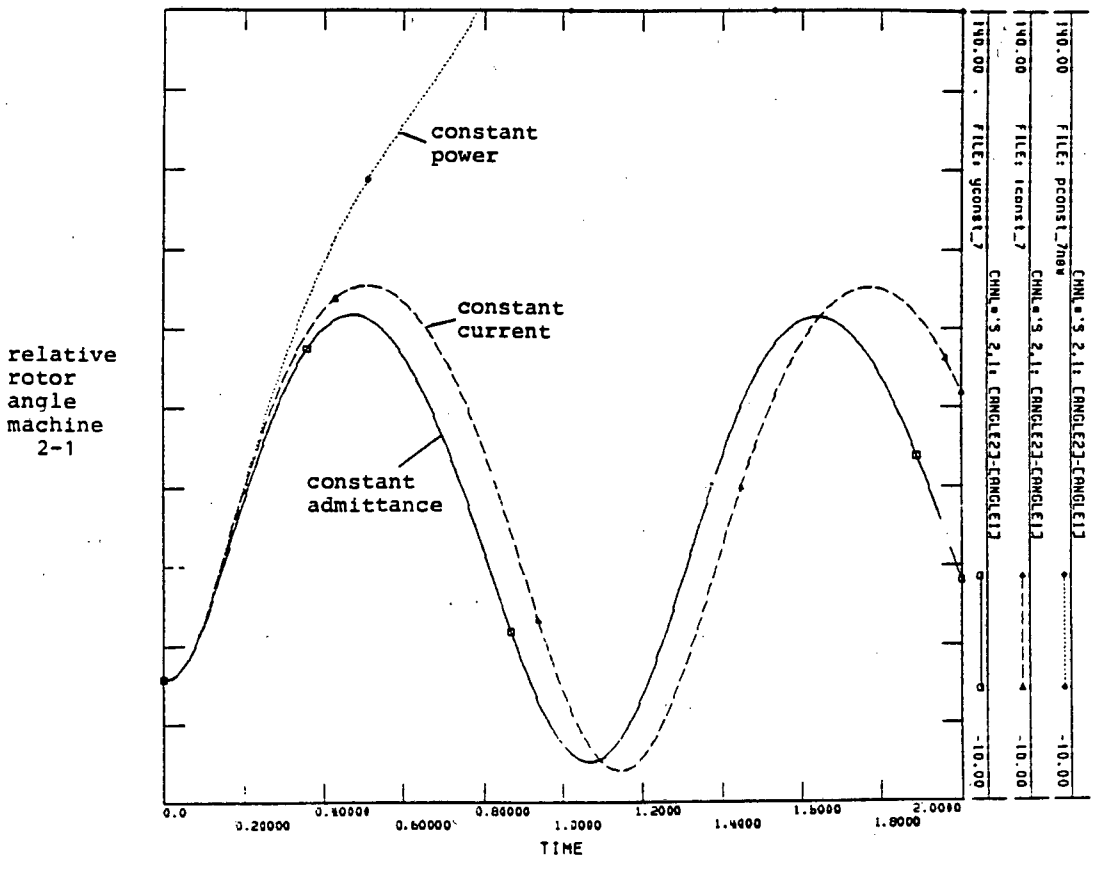

Figure 3.18 :
Comparison of the transient stability results obtained by using different static load models.

CASE 3.2

In this case study, the load at bus 8, which is local to generator 2, is modeled as constant power and the loads at busses 5 and 6 are modeled as constant admittance. Since the fault is close to generator 2, the results obtained by modeling this load as constant power will be compared to those obtained by modeling the load as constant admittance.

The simulation conditions for this case are listed in table 3.3 below:

Table 3.3: Simulation conditions -case 3.2

generator model	model 0.0 : only H and x'_d specified
load model	load at bus 8 P = constant load at bus 6 Y = constant load at bus 5 Y = constant
type of fault	three-phase
position of fault	on branch 5,7 near bus 7
start time	t = 0 sec
clearing time	t = 0.11 sec
breaker operation	branch 5,7 tripped (both CB's)
simulation time	2 seconds

Figure 3.12 showed the relative rotor angle for machines 2 and 3 with respect to machine 1, when all the loads (including the load at bus 8), were modeled as constant admittance. The results are repeated in figure 3.19.

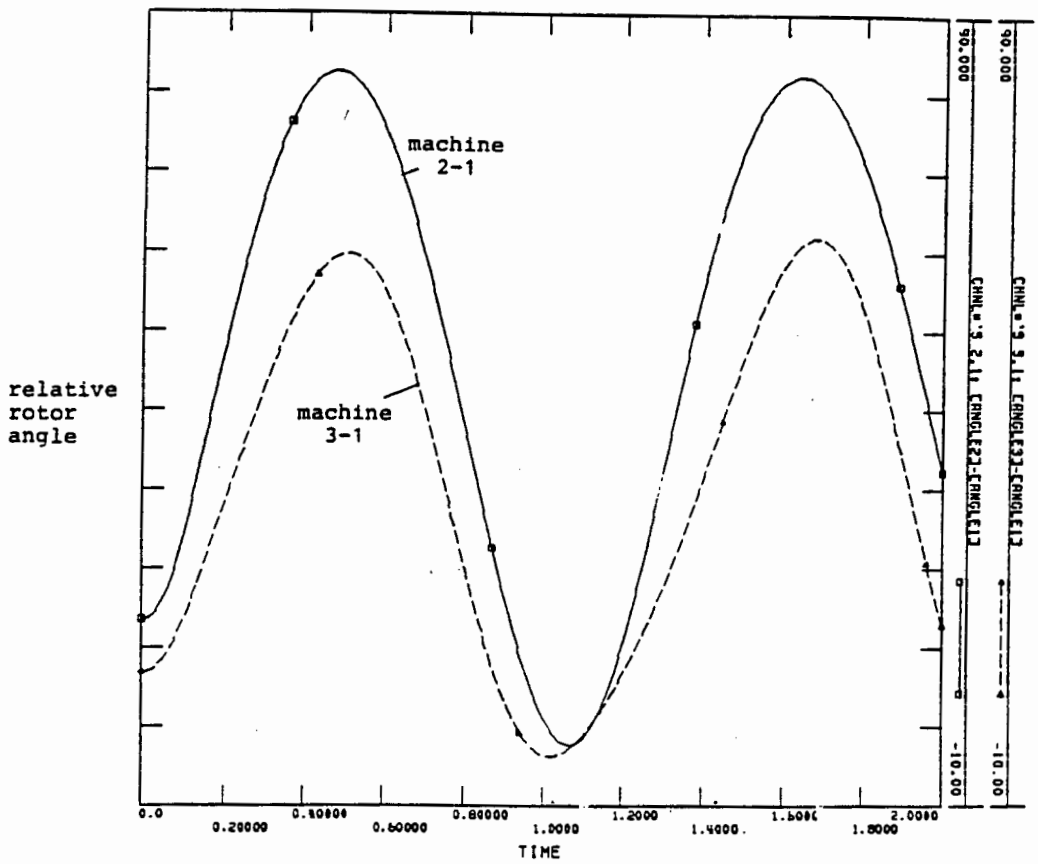

Figure 3.19 :
Relative rotor angles; Y = constant

Figure 3.20 shows the relative rotor angle for machines 3 and 2 with respect to machine 1 for case 3.2. The relative rotor angle between machines 2 and 1 reached a maximum of 80 degrees at t = 0.46 seconds. The results show a transiently stable system. The absolute rotor angles are shown in figure 3.21. In figure 3.21, the rotor angle of these machines reach a value of approximately 450 degrees within 2 seconds.

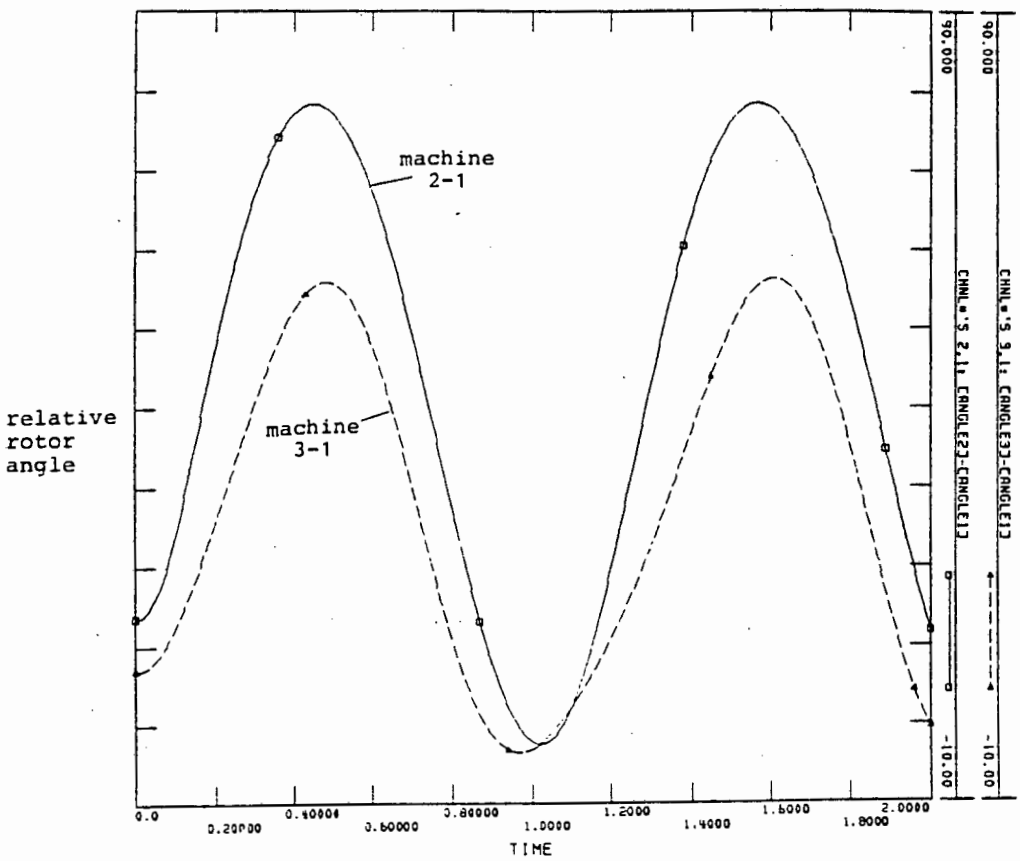

Figure 3.20 :
Relative rotor angles; local load P = constant

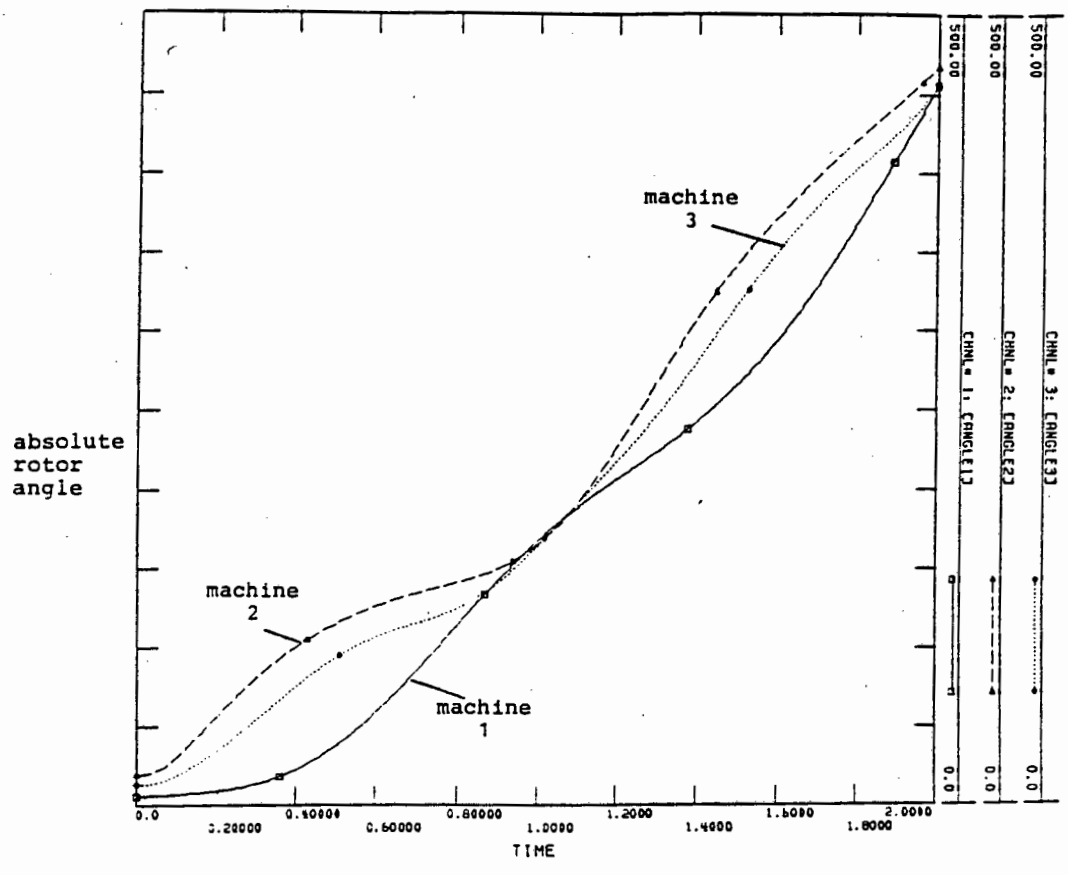

Figure 3.21 :
Absolute rotor angles; local load P = constant,

Figure 3.22 shows a comparison of the transient stability results produced by modeling the local load at bus 8 as constant admittance and as constant power. From
this figure, it is apparent that modeling the local load as constant power, gives optimistic results while modeling it as constant admittance gives conservative results.

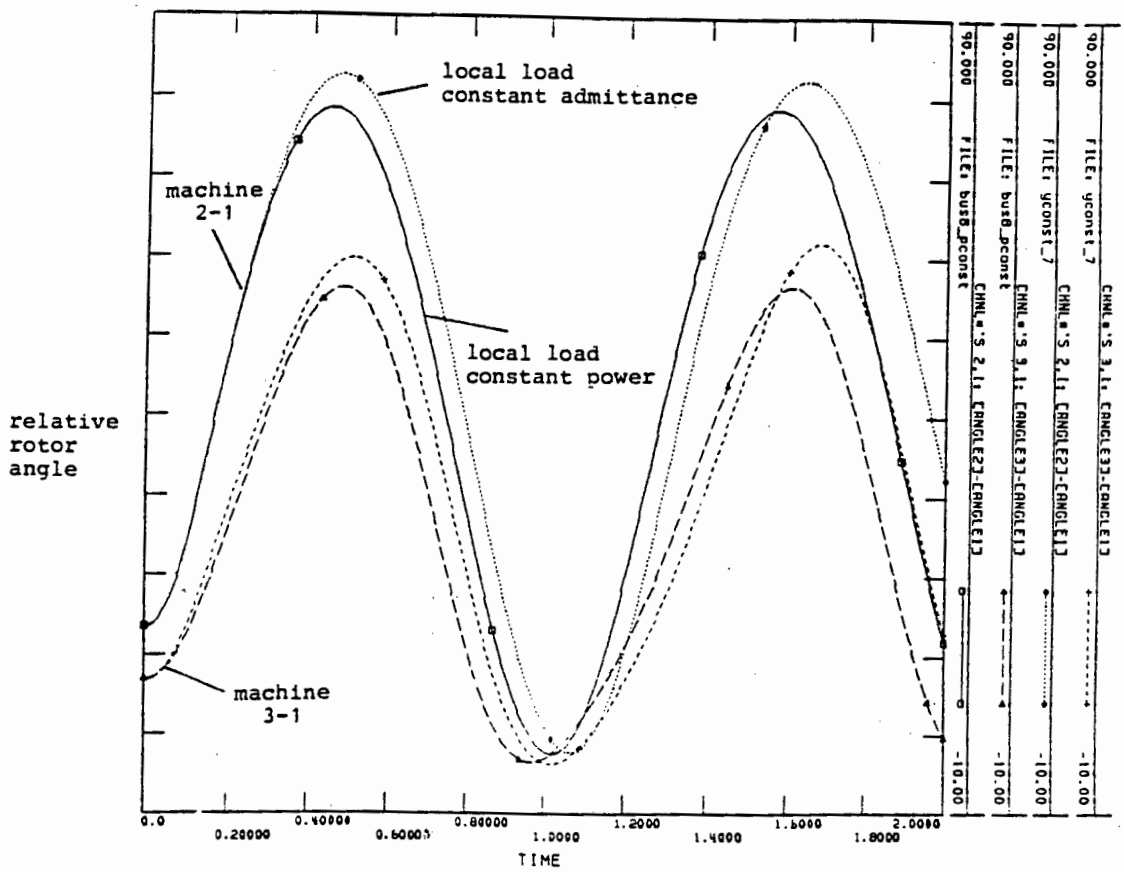

Figure 3.22:
Comparison; local load P = constant and Y = constant

The difference between the relative rotor angle amplitude of these two different load models is about 4 degrees. This angular difference is small and could be regarded as insignificant when the system is far from the transient stability limit. When the system is operating near the transient stability limit, however, this angular difference can make a difference in the interpretation of the results. False conclusions may be drawn regarding the system stability.

CASE 3.3

In this case, the local load at bus 8 is modeled as constant admittance and the remaining loads at buses 5 and 6 (see appendix 1) are modeled as constant power. The results of this case will be compared to those produced when all the loads are modeled as constant power. The simulation conditions for this case are listed table 3.4.

Table 3.4: Simulation conditions - case 3.3

generator model	model 0.0 : only H and x'_d specified
load model	load at bus 8 Y = constant load at bus 6 P = constant load at bus 5 P = constant
type of fault	three-phase
position of fault	on branch 5,7 near bus 7
start time	t = 0 sec
clearing time	t = 0.03 sec
breaker operation	branch 5,7 tripped (both CB's)
simulation time	2 seconds

The results are shown in figure 3.23. Modeling the local load as constant admittance, gives conservative results while modeling the local load as constant power gives optimistic results. The results produced by modeling the local load as constant admittance shows an unstable system. On the contrary, the results produced by modeling the load as constant power shows a marginally stable system.

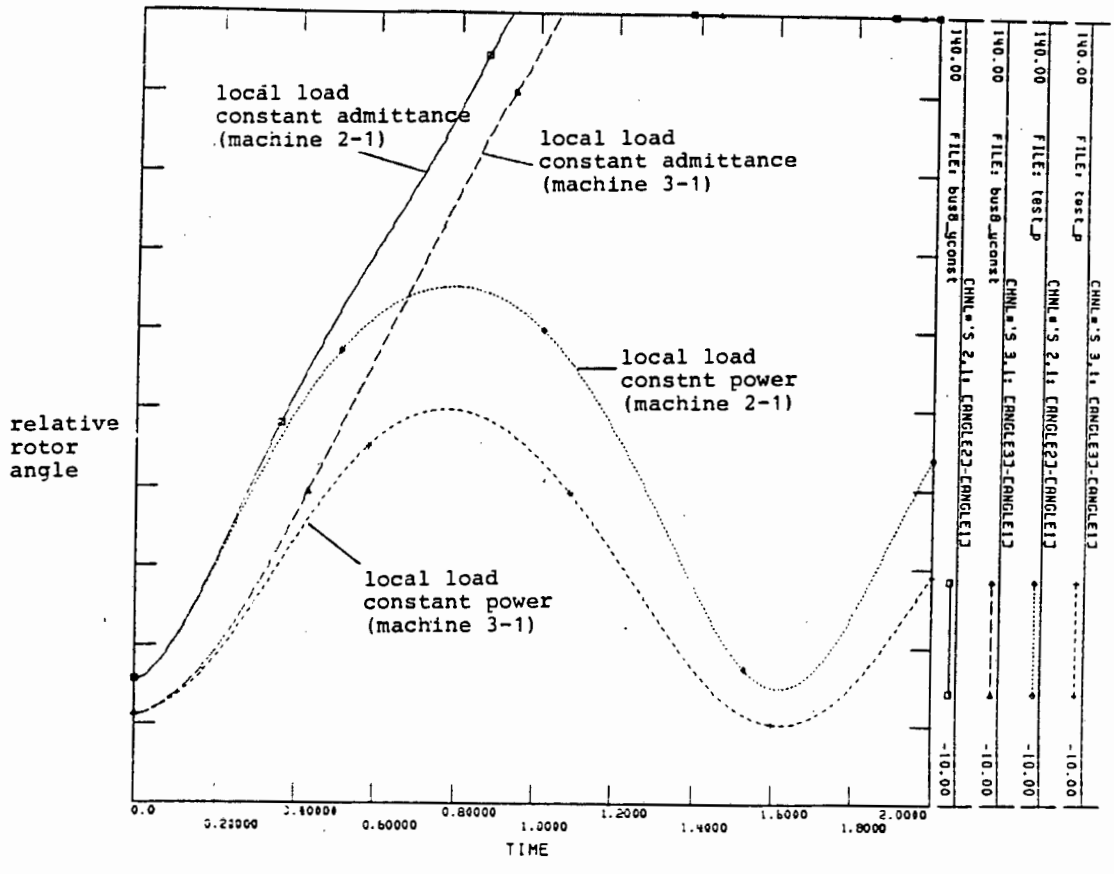

Figure 3.23:
Comparison; local load P = constant and Y = constant

It is apparent from this case study that accurate load modeling is very important because incorrect results could be deduced from the simulation studies. These results can affect some planning and operating practices, which are derived from computer modeling.

The above cases (3.2 and 3.3) have demonstrated that it is insufficient to make generalizations such as " modeling the power system loads as constant power produces pessimistic results while modeling the loads as constant admittance produces optimistic results ". The location of the load relative to the fault and generation should be taken into consideration when deciding what model to choose for the loads.

CASE 3.4

In this case study, the effects of the frequency sensitivity of the load on the transient stability results are investigated. Since the frequency dependency of the load contributes to the system damping, a load damping factor is introduced in the generator model. This damping factor has a typical value of 2 for loads such as centrifugal pumps and a value of 1 for loads such as large electric fans (ie loads whose torque is directly proportional to the speed of the motor).

The damping factor mentioned here is the factor D proportional to the speed in the swing equation (see equation 1.5, page 9). This factor represents the overall damping in the system. For example, the term can include the following :

(i) damping due to the damper windings
(ii) damping due to friction
(iii) damping due to the eddy currents in the rotor slots
(iv) damping due to the loads.

Studies in the past have indicated that the frequency dependency of the load, can be simulated by using a typical damping factor of 2 in the generator equations as a compensation factor. When this damping factor is used, only the voltage dependent load model used are used.

The simulation conditions for this case are listed in table 3.5.

Table 3.5: Simulation conditions - case 3.4

generator model	model 0.0 : only H and x'_d specified load damping factor = 2
load model	all loads are Y = constant
type of fault	three-phase
position of fault	on branch 5,7 near bus 7
start time	t = 0 sec
clearing time	t = 0.11 seconds
breaker operation	branch 5,7 tripped (both CB's)
simulation time	2 seconds

Figure 3.24 shows a comparison of the transient stability results when the damping is modeled and when it is not modeled. When damping is represented, the amplitude of the relative rotor angle is reduced. The amplitude of the second swing is lower than the first swing. Note that when damping is not represented, the amplitude of the relative rotor angle remains constant.

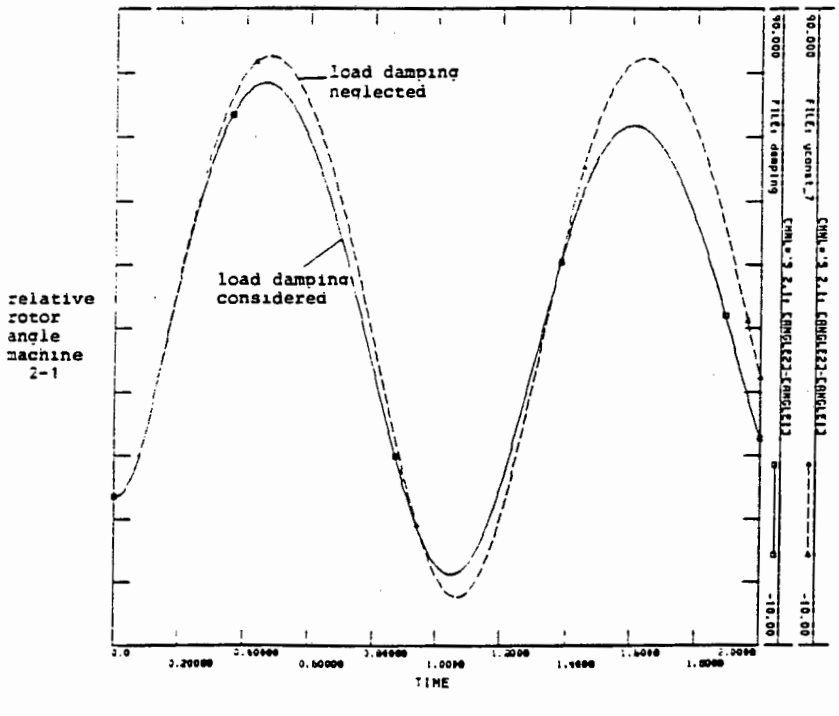

Figure 3.24 :
Transient stability results with and without load damping

Figures 3.25 and 3.26 show the phase portrait of the relative speed versus relative angle for the simulation without load damping and with load damping respectively. In figure 3.25, the portrait circles at a constant amplitude, immediately after the fault is cleared. Figure 3.26 shows that when damping is represented, the portrait circles inward. The amplitude of the relative rotor angle and the speed decrease.

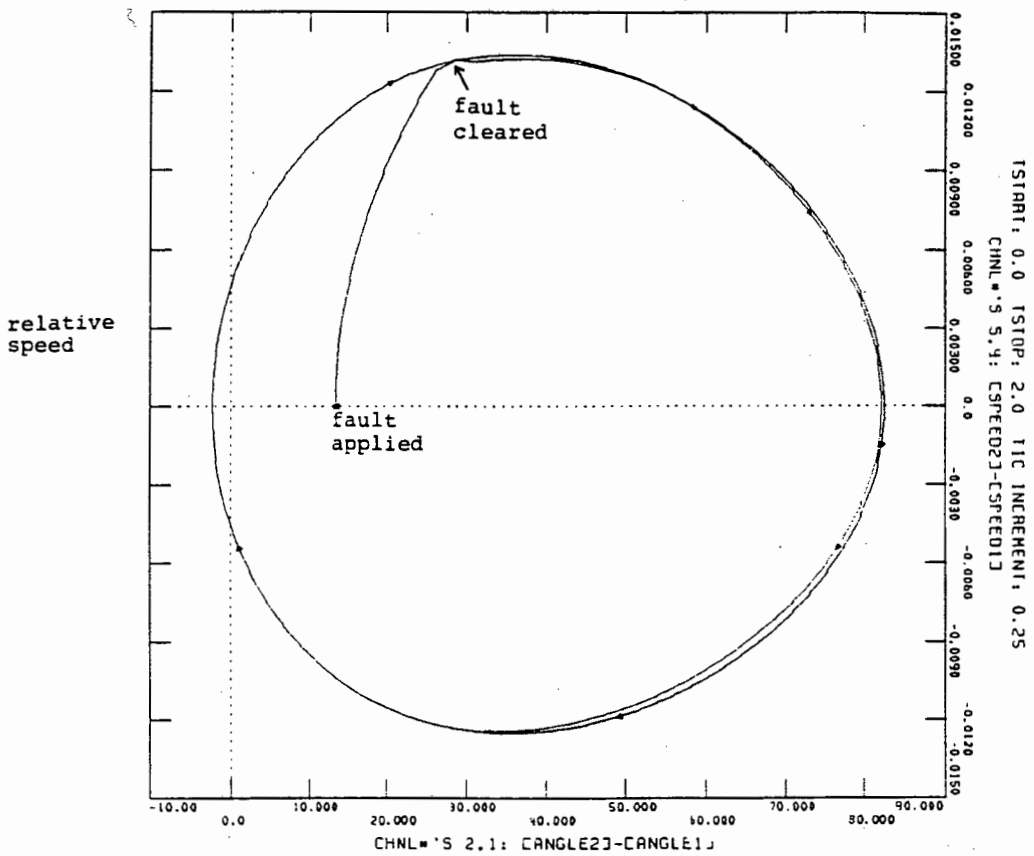

Figure 3.25 :
Phase portrait with damping neglected

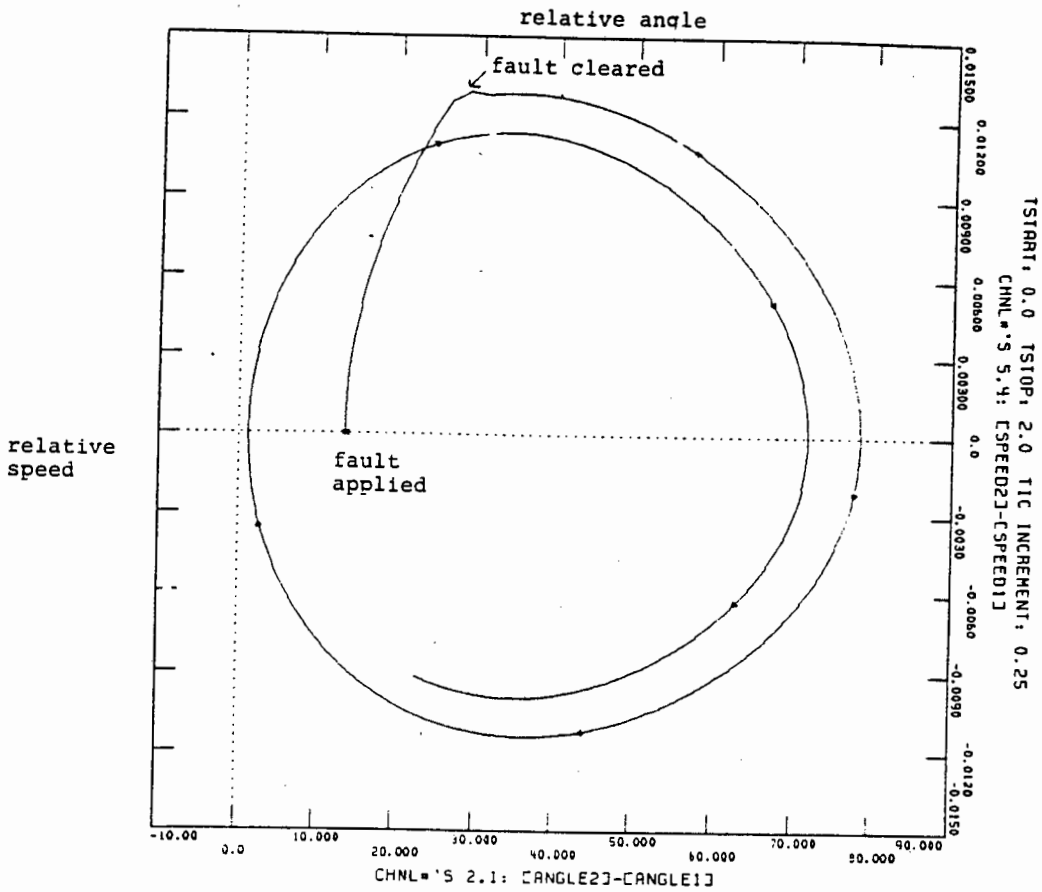

Figure 3.26 :
Phase portrait with damping represented

In order to observe the effects of damping on the system stability, it is necessary to extend the simulation time. Figure 3.27 shows the relative rotor angle for machine 2 and 3 with respect to machine 1, **for a simulation time of 20 seconds.** The results show that the system is stable. The relative rotor angle oscillations decay exponentially until the new stable operating point is reached.

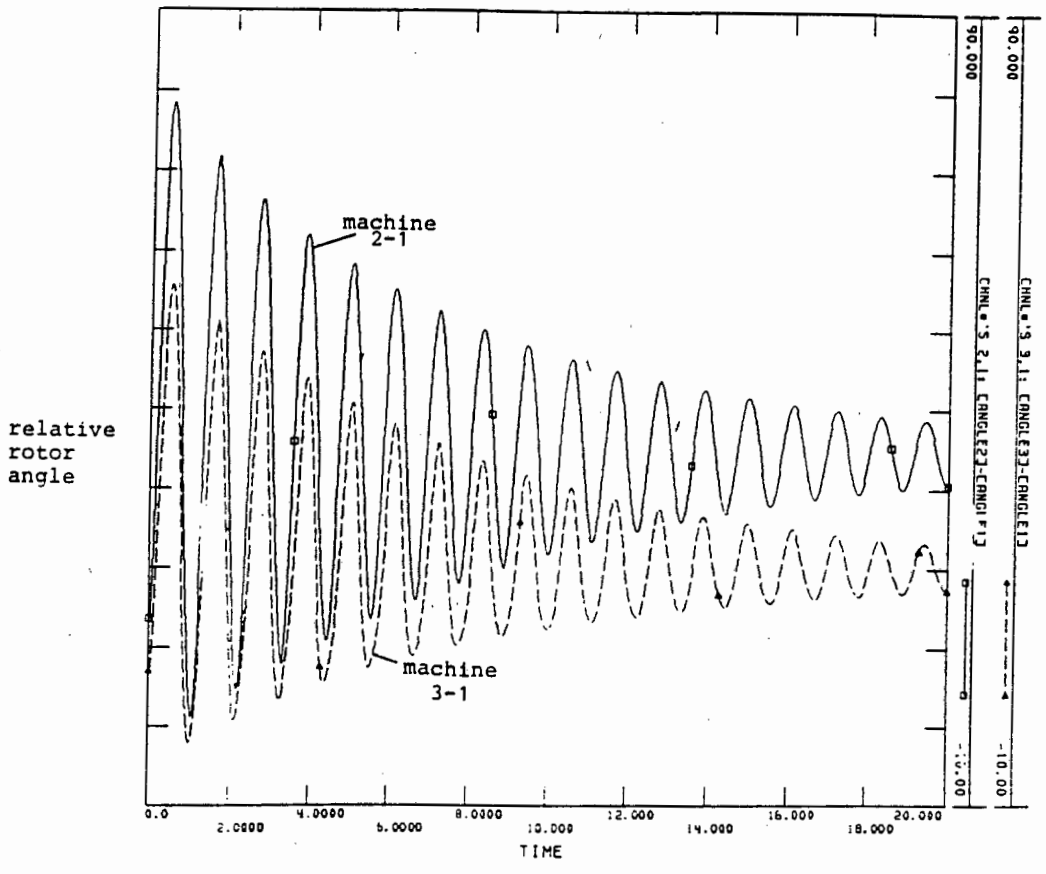

Figure 3.27 :
Frequency sensitivity of the load

Figure 3.28a shows a phase portrait of the relative rotor angle versus the relative speed of machine 2. The phase portrait starts at a pre-fault stable operating point. The speed increases rapidly during the fault. After the fault is cleared at t = 110 milliseconds, the portrait circles inwards showing a stable system.

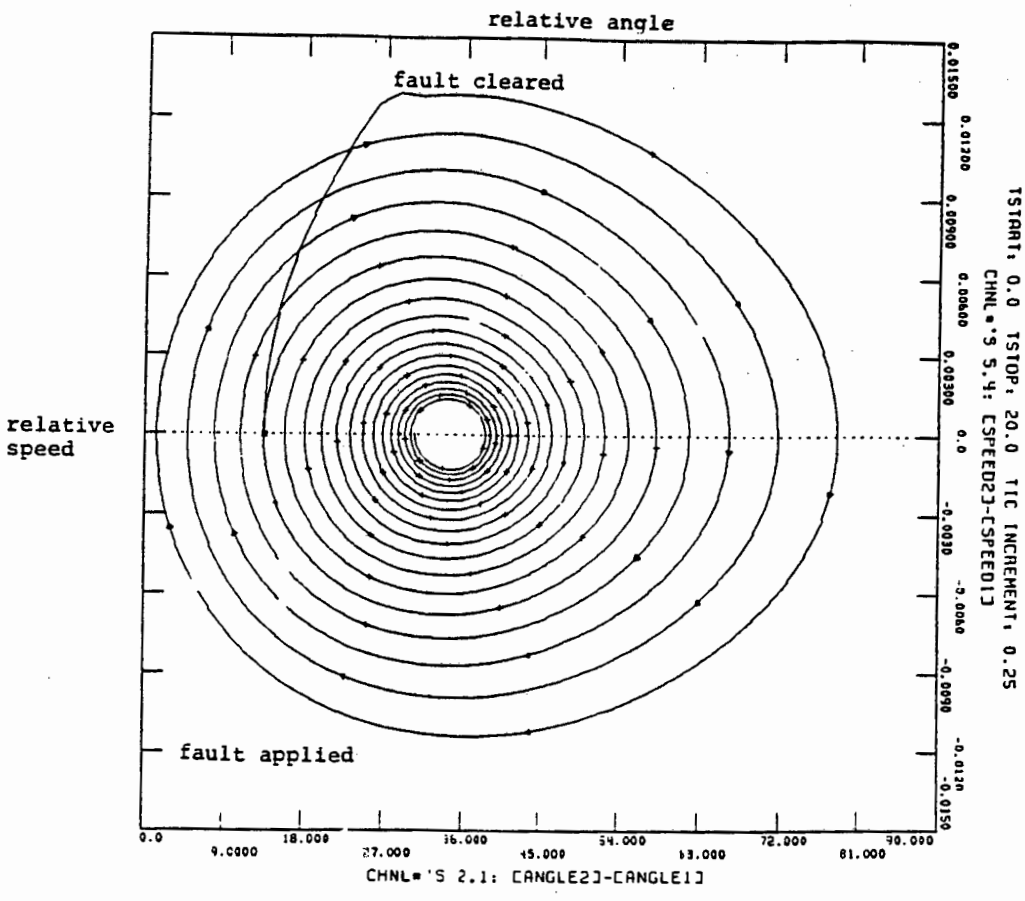

Figure 3.28a :
Phase portrait of relative angle
versus relative speed

Another approach of investigating the frequency sensitivity of the load, is to introduce a load model which varies with frequency. This approach is different from the previous one because it does not assume the actual dynamic load being modeled and thus no damping factor is introduced in the generator. The simulation conditions are shown in table 3.6.

Table 3.6 : Simulation conditions - load frequency model

generator model	model 0.0 : only H and x'_d specified
load model	all loads I = constant load frequency model (LOADF) included
type of fault	three-phase
position of fault	on branch 5,7 near bus 7
start time	t = 0 sec
clearing time	t = 0.11 sec
breaker operation	branch 5,7 tripped (both CB's)
simulation time	20 seconds

Figure 3.28b shows a plot of the relative angle of machine 2 and machine 3 with respect to machine 1. Once again, it is evident that the frequency behavior of the load only contributes to the system damping.

It is common practice to neglect the frequency dependency of the load in transient stability studies. This is because they contribute only to the system damping. When they are neglected, the results become pessimistic thus providing enough stability margin.

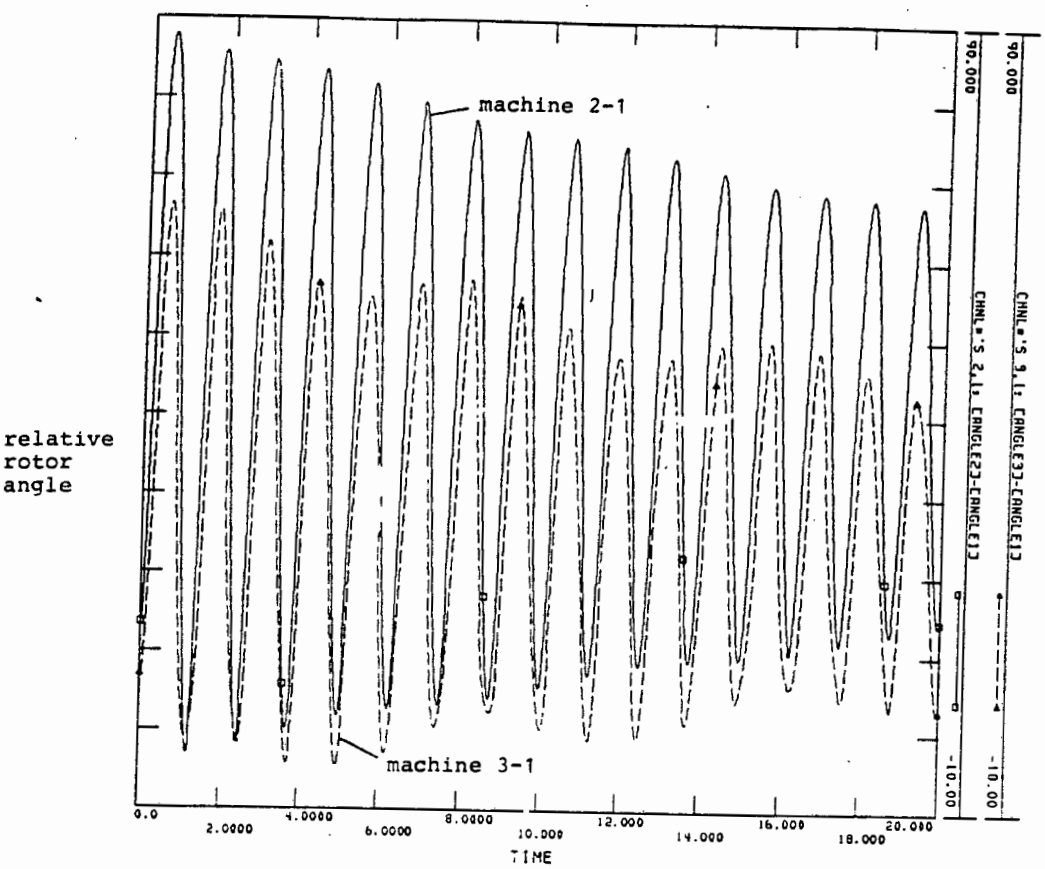

Figure 3.28b :
Frequency dependency of the load

CASE 3.5

In this case study, the location of the fault is changed. The fault is simulated on the transmission line between busses 6 and 9, near bus 9. Different static load models are used once more, to determine their effects on the transient stability limit.

The simulation conditions for this case are listed in table 3.7.

Table 3.7: Simulation conditions - case 3.5

generator model	model 0.0 : only H and x'_d specified
load model	all loads (1) Y = constant (2) I = constant (3) P = constant
type of fault	three-phase
position of fault	on branch 6,9 near bus 9
start time	t = 0 sec
clearing time	t = 0.18 sec
breaker operation	branch 6,9 tripped (both CB's)
simulation time	2 seconds

Figure 3.29 shows the relative rotor angle between machines 2 and machine 1 for different load models. Once more, **the transient stability results produced by modeling the load as constant power are more pessimistic than those produced by modeling the load as constant admittance or constant current.** In this figure, the result obtained by constant admittance modeling show a stable system, while those obtained by constant power modeling, show an unstable system.

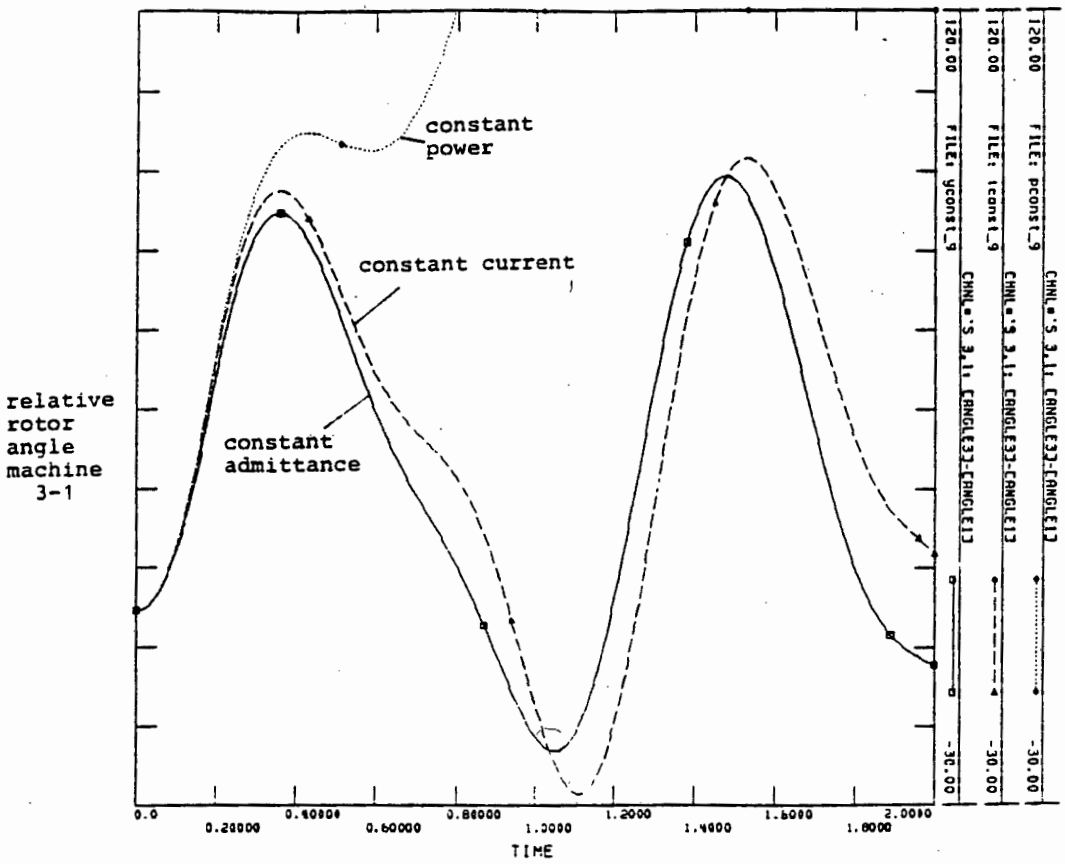

Figure 3.29 :
Comparison of the transient stability results
obtained by using different static load models

CASE 3.6

In this case the load at bus 6, which is remote from machine 3 (considering that the branch linking this load to machine 2 will be opened) is modeled as constant power and the other loads at buses 5 and 8 are modeled as constant admittances. A comparison will be made with the results obtained by modeling all the loads as constant admittances. The simulation conditions for this case are listed in table 3.8:

Table 3.8: Simulation conditions - case 3.6

generator model	model 0.0 : only H and x'_d specified
load model	load at bus 8 Y = constant load at bus 6 P = constant load at bus 5 Y = constant
type of fault	three-phase
position of fault	on branch 6,9 near bus 9
start time	t = 0 sec
clearing time	t = 0.18 seconds
breaker operation	branch 6,9 tripped (both CB's)
simulation time	2 seconds

A comparison of the results are shown in figure 3.30. Modeling the remote load as constant power gives conservative results while modeling it as constant admittance gives optimistic results.

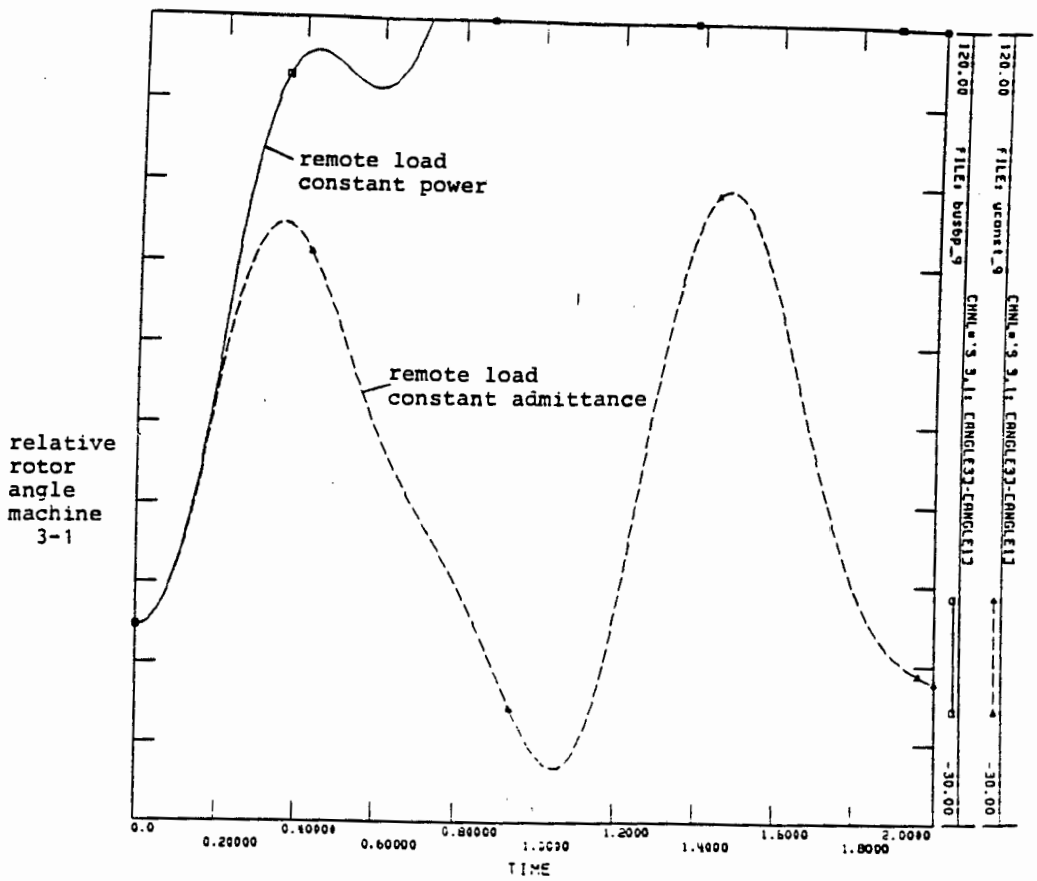

Figure 3.30 :
A comparison for different load models for a remote load

Cases 3.2 and 3.7 have indicated that when choosing a load model, the location of the load relative to the faulted generator must be considered.

The difference in the results produced by different static load models is small (less than 10 % for the previous case studies). When the power system is operating far from the transient stability limit, the choice of the load model is not critical. However, in the case where the system is operating near the transient stability limit, the choice of the load model is very critical because the simulation can give stable results for an otherwise unstable system.

CASE 3.7

In this case, the load at bus 5 (see appendix 1) will be modeled as a complex load. This complex load model represents the static and the dynamic behavior of the load. The structure of the load model is shown in figure 3.31. The load at bus 5 is broken into six different types namely: large motors, small motors, discharge lighting, transformer saturation, constant power and user defined static load model.

In this case, the objective is to investigate the dynamic behavior of large induction motors and their effects on the system transient stability. The type of modeling used is the second approach discussed in section 3.4.2.2. Only the percentage composition of large induction motors and constant power load, will be varied.

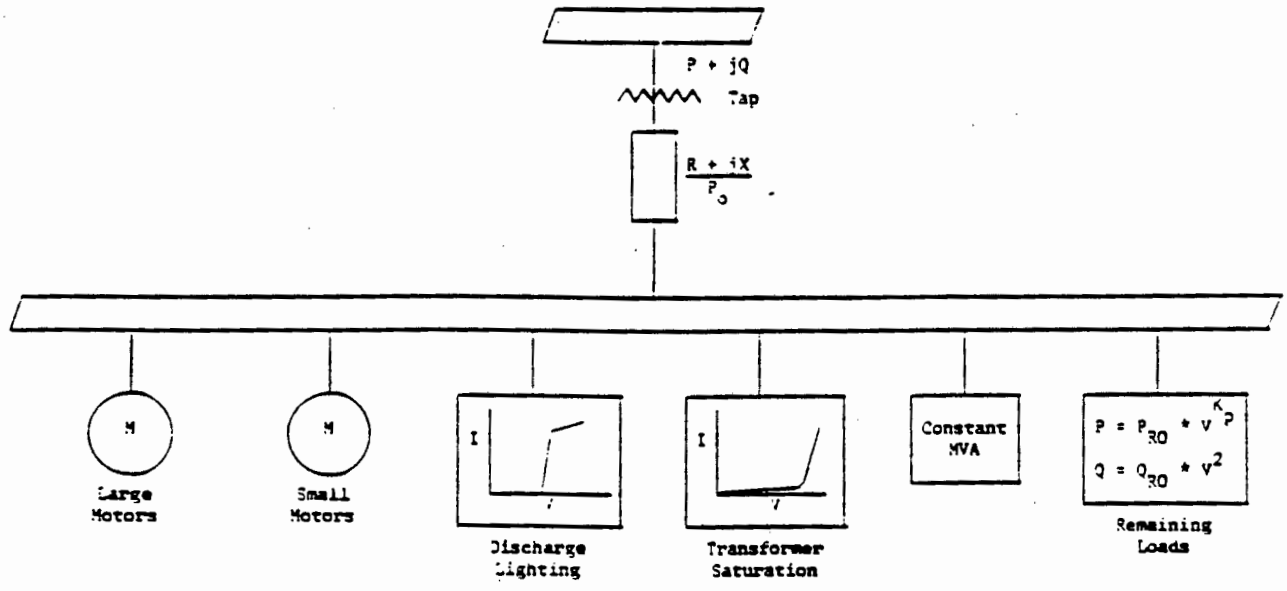

Figure 3.31:
Structure of the complex load model

The simulation conditions for this case are listed in table 3.9.

Table 3.9 : Simulation conditions - case 3.7

generator model	model 0.0 : only H and x'_d specified
load model	load at bus 5 complex loads at buses 6 and 8 are modeled as P = constant
type of fault	three-phase
position of fault	on branch 5,7 near bus 7
start time	t = 0 sec
clearing time	t = 0.08 sec
breaker operation	branch 4,5 tripped (both CB's)
simulation time	2 seconds

The load at bus 5 is varied as follows:

(i). 5 % Large Motors and 95 % Constant MVA load
(ii). 25 % Large Motors and 75 % Constant MVA load
(iii). 45 % Large Motors and 55 % Constant MVA load
(iv). 65 % Large Motors and 35 % Constant MVA load
(v). 85 % Large Motors and 15 % Constant MVA load

Figure 3.32 shows the active power consumption of the load at bus 5 for different load compositions listed above. During the fault, the active power consumption for 5% motor content drops from the initial value of 113 MW to 107 MW and remain constant at this value. After the fault is cleared, the active power consumption returns close to its initial value with only very small deviations.

For the 25% motor load content, the active power drops from 113 MW to 85 MW immediately after the fault occurs. The power consumption increases to 87 MW during the fault. After the fault is cleared, the power deviates by about 7 % from the original value, but this deviation is reduced with time.

For the other percentage content of large motors (45, 65 and 85%) the power consumption drops significantly, immediately after the

fault is applied. It then increases during the fault, with the largest percentage increase of 6 % for the 85 % large motor load content.

After the fault is cleared, the active power rises initially due to the rise in voltage, and then drops significantly. The higher the percentage content of large motors, the higher the drop in active power consumption. This is as a result of the increased dependency of the load to changes in voltage and frequency.

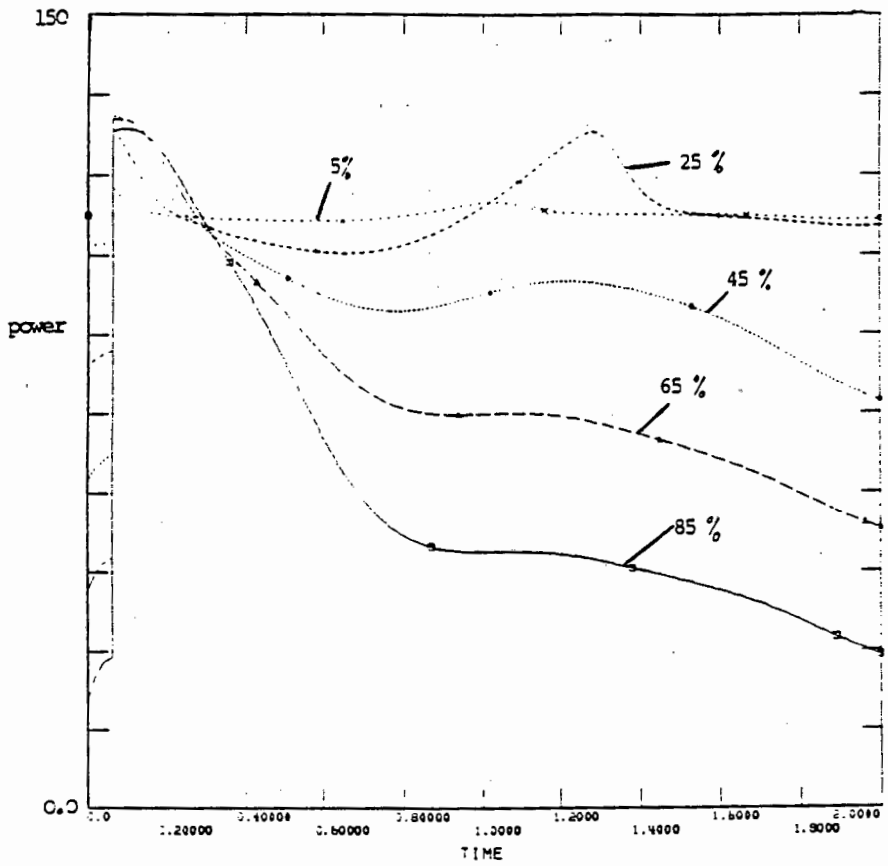

Figure 3.32:
Variation of active power consumption at bus 5 for different motor composition

Figure 3.33a and 3.33b shows the relative rotor angle of machine 2 and machine 3 with respect to machine 1 respectively. For the first swing, the amplitude of the relative angle between machines 1 and 2 is the largest when there is a highest percentage composition of large motors in the load.

On the contrary, the relative rotor angle amplitude is the lowest for small percentage composition of large motors.

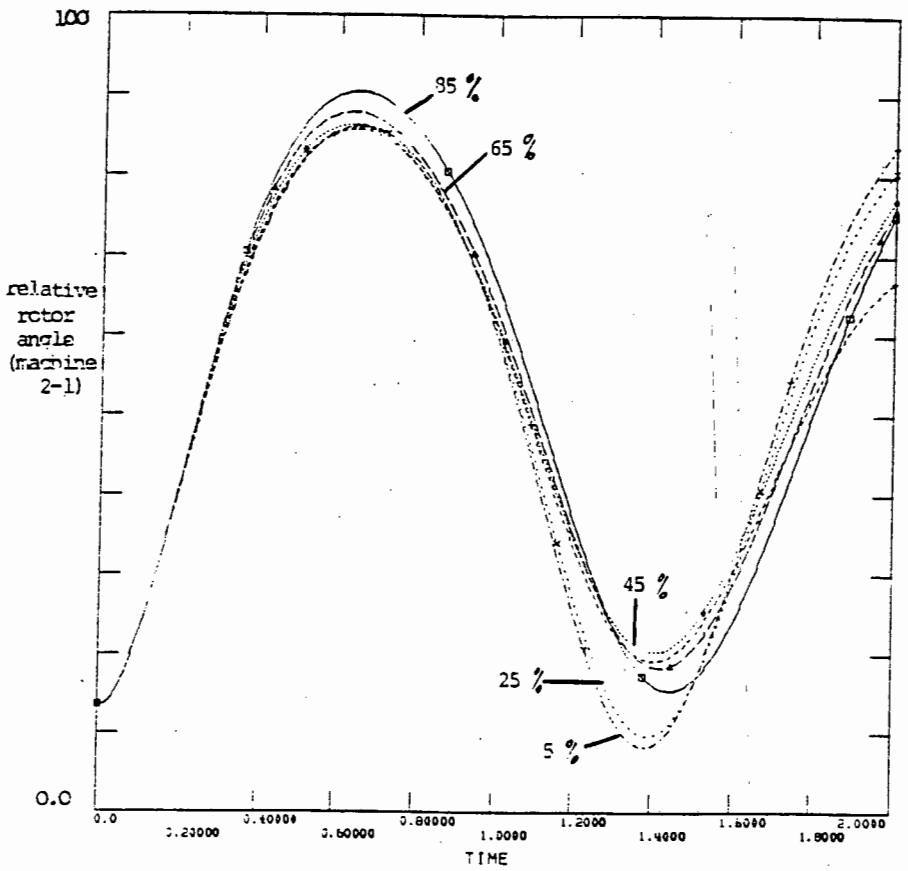

Figure 3.33a :
Relative rotor angle for machine 2 for different load compositions

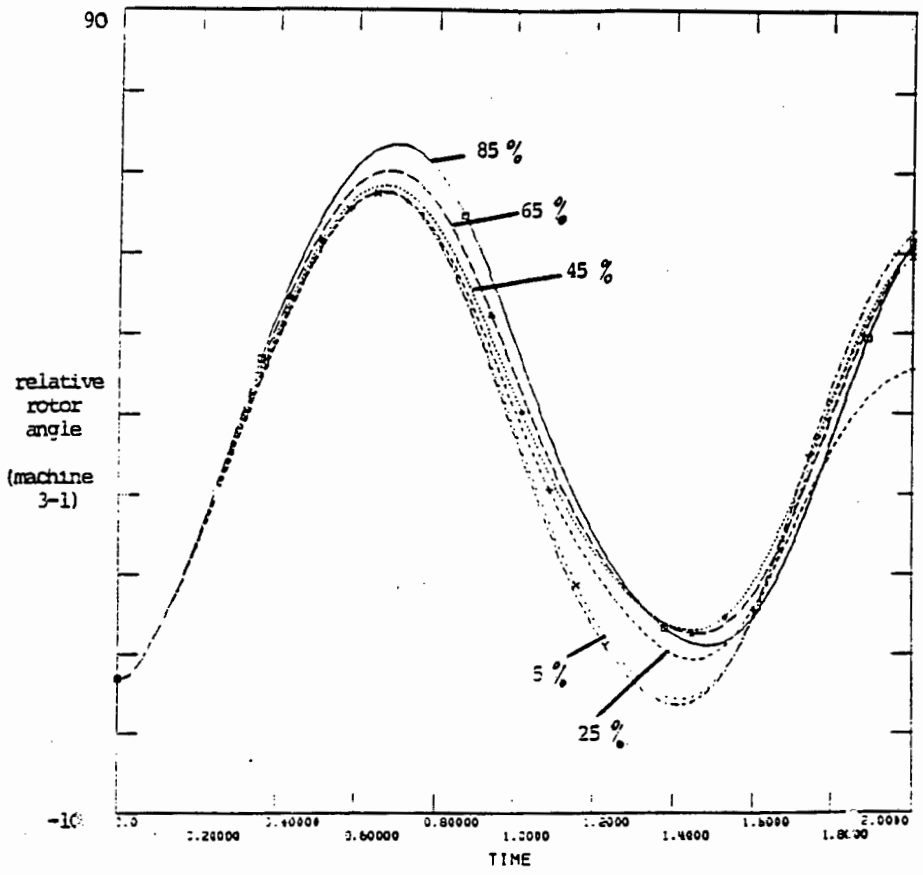

Figure 3.33b :
Relative rotor angle for machine 3 for
different load composition

If the load containing a high percentage of large induction motors is modeled with static characteristics, then the transient stability results are optimistic.

If the load containing a high percentage of large induction motors is modeled with dynamic characteristics, then the transient stability results are conservative.

The voltage profile for different load composition is shown in figure 3.34. The drop in voltage is higher for a high percentage composition of large motors. It takes a longer period of time for the voltage to recover when the load contains a high percentage of large motors.

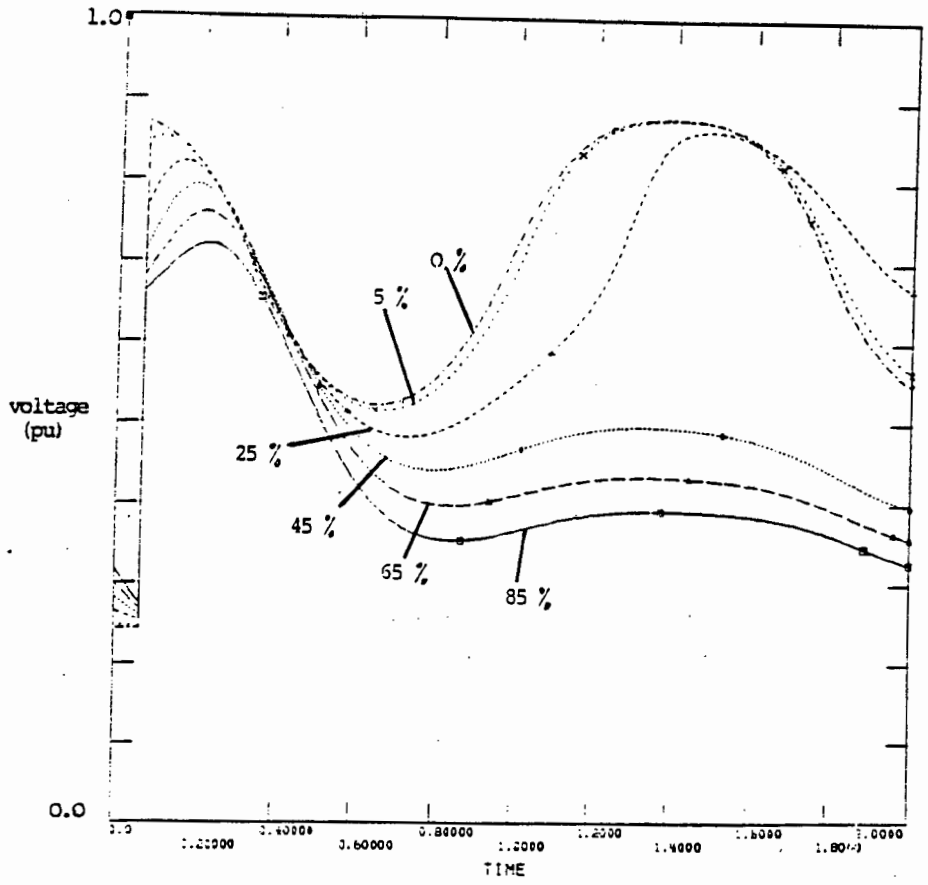

Figure 3.34:
Voltage profile for different load composition

The effects of different load composition on the absolute rotor angle of machine 1 is shown in figure 3.35. Because of the disturbance conditions for this case (listed in table 3.9), machine 1 will have to supply the load at bus 5 during and after the fault. The effect of modeling this load (at bus 5) will therefore have much influence on the performance of machine 1.

Figure 3.35 shows that the acceleration power increases as the percentage composition of large motors is increased. When the large induction motor content is 85 % of the total load, the rotor angle of machine 1 reaches 420 degrees within 2 seconds. When the dynamic behavior of the motors are modeled as 85 %, the rotor angle reaches 720 degrees within 2 seconds. This is consistent with the fact that , as the large motor composition in the load is increased, the active power consumption of the load drops. This causes the output power of machine 1 to be lower than when

the motors were not modeled as shown in figure 3.36.

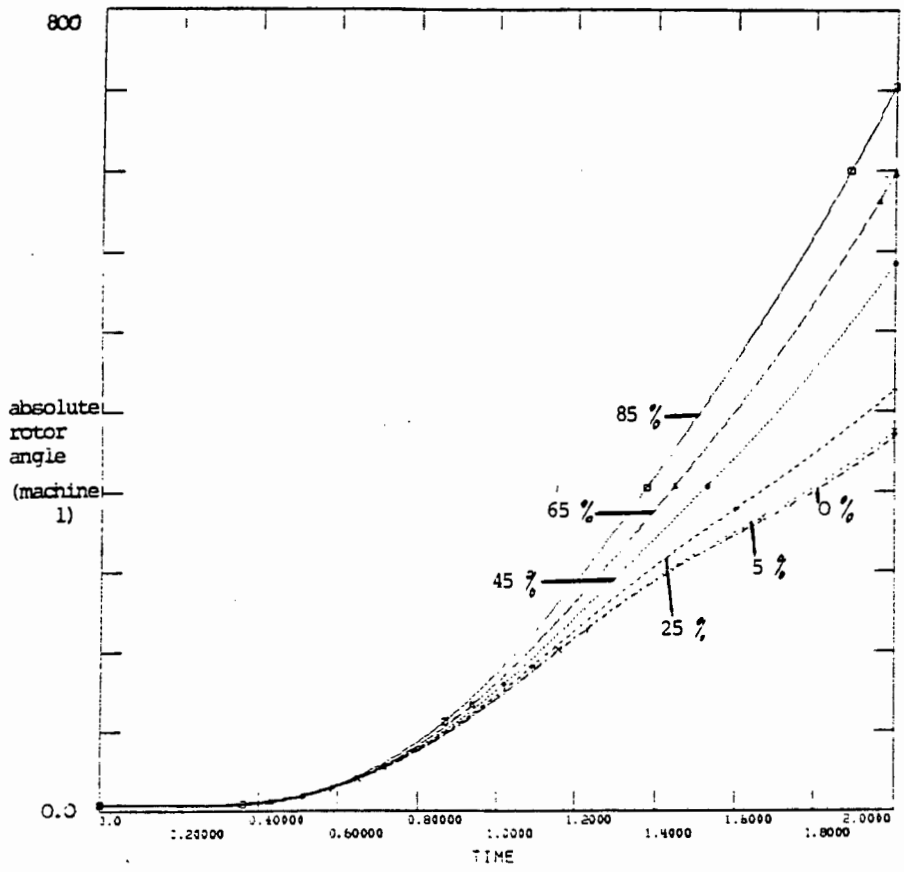

Figure 3.35:
Absolute rotor angle for different load composition (machine 1)

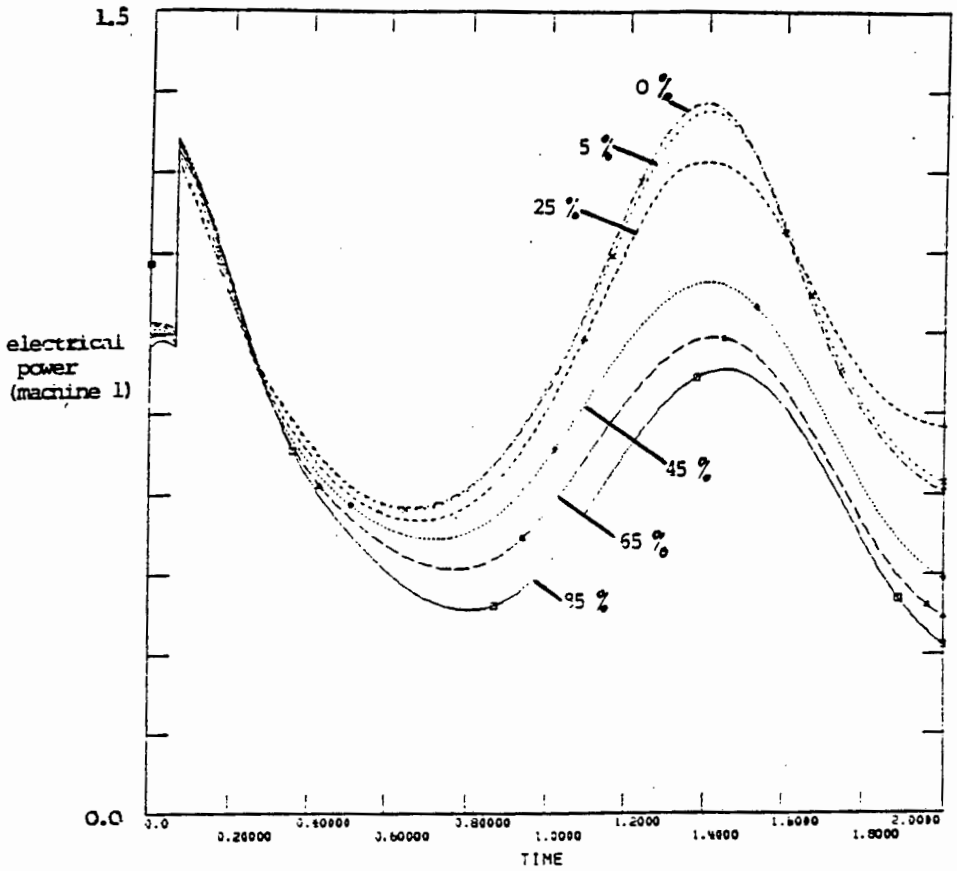

Figure 3.36:
Electrical power output from machine 1
for different load composition

For the same fault location and load model, similar observations can be made concerning the absolute rotor angle and the electrical power output of machines 2 and 3. The results are shown in figures 3.37 to 3.40 without further explanation.

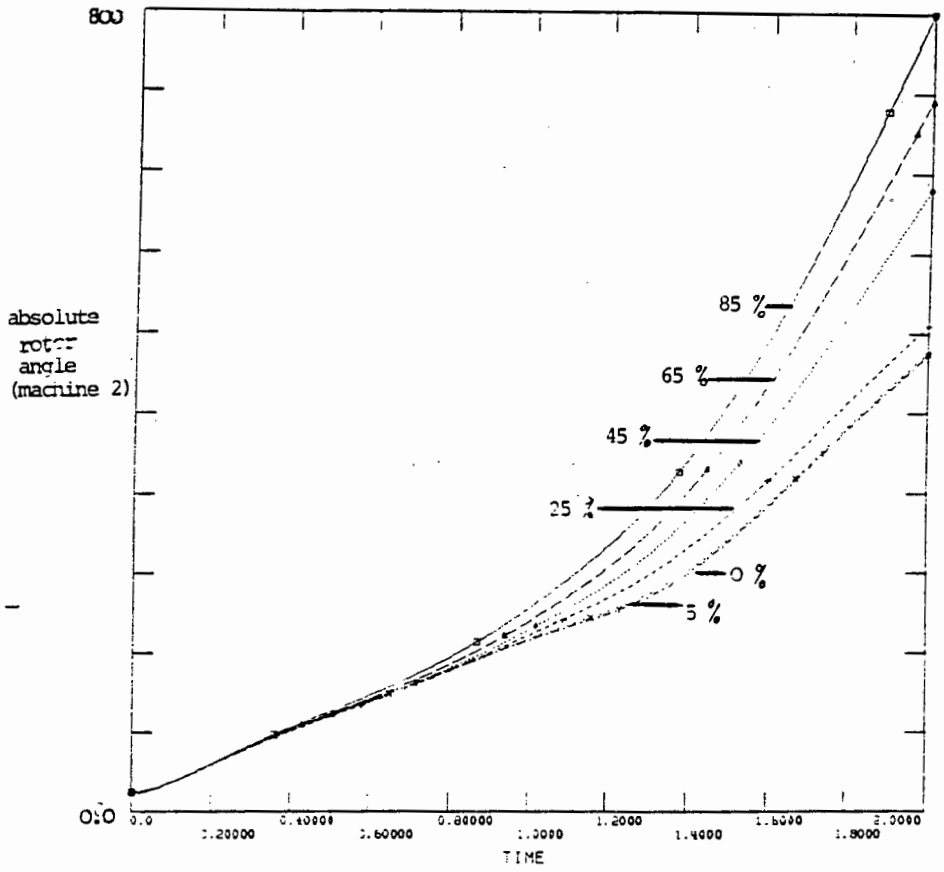

Figure 3.37:
Absolute rotor angles for machine 2,
for different load compositions

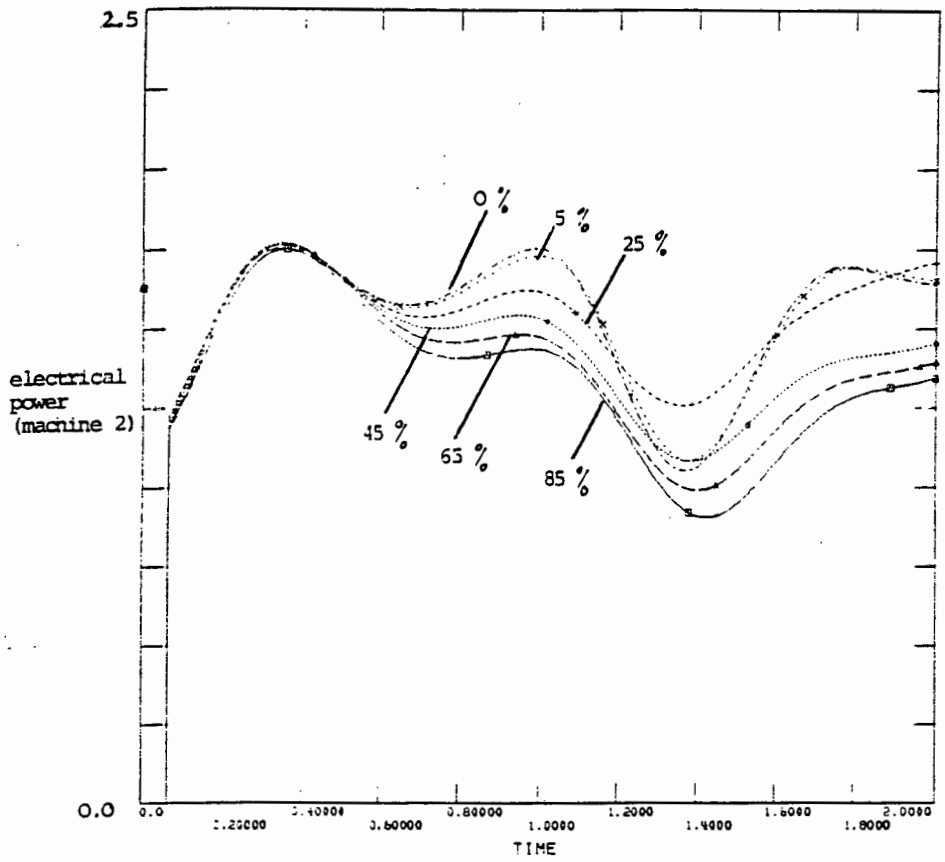

Figure 3.38:
Electrical power output for machine 2
for different load composition

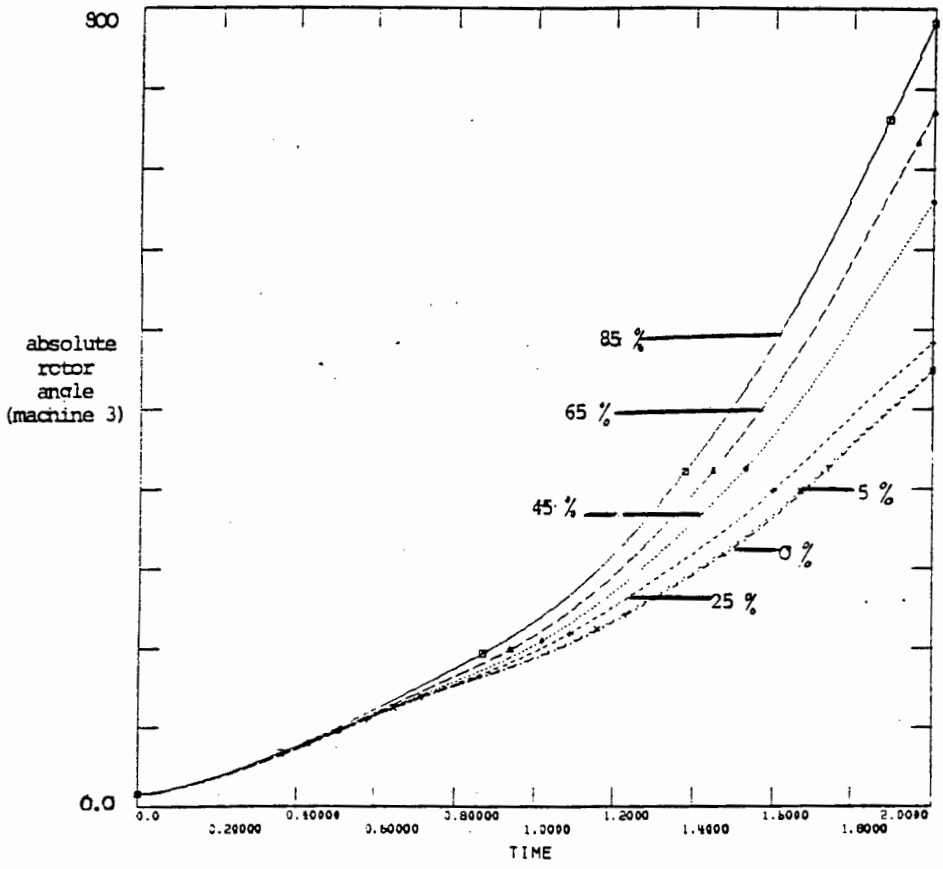

Figure 3.39:
Absolute rotor angle of machine 3
for different load composition

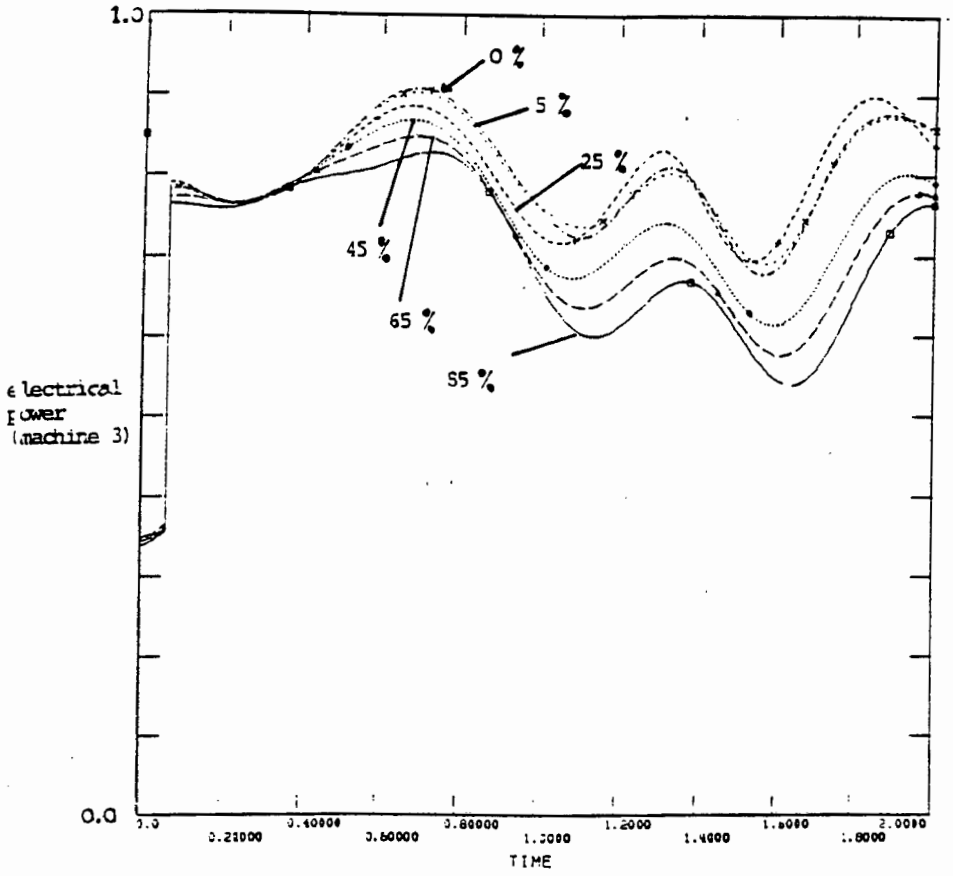

Figure 3.40:
Electrical power output for machine 3
for different load compositions

This case study has shown that the complex load model gives conservative transient stability results when there is a high percentage of large induction motors. When the percentage composition of large motors in the load are small, the transient stability results are optimistic.

CASE 3.8

In this case study, a 15.3 MVA induction motor is represented with its transient model, as part of the load at bus 5. The results are compared to those obtained by modeling this motor with its steady-state model and the static model (see figure 3.41). The simulation conditions for this case are listed in table 3.10 below:

Table 3.10 : Simulation conditions - case 3.8

generator model	model 0.0 : only H and x'_d specified
load model	15.3 MVA motor at bus 5 loads at buses 6 and 8 are modeled as P = constant
type of fault	three-phase
position of fault	on branch 5,7 near bus 7
start time	t = 0 sec
clearing time	t = 0.11 sec
breaker operation	branch 5,7 tripped (both CB's)
simulation time	2 seconds

The results are shown in figure 3.41. This figure shows a comparison of the results obtained by modeling the induction motor at bus 5 as a constant power , as a steady-state equivalent model and as a transient model.

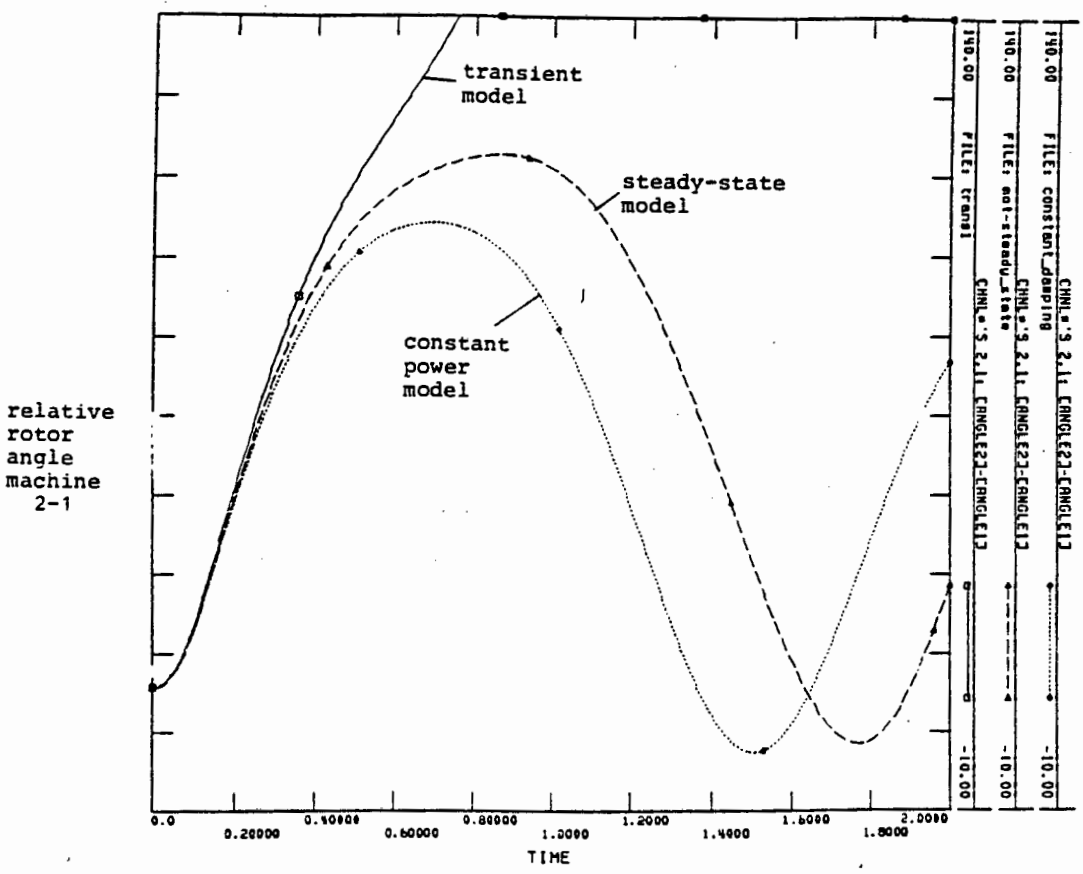

Figure 3.41:
Comparison of the transient stability results;
Static model,Steady-state model and transient model

For the same fault clearing time, the transient model gave unstable result, which are conservative, while both the steady-state model and the constant power model gave stable results. The transient stability results obtained by modeling the induction motor as constant power are the most optimistic.

Figure 3.42 shows the rotor angle of the synchronous generators. Machines 2 and 3 swing together but are out-of-step with machine 1.

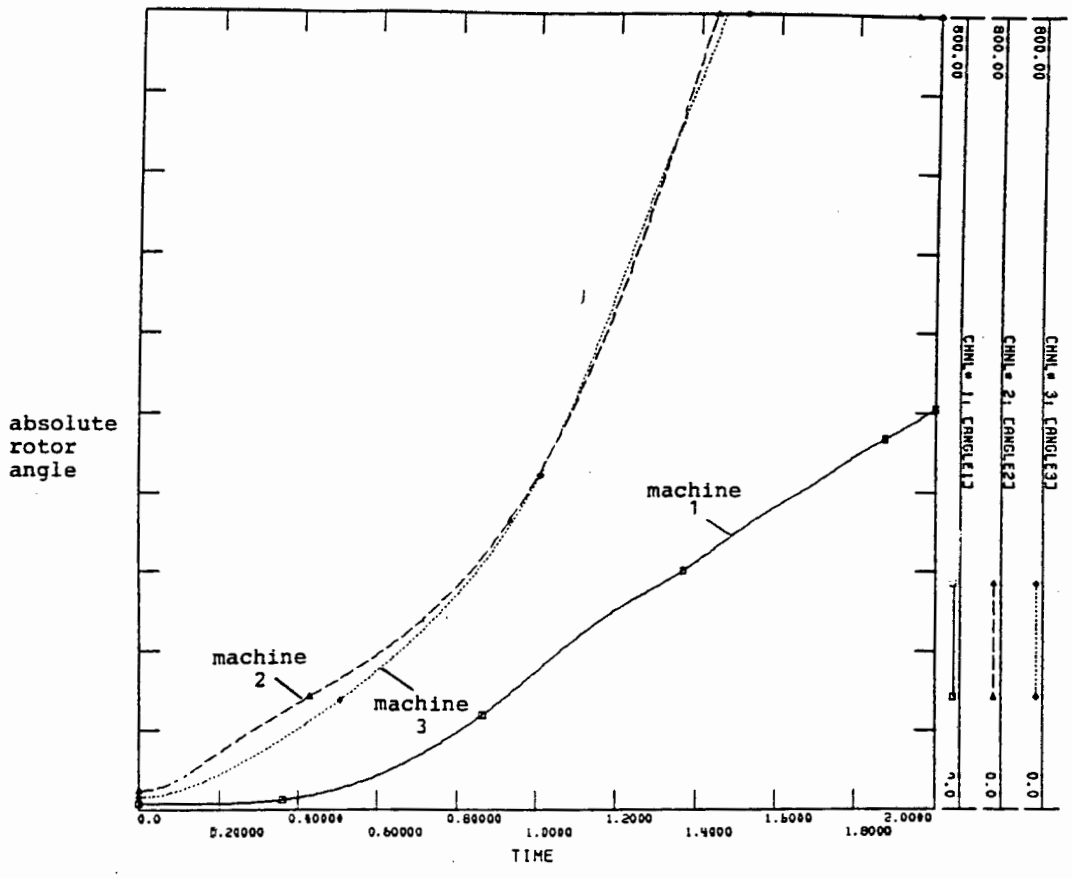

Figure 3.42:
Rotor angles of synchronous machines with motor modeled with a transient model

Figure 3.43 shows a comparison of the active power consumption of the motor when it is modeled with the steady-state equivalent model and the transient model. When a three phase fault occurs at bus 7 at time t = 0, the voltage at the motor terminal will drop and consequently the power consumption will also drop. For the steady-state model, the active power dropped from 13.5 MW to 2 MW and remained fairly constant for the duration of the fault. When the fault is cleared, the motor slowly returns to its prefault power consumption with minor oscillations.

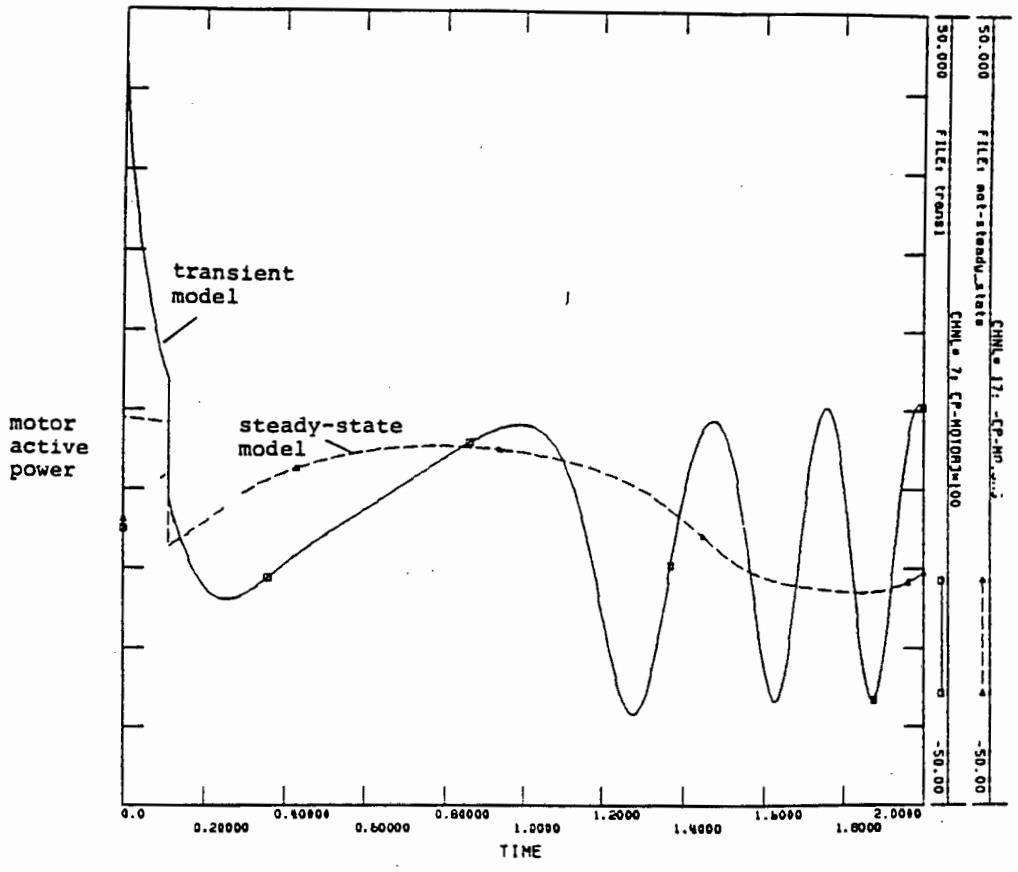

Figure 3.43:
Active power of the motor for different models

For the transient model, the motor power consumption also dropped but because of the trapped rotor flux, the induction motor now feeds into the fault. At the instant of the fault, the motor delivers 42 MW. During the fault, the power delivered decreases significantly and the decay is governed by the transient time constant of the motor. This transient response of the motor is responsible for causing rotor angle instability.

The results from case 3.1 to case 3.8 are summarized in the following table:

Summary of load modeling simulations

STATIC LOADS			
TRANSIENT STABILITY RESULTS			
LOAD MODEL	ALL LOADS	LOCAL LOAD	REMOTE LOAD
Constant Power	conservative	optimistic	conservative
Constant Current	optimistic	conservative	optimistic
Constant Admittance	more optimistic	more conservative	more optimistic

DYNAMIC LOADS		
LOAD MODEL		TRANSIENT STABILITY RESULTS
Constant power model		most optimistic
Complex model	high % large I.M	conservative
	low % large I.M	optimistic
Steady-state model		optimistic
Transient model		most conservative

The following conclusions can be drawn from the case studies performed :

1. When using static load models such as constant power, constant current and constant admittance, the relationship between the load model and the fault location should be considered.

2. Modeling a local load as constant admittance gives more conservative transient stability results, than when the load is modeled as constant power. Thus a local load should be modeled as constant admittance.

3. Modeling a remote load as constant admittance gives more optimistic transient stability results, than when the load is modeled as constant power. Thus a remote load should be modeled as constant power.

4. The frequency dependency of the load contributes only to the system damping. The transient stability results are conservative when frequency dependency of the load is neglected. Thus the frequency dependency of the load can be neglected in transient stability studies.

5. In order to determine the transient stability limit of a power system consisting of large induction motors, the motor must be modeled with its transient model because the results are the most conservative when this model is used.

6. The industrial power system loads should be modeled in detail. The percentage content of large and small induction motors should be considered. If there is a high percentage content of large motors, then the load must be modeled in detail. If the percentage content of large motor is small, then simple models for the industrial load could be used.

3.5 SUMMARY

This chapter has focused on load modeling for transient stability studies. A brief discussion on the problem of load modeling for stability studies was given. Then, different load modeling approaches were highlighted. In addition, the characteristics of different types of loads, namely; static loads and dynamic loads were discussed in detail.

Furthermore, methods used for aggregating power system loads were briefly discussed, namely; grouping of coherent induction motors and the equivalencing criteria for induction motors. Case studies were performed to simulate the effects of these different load models on the transient stability results. The relationship between the load model and the fault location was also considered in the case studies. The results from these case studies were given and conclusions were made.

Accurate load modeling was shown to be very important in transient stability studies. False conclusions concerning the stability of the system may be made, if the model for the load is chosen in an arbitrary way.

CHAPTER 4: VOLTAGE STABILITY

4.1. INTRODUCTION

In classical power system stability theory, the problem of stability was originally associated with synchronous generators. Most of the literature in the last decade concentrated on the study of the rotor angle stability and the effects of the control equipment (eg. automatic voltage regulators) on the rotor angle stability.

It has been recognized recently, that the stability problem does not only involve the rotor angle stability. The power system blackouts in France, Italy, USA etc. [35], have added a new dimension to the stability problem. These power system blackouts resulted largely because of the shortage of reactive power support in the network.

The objectives of this chapter are:

1. To review the state-of-the-art in voltage stability theory.
2. To present a description of voltage stability phenomenon by using a simple and direct example from literature.
3. To review the relationship between close multiple load flow solutions and voltage instability.

Analysis in this chapter is firstly conducted using a simplified representation of one generator and one load. This approach is adopted to prevent confusion between the factors responsible for voltage stability and those responsible for rotor angle stability. The factors affecting voltage stability will therefore be easily identified. This is obviously an oversimplification since in practice these two factors affect each other. Next, voltage stability will be studied by using an IEEE ninebus benchmark network.

The chapter begins by describing voltage stability. Then, the conditions in which voltage collapse may occur are outlined. Thereafter, steady state and dynamic aspects of voltage stability are explained by means of a simple example taken from the literature.

The effects of the following factors on voltage stability are then discussed:

a). changing parameters (load active and reactive power)
b). the uncoordinated tap changing
c). the generator voltage dynamics
d). the load dynamics.

The next aspect to be discussed is the relationship between heavy load conditions, close multiple load flow and voltage instability. Furthermore ,the literature on some voltage stability indicators will be reviewed.

Case studies are performed to investigate voltage collapse, due to increase in the load demand. The effects of the transformer tap changer action are also investigated. Finally, conclusions are made based on the discussions above.

4.2. THEORY OF VOLTAGE STABILITY

Voltage instability is the inability of the power system to maintain voltage magnitudes within specified operating limits during steady-state or transient conditions. During a voltage instability disturbance, the voltage exit the stable operating region and collapses.

The change in voltage is gradual but it can also be sudden at some point. This sudden change in voltage leads to voltage collapse. Any type of control action taken at this point will not save the voltage collapse.

Voltage collapse is associated with the use of high voltage transmission lines operating at their transmission capability limit, the relative shortage of reactive power reserves, the interconnection of bulk power systems and the availability of generation. Voltage stability has both steady-state and dynamic characteristics.

In the steady state, bifurcations of the equilibrium points are associated with the beginning of voltage collapse. These bifurcation points can be identified by sketching the active and reactive power against the load voltage. The knee point of these curves, where voltage stability is lost, is a bifurcation point. In steady state analysis, the dynamic behavior of power system elements is ignored.

In the dynamic state, the effect of the generator and load dynamics on voltage collapse is of concern. It should be noted that the static and dynamic problems, whether they are of angle or voltage variety, are not independent of each other. Traditionally, it was believed that the generator dynamics are solely responsible for the transient stabilities. This is no longer the case because load dynamics can cause voltage instability which can also lead to the loss of power system stability through the cascading process.

The steady-state and dynamic behavior of voltage instabilities are discussed below separately. Prior to this discussion, a comparison is made between the rotor angle stability and voltage stability.

4.2.1 Comparison of rotor angle stability and voltage stability

In a complex multimachine power system, the problems of rotor angle stability and voltage stability are not independent of each other. It becomes difficult, therefore, to single out specific properties and attribute them either as voltage

stability problems or rotor angle stability problems.

In essence, the rotor angle stability is an active power problem while voltage stability is a reactive power problem, because it is associated with the availability of reactive power in the network to support the voltage profiles.

These two stability problems can however, be studied separately by making some simplifying assumptions. In order to study " pure " rotor angle stability, a single machine and an infinite busbar example is used. The voltage behind the transient reactance is assumed to remain constant hence excluding the voltage dynamics. In order to study " pure " voltage stability, the rotating machine dynamics are excluded by assuming that the voltage behind the transient reactance is tied rigidly to the rotor angle(i.e there is no angular difference between the rotor angle and the field voltage angle. These two are lined up). The one axis voltage dynamics (direct axis) of the machine are included.

4.2.2 Steady-state aspects of voltage stability

Static stability is defined only for the steady state conditions. The system equations are assumed to have no time derivatives at all. All the equations defining the state are algebraic, and hence define the operating point of the load flow solution. In steady state stability, the state surrounding the stable operating region is neglected. A solution will be stable if any change in the system parameters produce a self adjusting change in the load flow operating point.

Figure 4.1 uses a simple example of a generator feeding a load through a reactance.

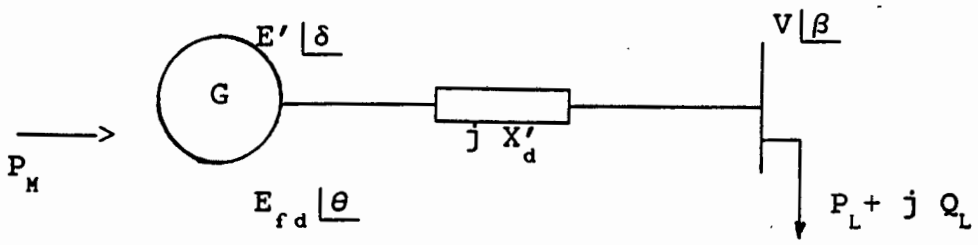

figure 4.1
Generator feeding a load through a reactance

The conventional approach of studying voltage stability was to plot the graph of V against P_L for increasing values of P_L and examine it. The typical V,P_L graph is shown in figure 4.2.

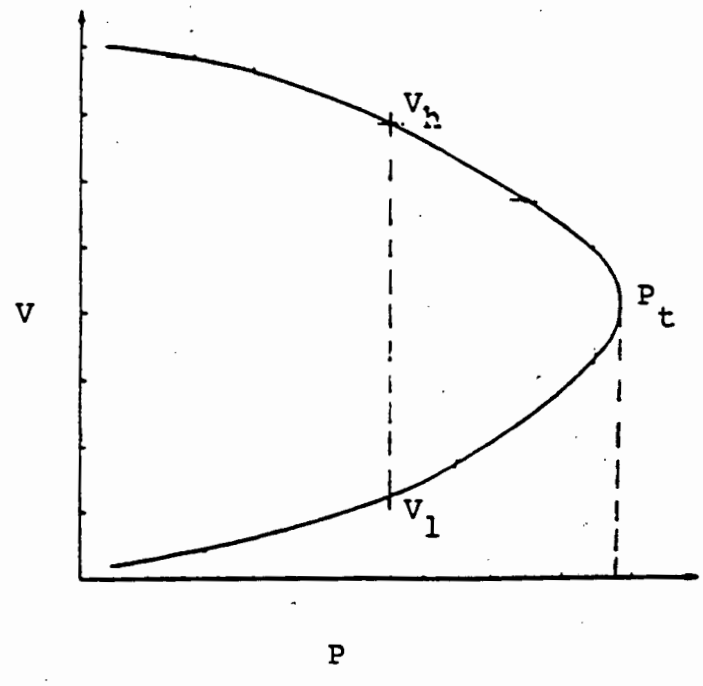

figure 4.2:
The conventional P-V curve for voltage stability

There are two load flow solutions V_h, the high voltage solution and V_l, the low voltage solution which is not practically usable. Thus V_h is taken as the only viable solution. By increasing the value of P_L step by step, the two load flow solutions approach each other at V_t. Increasing P_L beyond P_t will produce no load flow solution since the Jacobian matrix would be singular. The point (V_t,P_t) is the "knee point" of the P-V curve.

The other conventional approach to studying voltage collapse is to plot the graph of V against Q_L, the reactive power at the load bus. The Q-V curve is obtained by repeated load flow calculations, monitoring the voltage and the reactive power at a critical bus in the network. A reactive source is simulated at this bus and the MVAr limits are not enforced. The initial scheduled voltage is usually high (approximately 1.03 pu). A typical Q-V curve is shown in figure 4.3 :

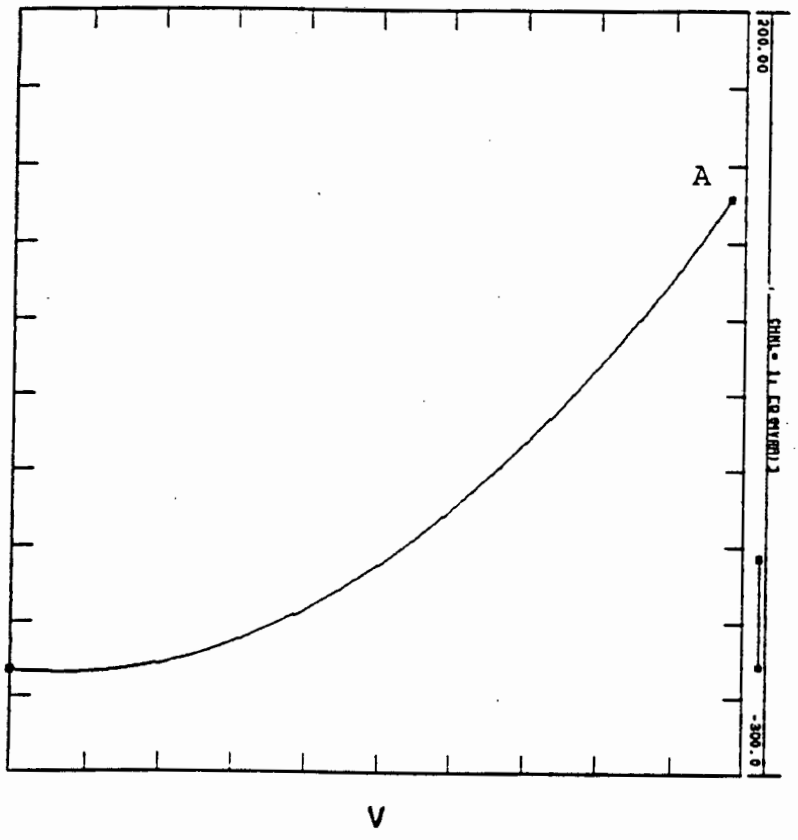

Figure 4.3
The conventional Q-V curve for voltage stability

Point A in figure 4.3 shows the initial load flow operating point for this bus. The scheduled voltage is reduced in small steps and the reactive power is monitored. The reactive power will decrease with the voltage reduction. The process continues until a further reduction in voltage results in an increase in reactive power requirement. This is the " knee point of the Q-V curve. The reactive power requirement at this bus is compared to the available reactive resources. If the reactive resources are less than the reactive power requirements, then the system will collapse.

Using static analysis only, erroneous conclusions concerning the voltage stability of the system may be drawn. This is because voltage stability is not only a steady-state problem but a dynamic problem too. It will be shown later in this chapter that by using bifurcation properties, the equilibrium point V_1 (see figure 4.2) can either be stable or unstable depending on the network conditions.

The model for the example in figure 4.1 can be written as follows [36]:

Rotor swing dynamics

$$f_1 = \frac{2H}{\omega_r}\frac{d^2\delta}{dt^2} + D\frac{d\delta}{dt} = 0 \qquad \text{.....(4.1)}$$

Direct axis voltage dynamics

$$f_2 = T'_{do}\dot{E}' = -\frac{x_d}{x'_d}E' + \frac{x_d - x'_d}{x'_d}\alpha V\cos(\beta-\theta) + \alpha E_{fd}$$

$$\alpha = 1 \,/\, (\cos(\delta-\theta)) \qquad \text{.....(4.2)}$$

where α is a constant coefficient that determines how rigid is the tie between the voltage behind the transient reactance and the rotor angle. For $\alpha = 1$, these two are lined up, enabling an independent analysis of voltage instability.

Load dynamics

$$f_3 = \dot{s} = f(p) \qquad \text{.....(4.3)}$$

where p denotes the parameter vector i.e. all the system parameters that can be varied. These parameters have no derivatives present."s" represents the dynamic state component of the load, eg. the slip of an induction motor.

Active and reactive power balance

$$f_4 = P_M - P_L = 0 \qquad \text{.....(4.4)}$$

The injections $P_M = P_L$ are constant and given.

$$f_5 = \frac{1}{X'_d} E'V \sin(\beta-\delta) + P_L = 0 \qquad \text{....(4.5)}$$

$$f_6 = \frac{1}{X'_d} (V^2 - E'V \cos(\beta-\delta)) + Q_L = 0 \qquad \text{....(4.6)}$$

The field voltage E_{fd} is constant and given.

The assumptions made in this example are:

a). The network is lossless
b). The turbine shaft power is equal to the load active power ($P_M = P_L$)
c). $\delta = \beta$ so that the rotor oscillations do not appear in the voltage equations. Hence voltage dynamics can be studied separately.

For the steady-state study of voltage stability, equation 4.3 does not appear since the load dynamics are ignored. Equation 4.1 subsequently disappears because rotor dynamics are assumed to have no influence on voltage dynamics.

Three equations, 4.2, 4.5 and 4.6 remain. The output quantity ($\beta - \delta$) in equations 4.5 and 4.6 can be eliminated. The system equations are thus reduced to two and are given by

$$f_2 = -\frac{x_d}{x'_d} E'^2 + \frac{x_d - x'_d}{x'_d} V^2 + (x_d - x'_d) Q_L + \alpha E_{fd} E' = 0$$

$$f_{56} = E'^2 V^2 - (x'_d P_L)^2 - (x'_d Q_L + V^2)^2 = 0 \quad \ldots\ldots\ldots\ldots\ldots (4.7)$$

The above equations have two state variables V, E′ both of which are one dimensional and three variable parameters P_L, Q_L, E_{fd} which may change the operating conditions. The following analysis uses the phase portrait of V and E′ to determine the steady state bifurcation points as the parameters P_L, Q_L and E_{fd} are varied.

Equation 4.7 can be used to plot the phase portrait of (V,E′) for different values of P_L, Q_L and E_{fd}. Figure 4.4 shows the phase portrait (V,E′) for E_{fd} = 1.8, P_L= 0.5, Q_L= 0.5, x_d= 0.146 and x'_d= 0.0608. Two loci are shown, the load flow locus and the equilibrium locus. The load flow equations are in a generalized form i.e the field excitation voltage setting and the internal generator voltage are included in the equations not only the bus voltages and injections. The intersection of these two loci depict the load flow solutions. There are only two solutions in this figure (because of the simple example chosen), otherwise in a multibus network there would be many solutions.

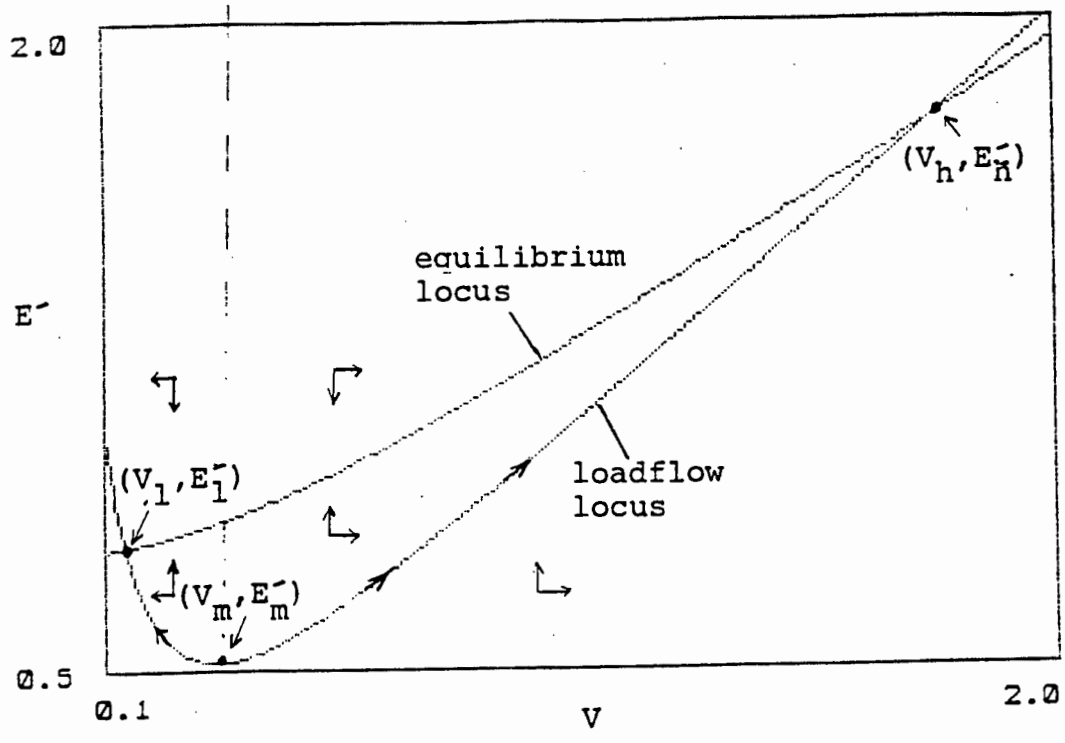

Figure 4.4:
A phase portrait for Efd=1.8, P_L=Q_L=0.5

There are three important points in figure , namely (V_h, E'_h), (V_l, E'_l) the load flow solution points and (V_m, E'_m) the minimum point of the load flow locus. When the parameters are varied, these points will move around the load flow locus and from their movement, the parametric stability can be deduced.

According to equation 4.7, the operating point is constrained within the load flow locus and dynamic movement along the locus is only dictated by the dynamics of E′ as given by equations 4.5 and 4.6. Because the trajectories of the phase portrait are constrained within the load flow locus, it follows that

$$\frac{\partial f_{56}}{\partial V} dV + \frac{\partial f_{56}}{\partial E'} dE' = 0 \qquad \text{.....(4.8)}$$

where V is differentiable, equation 4.8 becomes

$$\frac{\partial f_{56}}{\partial V} \dot{V} + \frac{\partial f_{56}}{\partial E'} \dot{E}' = 0 \qquad \text{.....(4.9)}$$

$\dot{V}$ is not a state variable because V is not a dynamic state variable. $\dot{V}$ however, provides information regarding the direction the trajectories will take on the load flow locus. Equation 4.9 can be written in the form :

$$\dot{V} = -\left(\frac{\partial f_{56}}{\partial V}\right)^{-1}\left(\frac{\partial f_{56}}{\partial E'}\right)\dot{E}' = \frac{1}{\left(\frac{\partial E'}{\partial V}\right)} * \dot{E}' \quad .....(4.9)$$

The direction of the trajectories therefore depends on the slope of $\frac{\partial E'}{\partial V}$ and on $\dot{E}'$. In figure 4.4, the slope of $\frac{\partial E'}{\partial V}$ is positive on the right side of the minimum point (V_m, E'_m) and negative on the left side of this point. The vector $\dot{E}'$ however, is negative above the equilibrium manifold and positive below the equilibrium manifold. Thus the direction of trajectories will be as shown in figure 4.4. The point (V_h, E'_h) is stable while the point (V_l, E'_l) is unstable when it is on the right side of (V_m, E'_m) and stable when it on the left side of this point. If the network conditions change such that the point (V_l, E'_l) moves to the right side of the (V_m, E'_m), the power system behavior changes.

When the load is increased (either P_L or Q_L or both), the high and low voltage load flow solutions approach each other. Since (V_l, E'_l) is an unstable point, when the two solutions become one, a bifurcation point (V_t, E'_t), the knee point of the P-V curve , results.

When the operating point of the power system reaches the point (V_t, E'_t), the gradients of the load flow locus and the equilibrium locus are colinear, so that

$$\begin{bmatrix} \frac{\partial f_2}{\partial V} \\ \frac{\partial f_2}{\partial E'} \end{bmatrix} = \beta \begin{bmatrix} \frac{\partial f_{56}}{\partial V} \\ \frac{\partial f_{56}}{\partial E'} \end{bmatrix}$$

Two rows in the Jacobian matrix [J] of the system will be multiples of each other, hence [J] will be singular. The singularity of [J] is an indication of voltage instability.

4.2.2.1 Effects of changing parameters

Changing E_{fd}

E_{fd} appears in the equilibrium equation but not in the load flow equation. By changing E_{fd} therefore, the load flow locus will remain fixed whils: the equilibrium locus changes.

Figure 4.5 shows that by decreasing E_{fd} the equilibrium locus moves to the right. The power system behavior changes as the equilibrium point (V_l, E'_l) passes the lower point of the load flow locus (V_m, E'_m) and also when the two equilibrium points (V_l, E'_l) and (V_h, E'_h) approach ea:h other at (V_t, E'_t). This makes these two points bifurcation points.

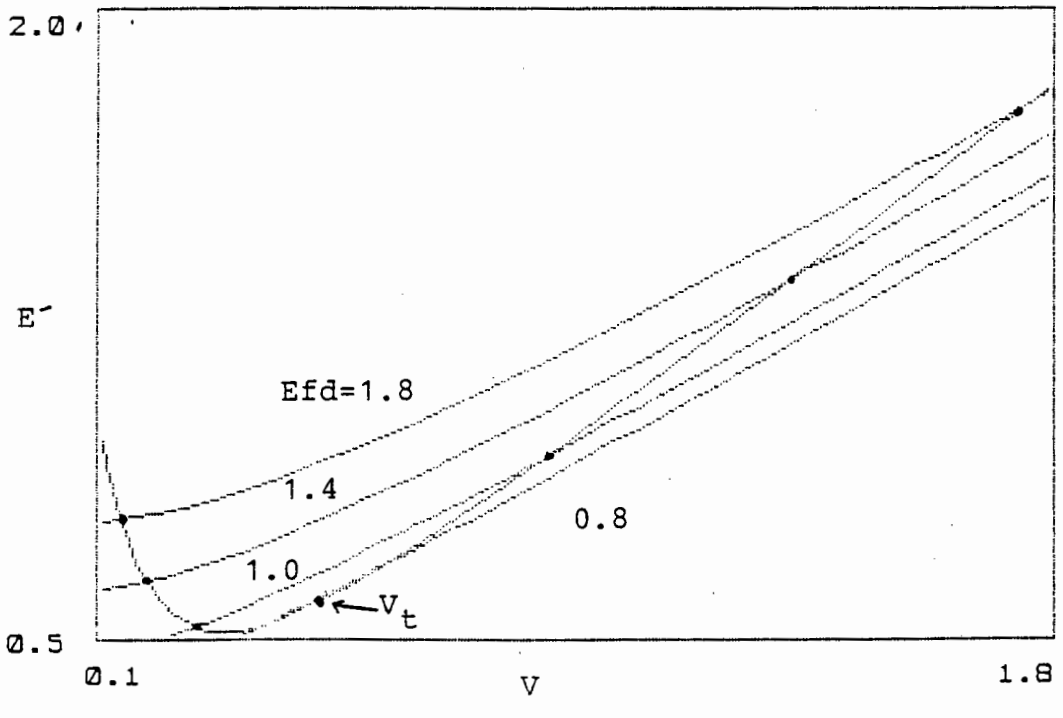

figure 4.5:
The effects of changing parameter E_{fd}, P_L= 0.5, Q_L= 0.5

Changing P_L

P_L appears in the load flow equation but not the equilibrium equation. Thus by changing this parameter, the equilibrium locus stays fixed and the load flow locus changes. By increasing P_L, as shown in figure 4.6 , the load flow locus moves upwards and two bifurcation points (V_m, E'_m) and (V_t, E'_t) can also be found.

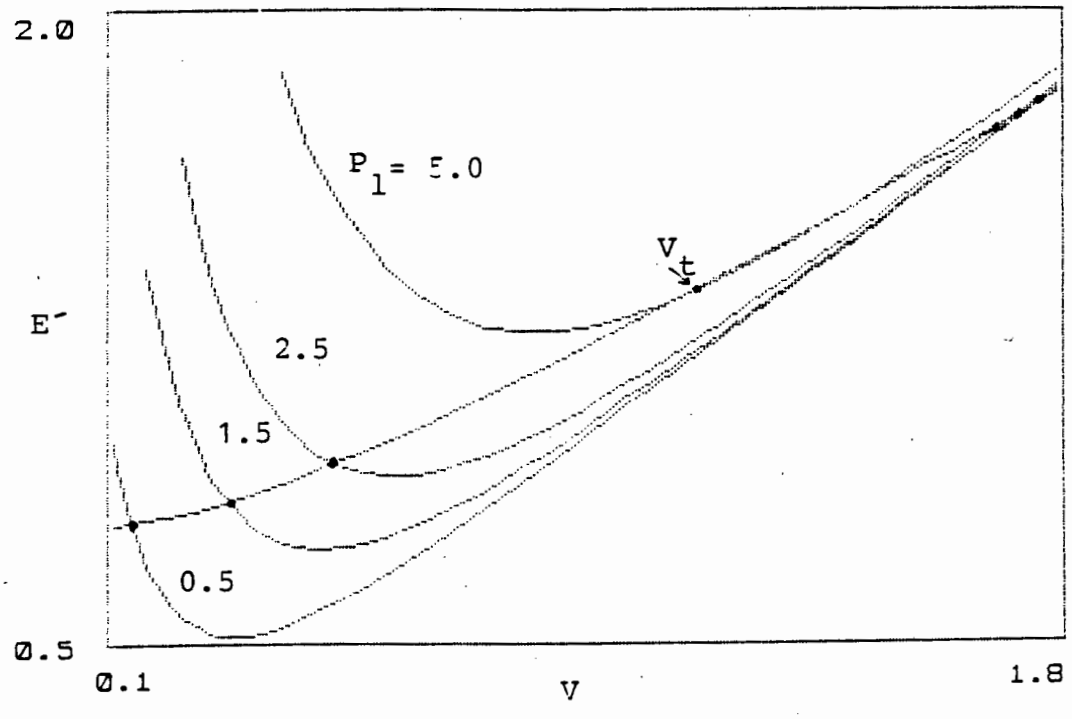

Figure 4.6
The effects of changing parameter P_L, E_{fd}= 1.8, Q_L= 0.5

Changing Q_L

Q_L appears in both the load flow equation and the equilibrium equation. This makes an analysis of the system behavior to parametric changes more difficult. Figure 4.7 below shows however, that the two bifurcation points (V_m, E'_m) and (V_t, E'_t) exist.

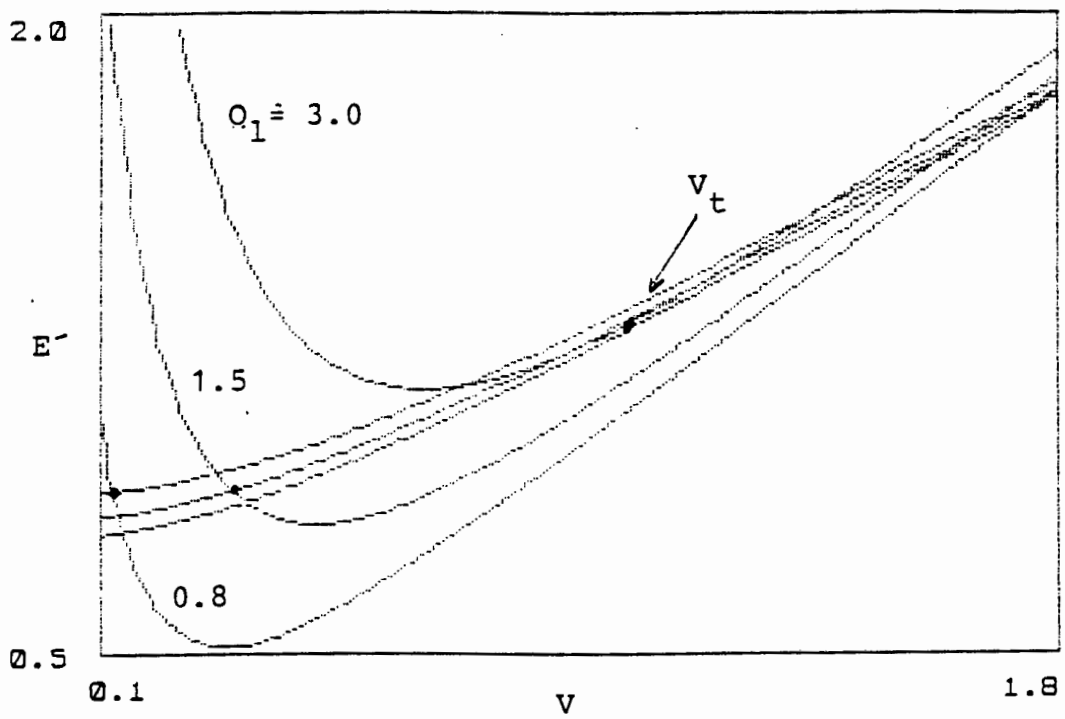

figure 4.7:
The effects of changing parameter Q_L, E_{fd}= 2, P_L= 0.5

4.2.2.2 *The effects of on-load transformer tap changing on static voltage stability*

A tap changing transformer will be added to the previous example as shown in figure 4.13. In this way, the effects of changing the transformer tap position on voltage stability can be studied.

It is well documented in the literature [37],[38],[39] that one of the main causes of voltage collapse is the action of uncoordinated tap changers. This section attempts to explain the relationship between the tap changer operation and voltage collapse.

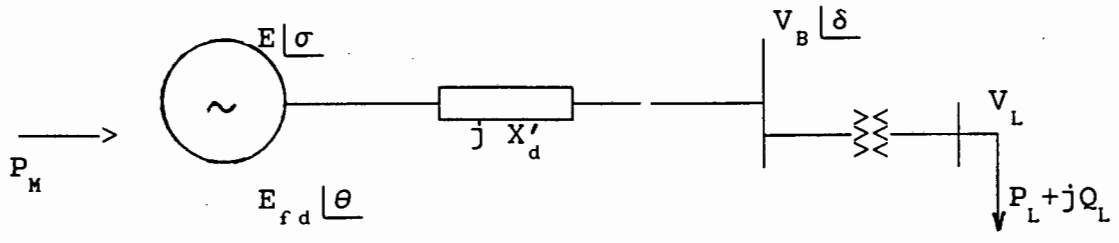

figure 4.8
Network showing tap changing transformer

The following assumptions are made in the analysis:

(a). The system is operated with the customary tap changer control which responds directly to the load voltage without constraints.

(b). No controllable reactive resources are included so that the basic effect of the tap changer is direct.

(c). The time lag of the tap changer operation is slow compared to the oscillations of voltage caused by generator and exciter dynamics.

The load model is very important especially when tap changing transformers are present. Chapter three discussed various load models in detail. The general load model for reactive power can be represented by a quadratic expression as follows:

$$Q = Q_{LO}(s) + q_L\tau + AV_L + BV_L^2 \qquad .....(4.10)$$

where $Q_{LO}(s) + q_L\tau$ is the load reactive power injection augmented by its change during τ, the period between command and execution. AV_L is the constant current component and BV_L is the constant impedance component. The dynamics of the load are represented in $Q_{LO}(s)$, which is a function of slip for an induction motor.

Since these dynamic state vectors are not very well understood, their effects on the stability limit will be ignored, although they may affect the stability limit. For this reason, $Q_{LO}(s) = Q_{LO}$ the static load injection.

The tap changer is a relay which responds to the load voltage V_L. Considering figure 4.13 above, assume that at switching, the setpoint is such that $V_{BO} = V_{LO}$ ie the setpoint is at the zero position. When at any time, the load voltage drops below the minimum allowable voltage V_L^m, a tap change will be ordered. This tap change will increase the reactive power flow in the load.

If the load voltage V_L is greater than V_L^m then the tap changer would have achieved its task. Further tap changes will not be necessary. However, if the load voltage is still less than V_L^m, tap changes will be ordered one after another until they reach their limit and the load voltage will slide down leading to a collapse. The increase of reactive power will not save this rapid drop of load voltage.

Another way of understanding the effect of the tap changer on voltage stability is to consider what happens when a unit

trips. The load voltage will drop and similarly the load active and reactive power demand will drop since they vary with the voltage.

For constant power loads, the tap changer will be used to try to keep the power constant. This causes more reactive current to flow through the lines to the load. The voltage drop will be increased and hence the voltage at the load bus will drop even further, thus accelerating the collapse of voltage.

4.2.3 Dynamic aspects of voltage stability

When voltage stability is studied from static characteristics of the power system, erroneous conclusions may be drawn because the dynamic characteristics of the generator, the control actions and the load would have been excluded [40]. The exclusion of these dynamics will prevert proper planning resulting in unforeseen system blackout as manifested by the blackouts in Tokyo, France, Florida, etc [35].

In dynamic stability studies, the response characteristics of the loads, the generators and the control equipment are crucial. Differential equations are used to model the behavior of these dynamics. These differential equations are linearized around an operating point (load flow solution) and the system equations are expressed in the state space formulation. For any changes in the network, the Jacobian matrix of the power flow equations and the eigenvalues of the linearized ("A") matrix are monitored.

Zaborszky [36] used a simple case of a generator with a static load and simple excitation control in order to determine the influence that the excitation control and generator dynamics have on voltage stability. He further modified this case by replacing the static load with a dynamic load. In both cases the dynamic behavior of the load and generator excitation influenced the position of the power system relative to the

bifurcation points.

Pai et al [41] used the 9 bus benchmark network to study the dynamic characteristics of voltage stability. The system equations are linearized around an operating point and the load level is incremented. Two cases are considered, the normal base loading and the system with base load which results in some of the generators hitting the Q-limits. For both cases, the voltage collapse conditions are monitored. This benchmark network will be used later to determine the steady state behavior of voltage stability.

Looking at these case studies [36],[41], an observation can be made that when studying the dynamic phenomena of voltage collapse, the bifurcation theory, the linearized dynamic model and the sensitivity analysis are used. This entails monitoring the singularity of the Jacobian matrix and observing the eigenvalues of the linearized matrix.

The static analysis only, is inadequate in predicting voltage instability accurately. However, the static criterion can be a meaningful guide to proposing dynamic stability margins [42].

The dynamic behavior of large induction motors has been cited as the main cause of voltage instability [43]. Factors such as the quantity and nature of mechanical loading, the motor rotor and load inertias and the proportion of constant impedance load play an important part in determining when voltage collapse occurs.

4.3 RELATIONSHIP BETWEEN HEAVY LOAD CONDITIONS, CLOSE MULTIPLE LOAD FLOW SOLUTIONS AND VOLTAGE INSTABILITY

The voltage profile in a power system can be most conveniently obtained from the solution of the well known nodal equation

$$P_i + jQ_i = \bar{V}_i \sum_{k=1}^{n} \bar{Y}^*_{ik} \bar{V}^*_k \qquad i = 1,2,\ldots n \qquad \ldots.(4.11)$$

Because of the non-linear nature of the load flow equations, the solution for the above equation may possess several mathematical solutions [44],[45]. A power system with n nodes will have 2^n possible solutions. Thus the existence of multiple load flow solutions.

For a heavily loaded power system, these multiple load flow solutions approach one another to become very close solutions. When performing load flow studies under these conditions, infeasible solutions may results. It should be kept in mind that these close multiple load flow solutions may not have the same dynamic structure (e.g one solution may be stable and the other unstable) and thus bifurcation points may result. The resulting bifurcation points, link voltage instability to the multiple solution structure.

4.4. VOLTAGE STABILITY INDICATORS: A LITERATURE REVIEW

The subject of voltage stability is receiving growing attention and much research is being conducted. At this stage however, there are no conclusive results. Listed below is a literature review of some technical papers on voltage stability.

Sekine and Yokoyama [46] proposed a method which makes it possible to derive very close multiple load flow solutions for ill-conditioned or heavily loaded power system. The physical stability of each solution was studied and it emerged that in order to test voltage stability, the power-voltage

characteristics of the load and the response characteristics of the controller must be taken into account.

The same authors [47] studied the dynamic stability of a model system by using eigenvalue methods, considering the dynamic response of loads and control equipment. They have shown that it is possible to detect voltage instability by eigenvalue method, and that voltage instability is influenced by the dynamic behavior of the loads and control equipment.

De Marco and Bergen [48] asserted that voltage collapse may be modeled as a large deviation in the system dynamics. They proposed a security measure for electric power systems to indicate vulnerability to voltage collapse. This measure accounts for random disturbances in load and nonlinear dynamics of voltage dependent loads, and is based on the expected exit time of the randomly perturbed system from the region of attraction of the system.

Kwatny et al [49] analyzed static bifurcations of the load flow equations using the Liapunov-Schmidt reduction and Taylor series expansion of the reduced bifurcation equation. It was shown that the static bifurcation of the load flow equations are associated with either divergence-type instability or when the load flow equations looses causality.

Kessel and Glavitsch [50] derived a voltage stability indicator L, ranging from zero to one, with a value of one indicating voltage collapse and a value between zero and one indicating voltage stability. This indicator L can be calculated from a known system state (load flow). Voltage stability is guaranteed if L is less than one.

Barbier and Barret [18] used static analysis to calculate the critical voltage at a load bus under maximum transfer conditions. This critical voltage is then used as a threshold value to which the actual bus voltage can be compared.

Lemaitre et al [51] noted that voltage levels or load flow divergence are not sufficient accurate indicators of voltage instability. They proposed a real time dynamic indicator which could be used as a forecasting tool. This dynamic indicator is derived considering the existence of secondary voltage control, the control law governing the compensation of reactive energy and the load response. This tool will also give an indication of voltage instability to the operator well ahead of time, so that there is sufficient time to take appropriate preventive steps.

4.5 CASE STUDIES

In the following sections, case studies are performed to determine the effects of the load on voltage instability. The example in figure 4.9 is used. The voltage stability of the network is studied by a parametric load flow, i.e the active and reactive power of the load are increased in small steps.

The generator is modeled as an infinite bus and the load is modeled as a constant power.

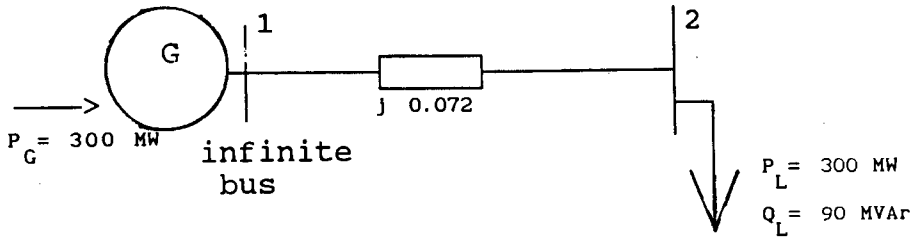

Figure 4.9:
A single machine and a single load example

CASE 4.1

In this case study, the effects of the active and reactive power load on voltage stability are investigated. The active and reactive power of the load are increased in small steps until voltage collapse occurs. The simulation conditions for this case are listed in table 4.1:

Table 4.1: Conditions for case 4.1

Network investigated	A single machine and a single load (figure 4.8)
Parameters changed	1. Real power load only 2. Reactive power load only 3. Apparent power

This case study shows that voltage collapse is highly dependent on the amount of loading in the system.

Table 4.2 shows the load flow solution for the load demand of 300 MW and 90 MVAR. This is the initial load flow operating point. This table also shows the knee point conditions.

Table 4.2: Load flow results for initial and knee point conditions (active power increased)

Bus Number	Voltage (pu)	Angle (degrees)	Active power	Reactive power	
2	0.958	-12.4	300.0	90.0	Initial conditions
2	0.737	-38.2	665.0	90.0	Knee point conditions

Figure 4.10 shows the P-V curve for an increase in active power. The initial voltage magnitude is 0.957 pu with an angle of -12.4 degrees. As the active power is increased, the voltage drops to 0.737 pu, with an angle of -38.2 degrees. This is the point at which voltage collapse begins. The load has increased by 122 % from the initial operating conditions.

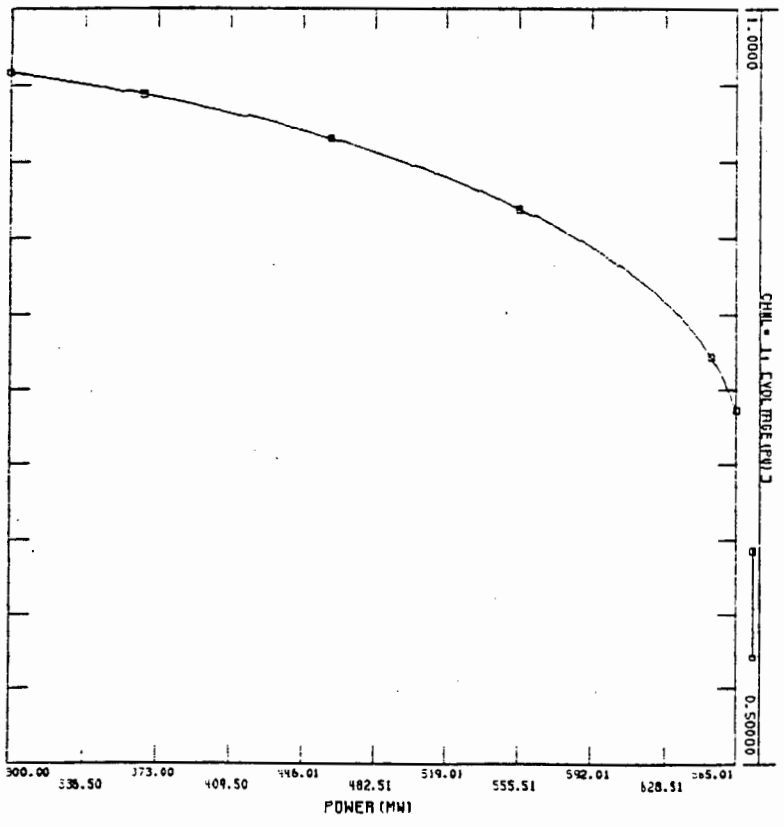

Figure 4.10:
P-V curve showing voltage collapse conditions

Figure 4.11 shows the load Q-V curve when the reactive power is increased from 90 MVAR in small steps, with the active power kept constant at 300 MW. The initial conditions and the knee point conditions are given in table 4.3.

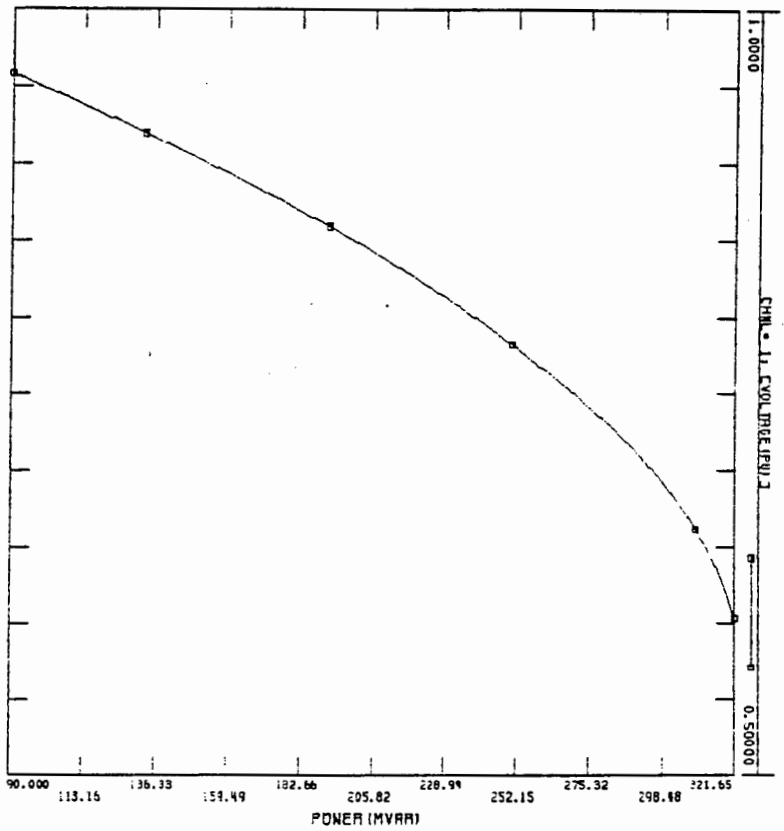

Figure 4.11:
Q-V curve showing voltage collapse conditions

Table 4.3 : Loadflow results for initial and knee point conditions (reactive power increased)

Bus Number	Voltage (pu)	Angle (degrees)	Active power	Reactive power	
2	0.958	-12.4	300.0	90.0	Initial conditions
2	0.603	-20.0	300.0	321.6	Knee point conditions

Voltage collapse occurs when the voltage has a magnitude of 0.6 pu with an angle of -20 degrees. As expected, the voltage angle is affected only slightly as compared to the voltage magnitude. Only a 257 % increase of reactive power load was responsible for voltage collapse as compared to a 568 % increase of load active power.

Figure 4.12 shows the S-V curve when the load is increased with a constant power factor. The initial conditions and the conditions before collapse are listed in table 4.4.

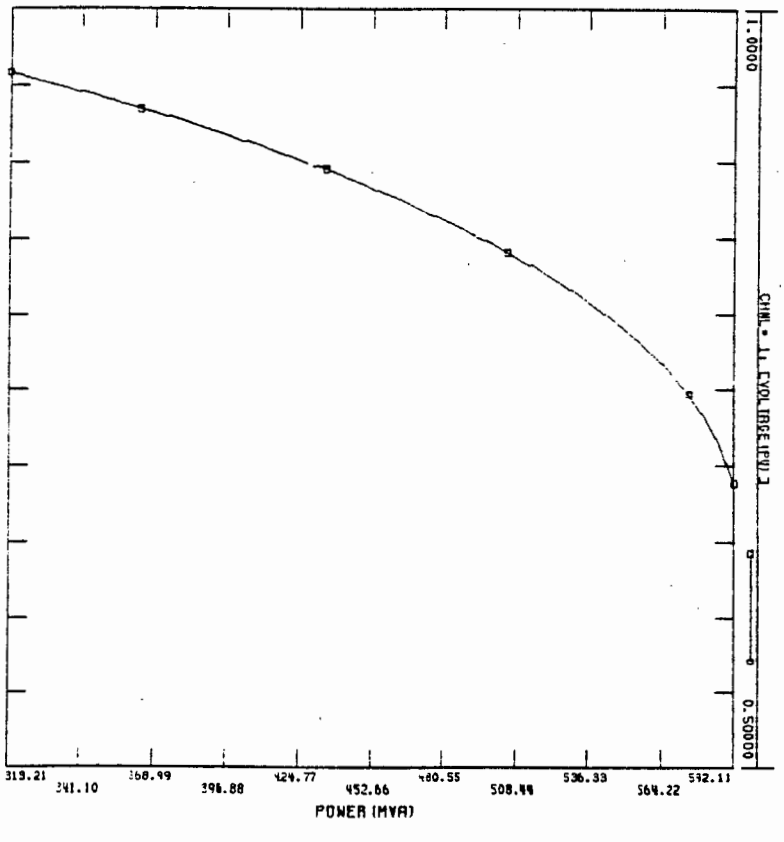

Figure 4.12:
S-V curve showing voltage collapse conditions

Table 4.4 : Loadflow results for initial and knee point conditions (Apparent power increased)

Bus Number	Voltage (pu)	Angle (degrees)	Apparent power	
2	0.958	-12.4	313.2	Initial conditions
2	0.689	-34.3	592.1	Knee point conditions

Voltage collapse occurs when the voltage has a magnitude of 0.689 pu with an angle of -34.3 degrees. The load demand at this point is 592 MVA which represents 89 % increase from the initial conditions.

Comparing the results of figures 4.10, 4.11 and 4.12, it can be shown that the results obtained by increasing the reactive power only, are the most conservative, i.e the voltage magnitude at the point of collapse is the lowest. The results obtained by increasing only the real power, are the most optimistic.

The P-V curve is the most commonly used method in voltage stability analysis because in most cases, the active power increase of the load is greater than the increase of reactive power. It is however, important that the Q-V curve be used when analyzing voltage collapse because of the strong coupling between the reactive power and the voltage.

CASE 4.2

In this case, a different type of a Q-V curve will be used to determine the minimum reactive power requirement at the load in order to prevent voltage collapse. A source of reactive power is simulated at the load bus and the voltage is decremented in small steps while monitoring the reactive power. The results are shown in figure 4.13 :

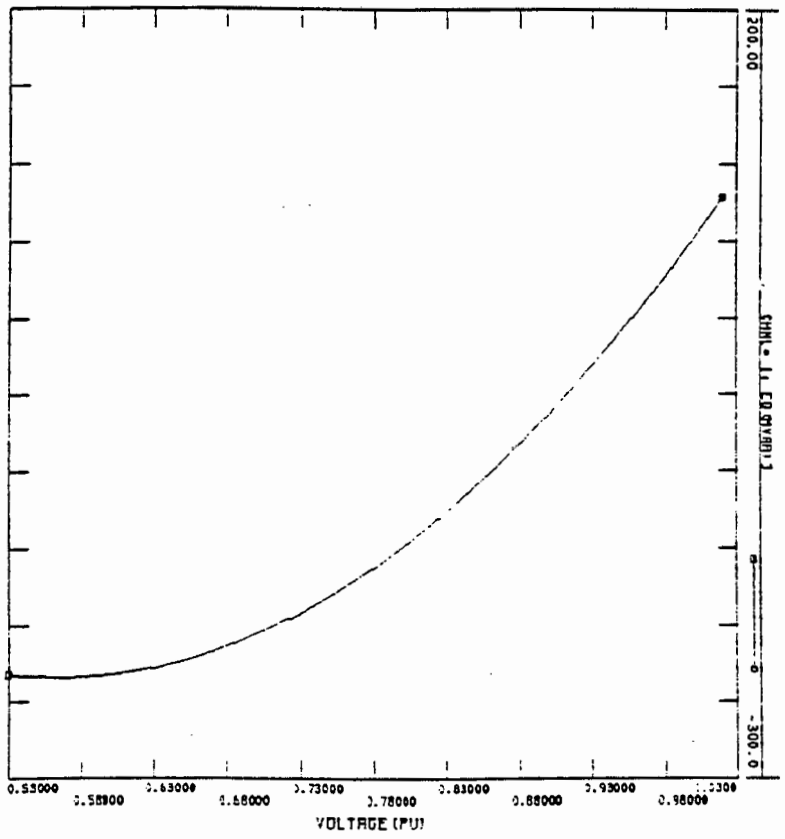

Figure 4.13:
Q-V curve to determine minimum Q requirements at a bus in order to prevent voltage collapse

Figure 4.13 shows that as the voltage is decreased, the reactive power requirement at the load bus increases. Decreasing the voltage even further reduces the reserve of available reactive power resources. When there is no more reactive power reserves, a slight reduction of voltage will result in voltage collapse. This occurs at the knee point (minimum point) of the Q-V curve. The voltage at this point is 0.55 pu and the reactive power shortage is -228 MVAR.

This amount of reactive power is then compared to the available reactive power resources. If the resources are not adequate to meet this requirement, then there is a risk of loosing voltage stability. In order to prevent voltage collapse, a reactive power injection of 228 MVAR would be required at the bus.

CASE 4.3

In this case the effects of changing the transformer tap position on voltage stability will be investigated. The diagram of figure 4.14 will be used for this purpose.

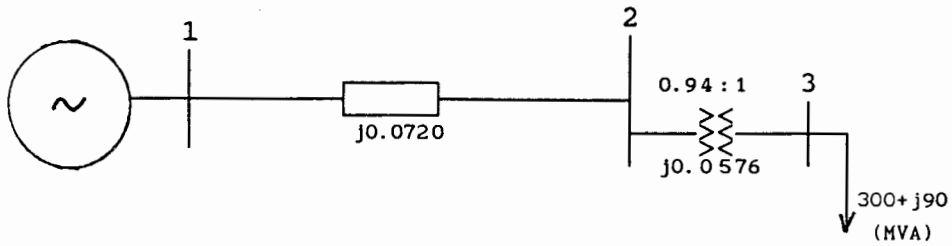

Figure 4.14 :
Load tap changer example

Figure 4.15 shows the P-V curve for an increase in the active power of the load only, with the taps of the transformer locked at their initial position. The loadflow results for the initial and knee point conditions are given in table 4.5.The initial voltage magnitude is 0.97 pu and the voltage magnitude just before collapse is 0.77 pu. The load increase at the knee point of the P-V curve (i.e just before collapse) is 61 % from the initial load of 300 MW.

Table 4.5 : Loadflow results for initial and knee point conditions (fixed transformer taps)

Bus Number	Voltage (pu)	Angle deg	Active power	Reactive power	Tap ratio	
2 3	0.935 0.971	-12.7 -17.2	0.0 300.0	0.0 90.0	0.938	Initial conditions
2 3	0.769 0.777	-25.5 -36.5	0.0 438.7	0.0 90.0	0.938	Knee point conditions

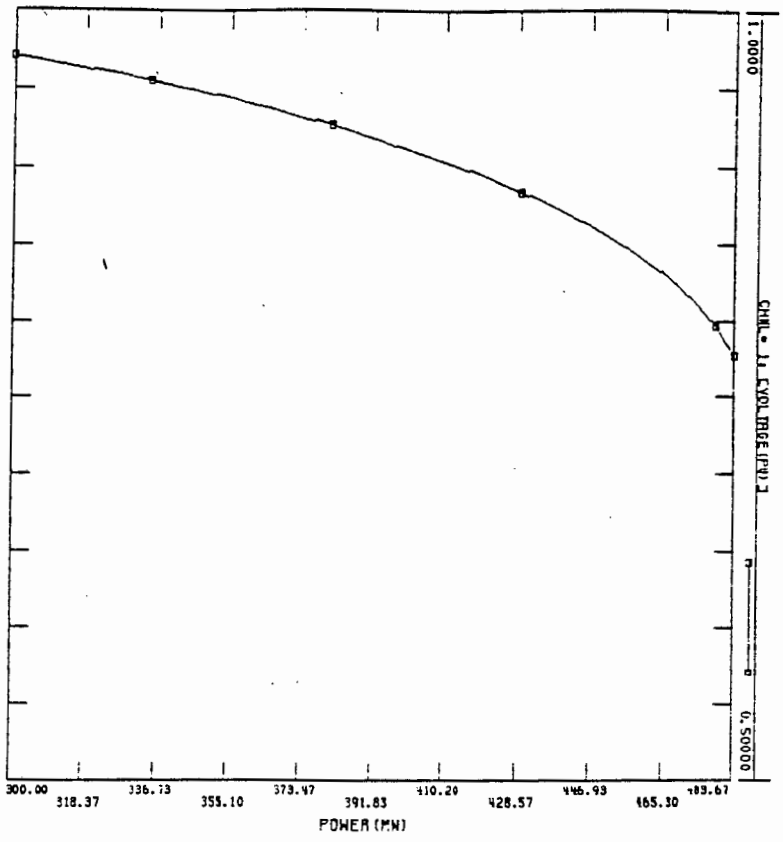

Figure 4.15:
P-V curve with transformer taps locked

Figure 4.16 shows the P-V curve for the case where the taps are allowed to vary. The initial voltage magnitude is the same as before at 0.97 pu. The transformer taps are allowed to vary to +/- 15 % of the nominal tap (usually 1 pu), and regulate the load voltage to a minimum of 0.95 pu and a maximum of 1.05 pu. The loadflow results are given in table 4.6.

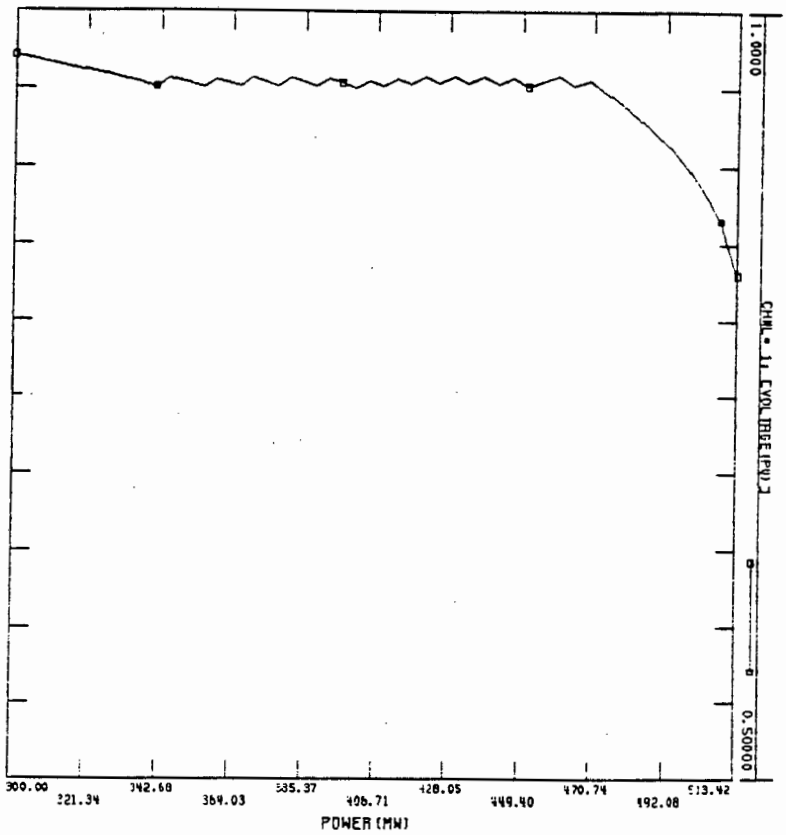

Figure 4.16:
P-V curve showing transformer taps adjustment

Table 4.6 : Loadflow results for initial and knee point conditions (transformer taps not fixed)

Bus Number	Voltage (pu)	Angle deg	Active power	Reactive power	Tap ratio	
2 3	0.935 0.971	-12.7 -17.2	0.0 300.0	0.0 90.0	0.938	Initial conditions
2 3	0.739 0.829	-25.5 -38.7	0.0 513.4	0.0 90.0	0.850	Knee point conditions

Figure 4.16 shows that after a load increase of 13 % i.e at 340 MW, the load voltage is close to the minimum limit specified for regulation. Step changes of the taps are ordered and the load voltage increased above 0.95 pu. A further increase of load causes the voltage to drop and thus more step changes are ordered.

This process is repeated until the tap reach their limit. This occurs when the load increase is 57 % (470 MW) higher than the initial load. Beyond this point, no further voltage control is possible and the voltage collapses rapidly. The voltage magnitude before collapse is 0.83 pu with a load increase of 71 %. The rate of change of voltage to an increase in power, when the taps have reached the upper limit, is greater than that of figure 4.16.

Comparing figures 4.15 and 4.16, the effects of the transformer tap adjustment on voltage collapse, can be clearly seen. When the taps are adjusted, voltage collapse occurs at a higher level of secondary voltage, because the changing taps try to improve the voltage at the load side without considering the availability of reactive power resources in the system.

Figure 4.17 shows the P-V curves for the high voltage and the low voltage side of the transformer. Monitoring only the low voltage side of the transformer, can give the impression that the system is far from voltage collapse. This may subsequently delay the appropriate control action necessary to prevent voltage collapse. Monitoring the high voltage side of the transformer, provides an indication of the change in voltage, hence appropriate control action may be taken to prevent the rapid slide of voltage into collapse.

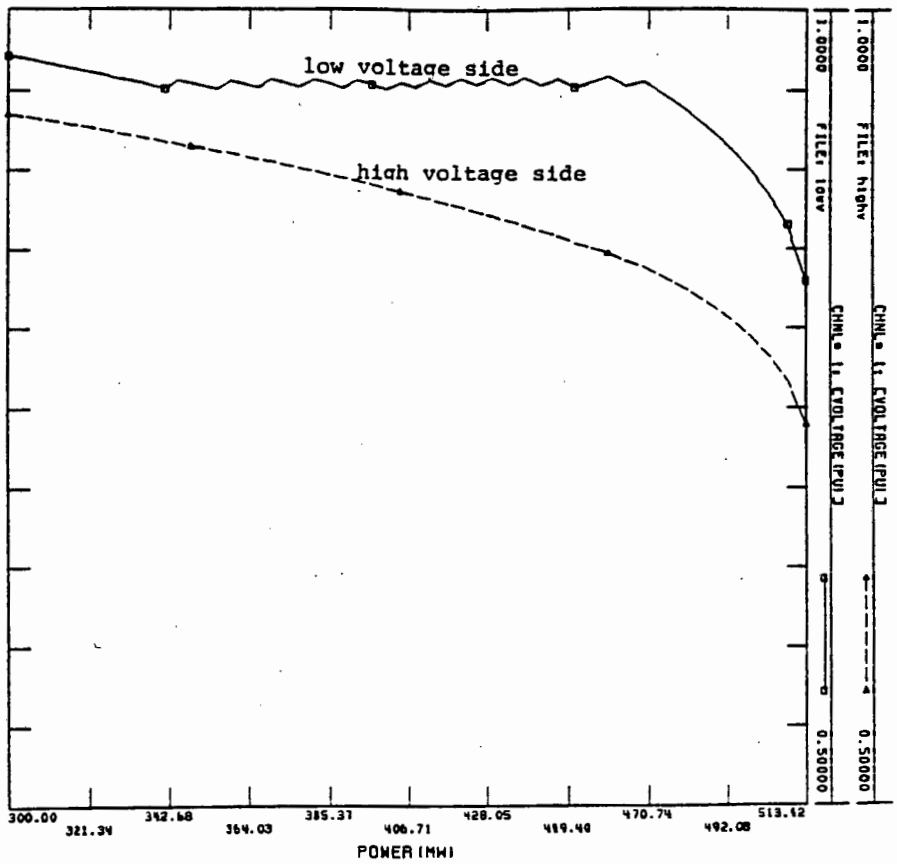

Figure 4.17 :
P-V curve for the low and high voltage side
of the transformer

The same procedure as in cases 4.1 to 4.3 can be used to study voltage stability in a complex multi-machine system. The difference is that in this case, sensitivity analysis must be performed to determine the bus with the greatest sensitivity of voltage to changes in power. This analysis will indicate the area from which voltage instability is likely to begin.

The ninebus example of Appendix 1 will now be used to simulate voltage instability. A sensitivity analysis, performed on the industrial-grage software package POWSYS,has shown that when the system load is increased, the voltage drop at bus 5 is the most sensitive to this change. This is an indication that voltage collapse due to load increase, will most likely occur at bus 5. Table 4.7 shows the loadflow results for the knee point conditions. See Appendix 1 for the initial condition loadflow results.

Table 4.7 : Loadflow results for the knee point conditions

Bus Number	Voltage (pu)	Angle deg	Active power	Reactive power
1	1.040	0.0		
2	1.025	-46.0		
3	1.025	-49.5		
4	0.852	-24.5		
5	0.778	-50.0	331.4	50.0
6	0.808	-46.5	238.6	30.0
7	0.950	-52.0		
8	0.925	-59.4	265.2	35.0
9	0.963	-52.4		

Figure 4.18 shows the P-V at bus 5 for changing loads. Voltage collapse occurs when the voltage is at 0.78 pu at a loading of 165 % above the normal base loading.

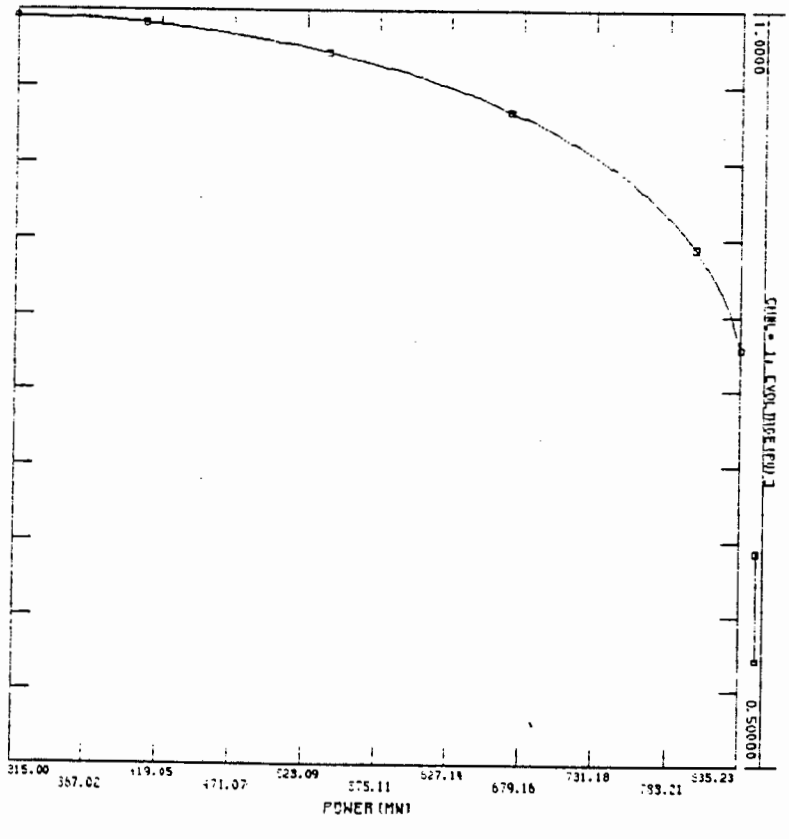

Figure 4.18:
P-V curve for load at bus 5

The minimum reactive power requirements at bus 5 are shown in figure 4.19. This figure shows that in order to avoid voltage collapse in the network, the available reactive power resources must be capable of providing 220 MVAr.

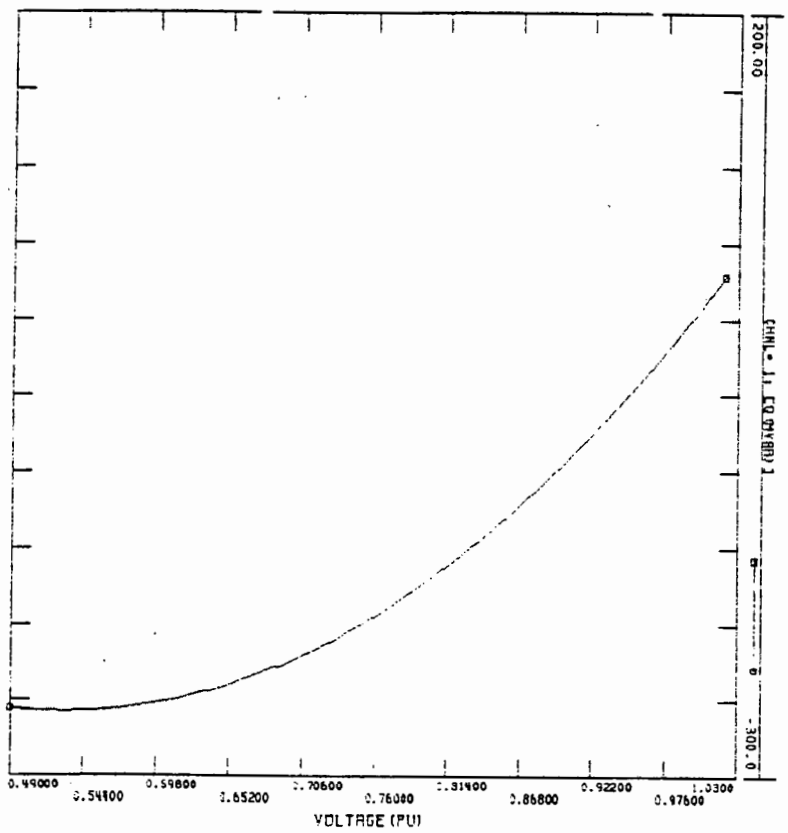

Figure 4.19 :
Minimum Q requirements at bus 5

4.5. SUMMARY

The review of the literature has indicated that the research on the causes of voltage instability and the measures used to guard against voltage collapse has not been exhausted yet. There is a general consensus however, that some of the causes of voltage instability are:

1. the shortage of reactive power support
2. the uncoordinated change of the transformer taps
3. the transfer of large amounts of power over long high voltage transmission lines.

Most of the available literature, studied voltage instability from the static point of view. They cited the singularity of the Jacobian matrix as a suitable indicator to voltage collapse. There are various papers however, which have pointed out that voltage instability could also be caused by the dynamic behavior of generators, loads and control equipment. To study the dynamic behavior, these papers used the state space technique and they cited the eigenvalues of the linearized "A" matrix as an indicator of voltage instability.

Voltage stability was shown to have a close relationship with multiple load flow solutions which occur when the power system is heavily loaded.

The steady state analysis of voltage stability was shown to have some shortcomings because erroneous conclusions about the system stability could be made. The most important fact highlighted was that both the steady state and dynamic aspects of voltage stability need to be considered in order to have an understanding of the voltage stability problem.

Case studies were performed using a single machine and a load, and a ninebus three machine system, to determine the occurrence of voltage instability. It was shown that increasing parameters

such as active and reactive power of the load, could cause voltage collapse in a network.

The results have also shown that voltage collapse is related to heavy loading network conditions. The use of uncoordinated transformer taps was also shown to accelerate the collapse of voltage.

CHAPTER 5 : MOTOR STARTING AND VOLTAGE DIPS

5.1 INTRODUCTION

In this chapter, the effects of voltage dips on the behavior of large motors will be investigated. Voltage dips, of different magnitude and duration will be applied on a simple network, and the behavior of the motors will be observed. In addition, the factors affecting induction motor starting and the motor performance during starting are discussed.

Voltage dips occur randomly on a power system. Their magnitude and duration depends on the type of the disturbance applied. It is thus difficult, from the planning point of view, to know beforehand what types of voltage dips will affect the power system and which dips will have damaging effects on the motors.

It is therefore necessary to analyze the effects of a wide range of voltage dips for different durations. Adequate protection schemes can then be designed to prevent subsequent damage to the motors.

In industrial plants where more than 75 % of the loads are dynamic (i.e induction and synchronous motors), the problem of starting large motors is of concern. A typical industrial power plant problem would be to ensure that when starting a large motor, the other motors which are connected in parallel to the motor being started, do not stall. The concept of load stability stems from this problem.

The chapter begins by investigating the behavior of large induction motors under starting conditions. Next, the factors which affect induction motor starting are investigated. A simple network is used for this purpose. Furthermore, voltage dips of different severity and duration are simulated and the induction motor behavior is observed. Finally, a summary of the chapter is provided at the end.

5.2 INDUCTION MOTOR STARTING

The starting and running characteristics of induction motors depend mainly upon the design and construction of the rotor. The rotor is constructed such that the starting current is as low as possible and the starting torque high. There are two basic types of rotor construction namely, the squirrel cage rotor and the wound rotor.

In the squirrel cage rotor, uninsulated bars are inserted into slots, and are laid axially or skewed at a slight angle across the core. These bars are short-circuited at both ends of the rotor. In the wound rotor, thoroughly insulated windings are placed in the slots with the terminal ends of each phase fastened to slip rings.

The squirrel cage rotor design is preferred because of its simplicity and the fact that the motor can provide long, reliable service at a relatively low cost. This type of motor is thus a general purpose machine for applications not requiring variable drives.

Large squirrel cage induction motors are usually fitted with a second cage to enhance starting characteristics. The advantages of single-cage and double cage induction motors were discussed in chapter 3.4.2.2. This type of rotor construction enables direct-on-line starting, the most severe form of starting which requires large amounts of starting torque and reactive power.

Other starting methods namely : the star-delta switching, the use of auto transformers and primary resistors are necessary in order to limit the starting current. These methods however, also reduces the starting torque which is undesirable.

Figure 5.1 shows the network used to determine the behavior of large induction motors under starting conditions. The simulation conditions are as follows:

(a). A 15.3 MVA induction motor is connected to bus 2 through a transformer.

(b). The motor is modeled by a double cage equivalent circuit.

(c). The motor is started direct on line at time t = 0 sec.

(d). The driven load torque is a quadratic function of speed i.e. $T_m = a + b\omega + c\omega^2$ and $T_m(0) = 1$ pu.

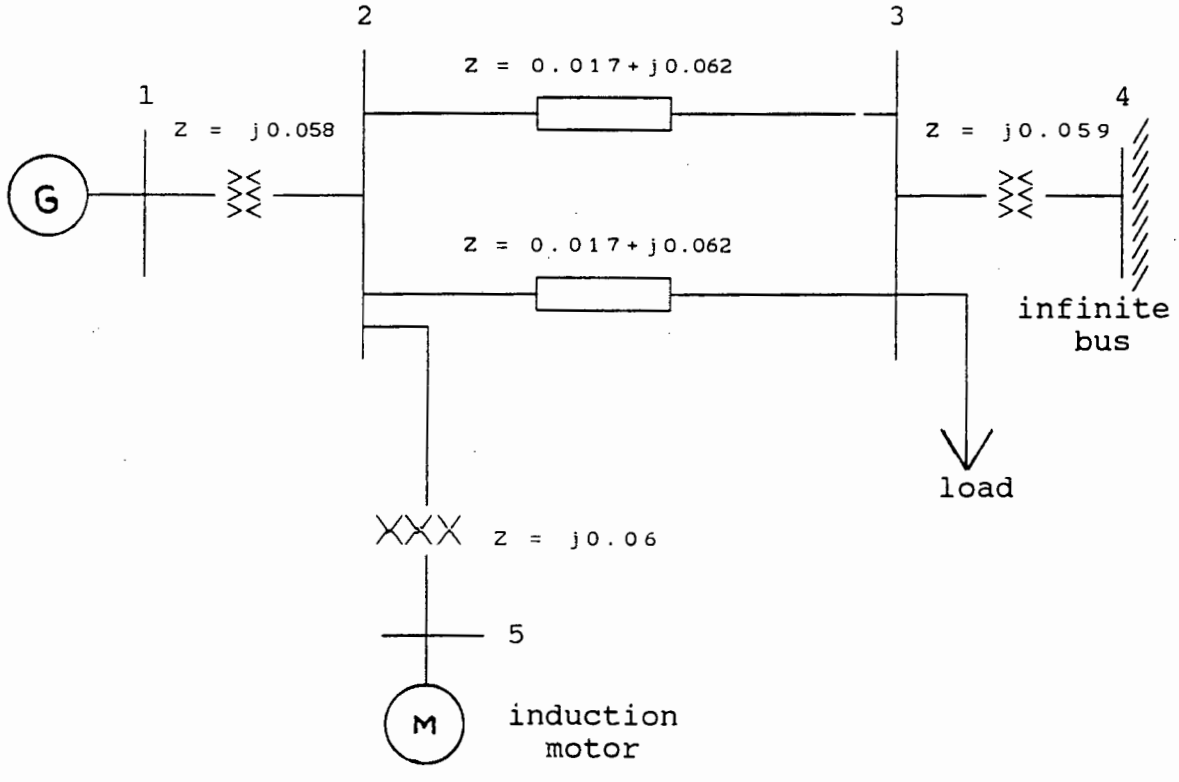

Figure 5.1 :
Network example used for motor starting
showing branch impedance

The results are shown in figure 5.2. Immediately upon switching, the voltage at the motor terminal dropped by 10 %. This low voltage is maintained until the motor electrical torque is equal to the load mechanical torque. It took 18 seconds for the motor to reach full load conditions.

Figure 5.2 shows that during switching, the active power drawn by the motor increases to 53 % of the full load power and continues to increase during the starting period. At 15 seconds, the motor draws full load power but continues to accelerate because the developed electrical torque is still less than the required torque to drive the load. The active power then overshoots the full load value by 133% for only 3 seconds before the voltage recovers. The motor reaches full load conditions after 18 seconds from starting.

The reactive power drawn by the motor during starting is very high (about 10.2 times the full load value). This amount of reactive power is drawn until the motor reaches full load conditions. The current drawn by the motor is also very high and may cause permanent damage to the motor by overheating the windings. Any type of thermal protection designed for the motor must be able to withstand these large currents.

The slip of the induction motor is initially at unity before starting. After starting, the slip then decreases almost linearly with increasing time until full load conditions, where the slip is very small (1% in figure 5.2 above).

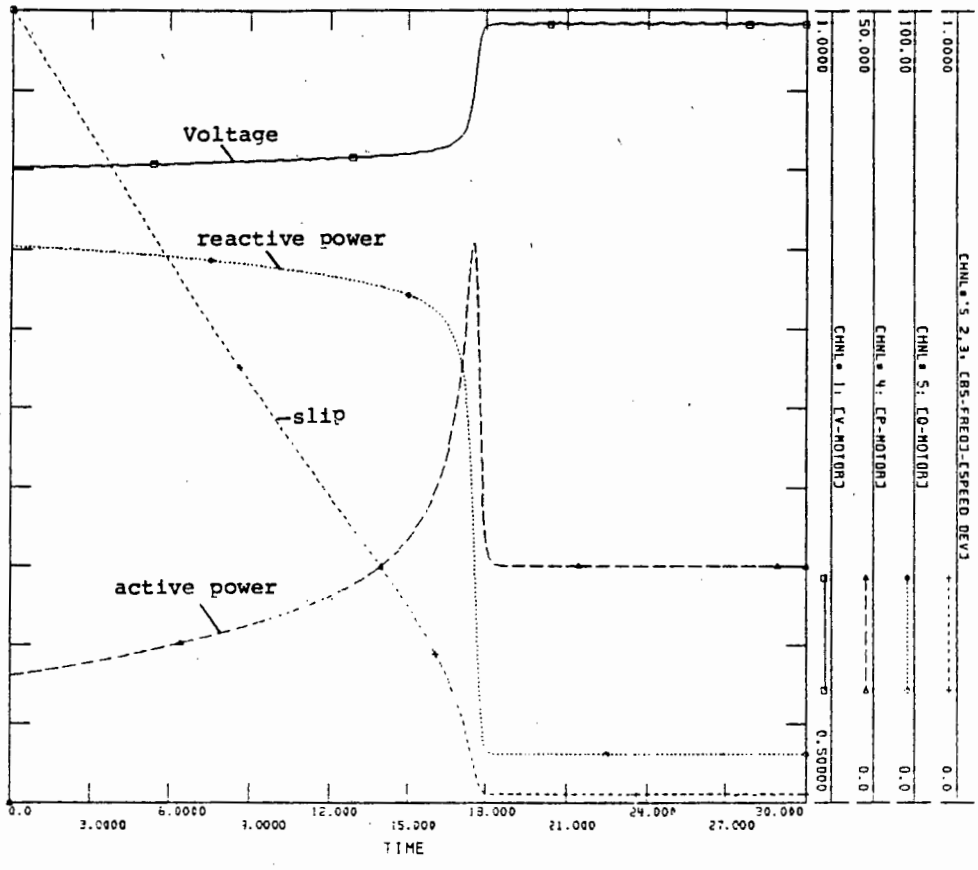

Figure 5.2:
Induction motor behavior during starting

The factors affecting induction motor starting time are discussed below :

5.2.1 Factors affecting induction motor starting time

There are various factors which affect the starting time of the induction motor. These are the type of the drive load (i.e. either a pump or fan etc), the amount of load at starting (either full load or fraction thereof), the MVA rating of the machine, the reactance of the feeder transformer and the torque/slip characteristics of the motor itself.

The different types of loads can be modeled by varying the exponent (D) of the mechanical torque equation $T_m = (a + b\omega)^D$, where a and b are constants.

Figure 5.3 shows the effect of the type of load on the starting time. The motor started within 18 seconds for the load torque/slip relation of the second order. When the exponent was changed to 1.5, the motor took 21 seconds to start and for a linear load (exponent of 1), the motor took 31 seconds to start. Thus the type of load can affect the starting time to a large extend.

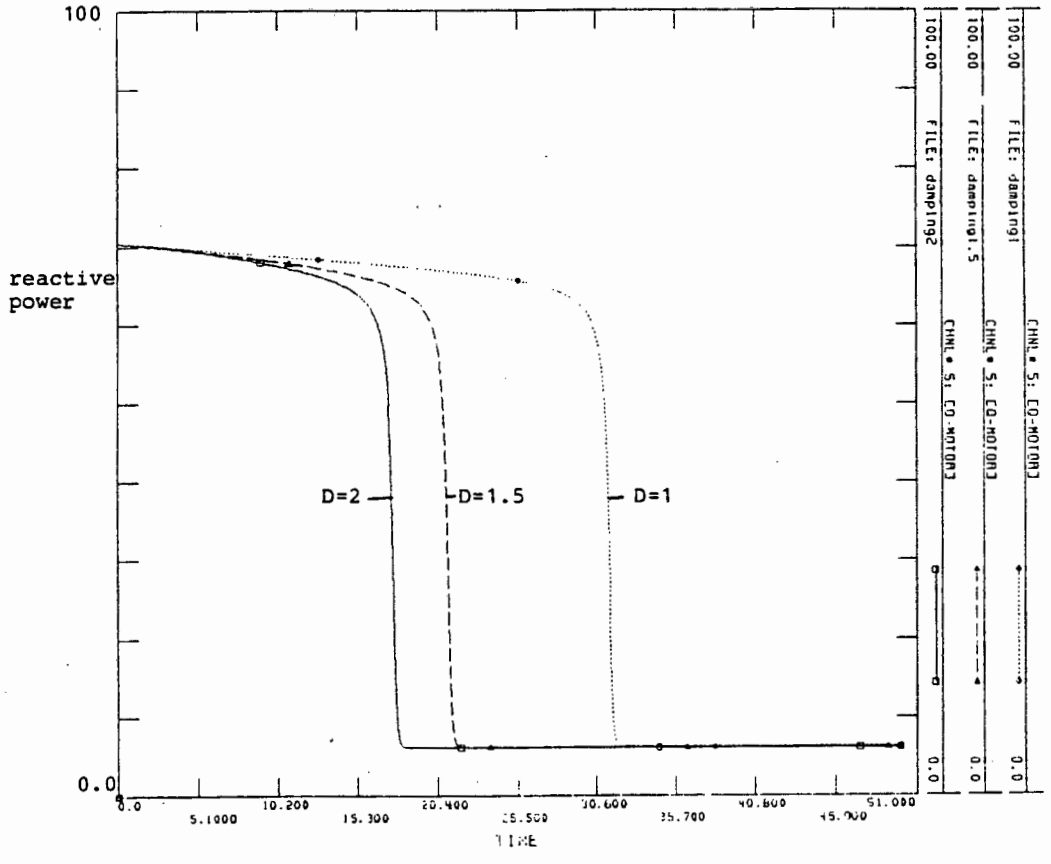

Figure 5.3:
Influence of the load type on the starting time

Figure 5.4 shows the effect of the motor rating on the motor starting time. The inertia of the machine is kept constant for different machine ratings. A 20.3 MVA motor took 20 seconds to start as compared to 18 seconds for 15.3 MVA motor and 16 seconds for a 10.3 MVA motor. Thus the higher the motor MVA rating, the longer it takes the motor to start.

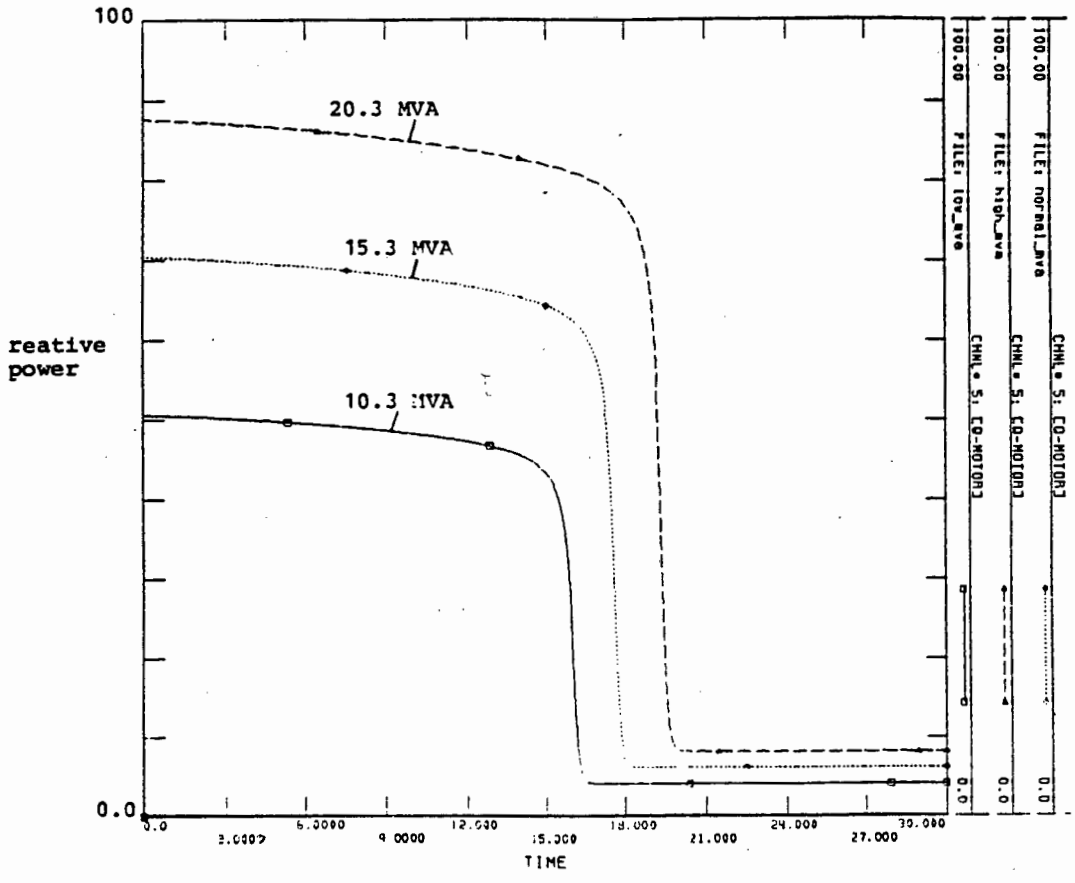

Figure 5.4:
Influence of the motor rating on the starting time

Figure 5.5 shows the effect of the initial load torque on the motor starting time. The longest starting time of 18 seconds occurred when the motor is started with full load torque. When the motor is started with 75% of full load torque, the starting time reduced to 16 seconds and for 50% of full load torque, the starting time reduced to 14.5 seconds.

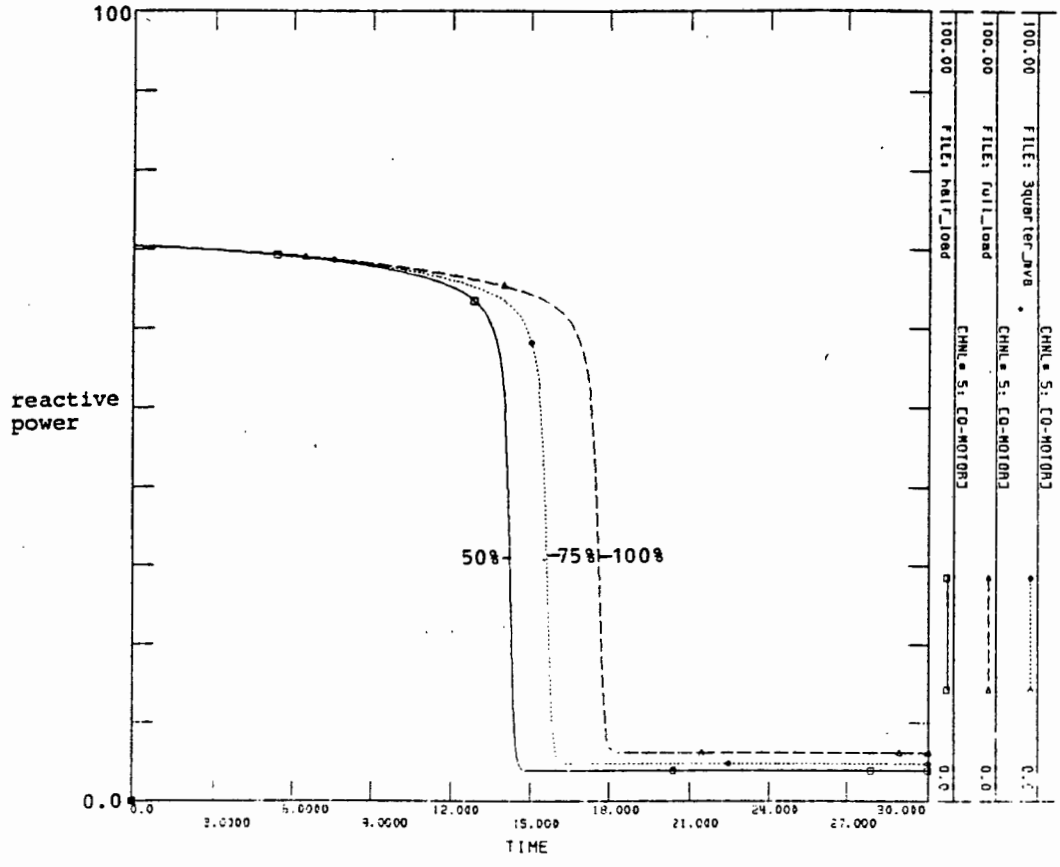

Figure 5.5:
Influence of initial load torque on starting time

Figure 5.6 shows the effect of the transformer reactance on motor starting. A 3%, 6% and 9% transformer reactance, on transformer MVA base, were used to simulate their effects on the starting time. The highest reactance of 9% had the effect of increasing the starting time to 19.5 seconds. For the 6% reactance, the motor took 18 seconds to reach running conditions and for the 3% reactance, 16.5 seconds.

Thus the motor with the highest transformer reactance will take longer to reach full load conditions.

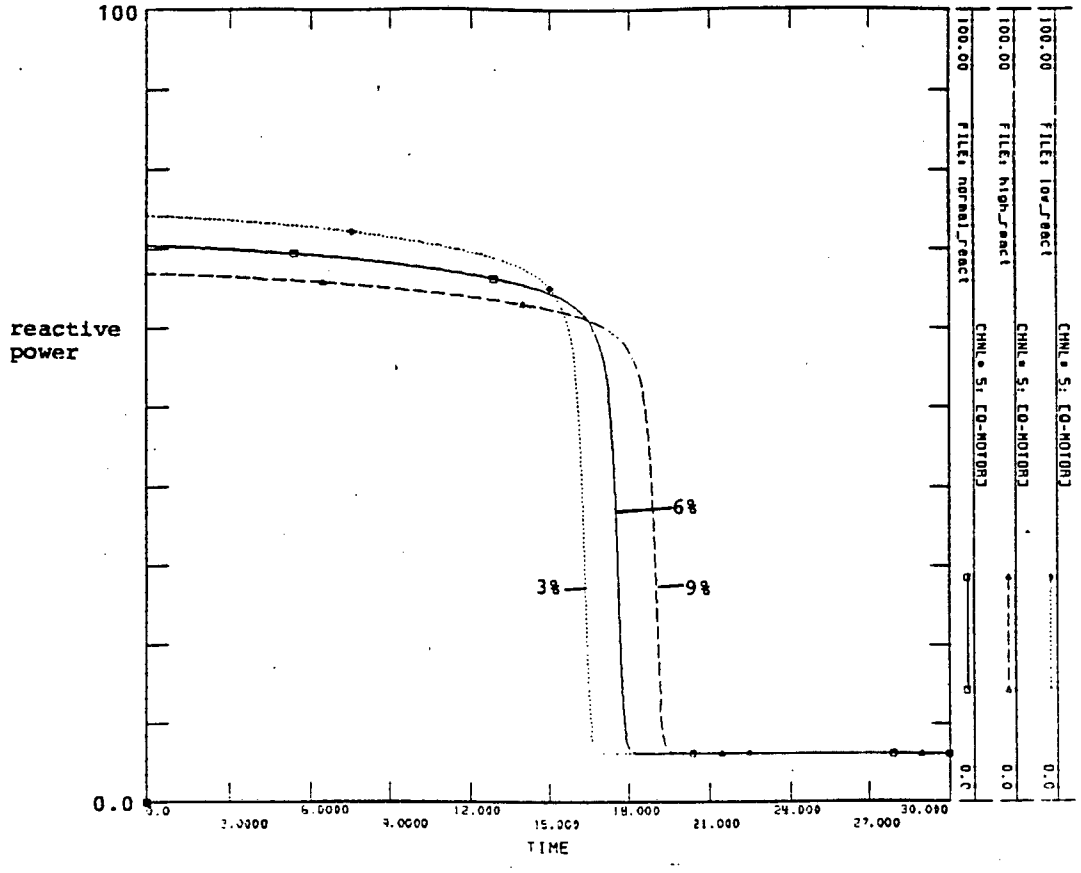

Figure 5.6:
Influence of the transformer reactance on
the motor starting time

5.3 EFFECTS OF VOLTAGE DIPS ON THE MOTOR BEHAVIOR

In this section, figure 5.1 will be used to determine the effects of different voltage dips, lasting for different duration, on the induction motor performance. A voltage dip is simulated on bus 2 (figure 5.1) as a three-phase fault through an impedance. This impedance is varied to obtain different dips. The damping due to the load attached to the motor is not modeled.

Figure 5.7 shows the slip of the induction motor when it is subjected to different voltage dips for 1 second. The motor can withstand a 10% voltage dips within 1 seconds. The slip increases by 0.2% during this dip and remains constant during the dip. When the voltage recovers, the slip then returns to its initial value. For a 20% dip, the slip increases by 0.6% and returns to its initial value after voltage recovery. The motor can also withstand this dip for 1 second.

A 50% dip caused the motor slip to rise with no sign of reaching a constant value during the dip. The slip increased by 4% within 1 second. After the voltage recovers, the slip returns to its initial value with small oscillations (less than 0.2%). Depending on the application of the motor, these small oscillation may or may not be acceptable.

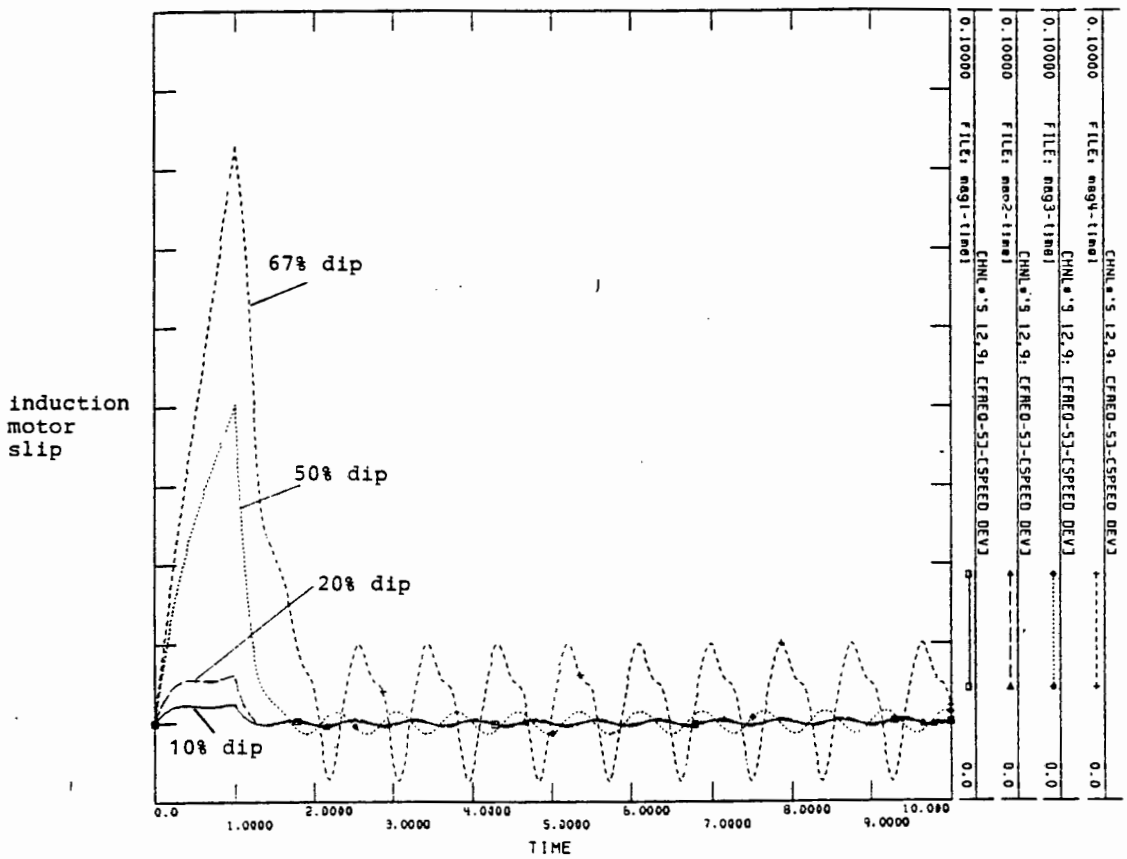

Figure 5.7:
Motor slip under different voltage dips for 1 second

A 67% voltage dip caused the motor slip to rise sharply for the duration of the dip, increasing by more than 7% within 1 second. The motor cannot survive this dip because after the voltage recovered, the oscillations of the slip are large (about 1%) and do not show any sign of dying down after 10 seconds. Pulsating torques will be produced at the shaft and the motor may stall. The motor cannot withstand voltage dips larger than 50% within 1 seconds.

Figure 5.8 shows the slip of the induction motor subjected to a 90 % voltage dip lasting for different durations. This motor can withstand a voltage dip of 90 % for 0.2 seconds. As the duration of the dip is increased, the motor slip oscillates with increased amplitudes. For a 90 % dip lasting for 0.5 seconds, the slip initially increases to 6 % when the voltage recovers and then decrease momentarily. The slip increases again showing that the motor would stall.

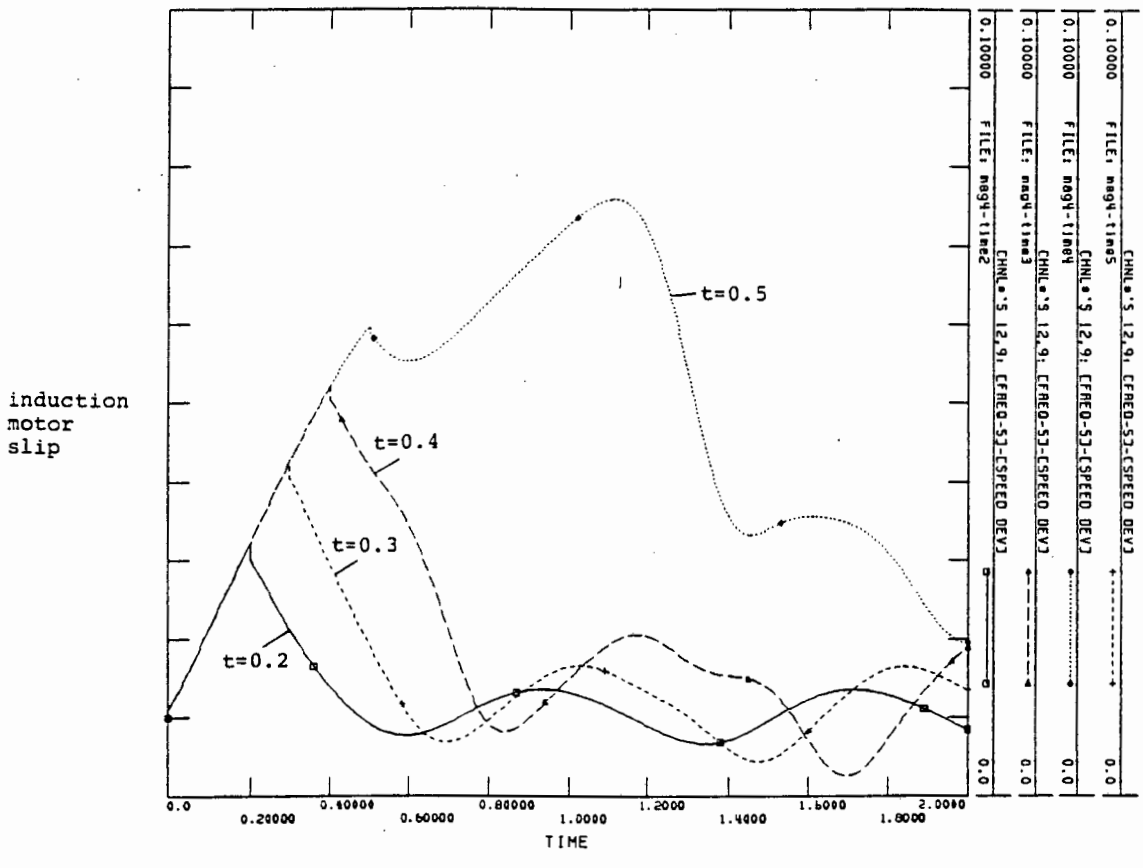

Figure 5.8 :
Motor slip for 90 % dip for different durations

5.4 SUMMARY

This chapter investigated the behavior of large induction motor under starting conditions. Starting a large motor causes voltage dips which last for a relatively long time. It is thus necessary to perform voltage dips studies to ensure that the other motors connected in parallel with the motor being started, do not stall.

The factors that can affect the starting duration of induction motors were shown to be the type of driven load, the rating of the motor, the amount of load at starting and the reactance of the motor transformer.

Voltage dips studies were also performed to determine the strength of the induction under the dips of different magnitudes and durations. The slip was used as an indicator of stability.

CHAPTER 6 : GENERAL CONCLUSIONS AND SCOPE FOR FUTURE RESEARCH

6.1 GENERAL CONCLUSIONS

The main conclusions of this thesis can be briefly stated as follows :

1. The different generator models used, produced different transient stability results. The results obtained by using the models are as follows :

   model 0.0 - most optimistic
   model 1.0 - most conservative
   model 2.1 - conservative and
   model 2.2 - optimistic

2. Model 0.0 must only be used for the first swing transient stability study.

3. Model 1.0 should be used only when the detailed parameters of the machine are not known.

4. Model 2.1 represents limited damping due to the currents in the rotor slots. This model should be used for representing hydrogenerators.

5. Model 2.2 represents more damping due to the currents in the rotor slots. The model should be used for representing turbogenerators without damper windings.

6. Modeling a local load as constant admittance gives more conservative transient stability results, than when the load is modeled as constant power. **Thus a local load should be modeled as constant admittance.**

7. Modeling a remote load as constant admittance gives more optimistic transient stability results, than when the load is modeled as constant power. **Thus a remote load should be modeled as constant power.**

8. When using static load models such as constant power, constant current and constant admittance, the **relationship between the load model, the location of the load and the location of the fault should be considered.**

9. The frequency dependency of the load contributes only to the system damping. The transient stability results are conservative when frequency dependency of the load is neglected. Thus the frequency dependency of the load can be neglected in transient stability studies.

10. Modeling an induction motor with its transient model gives conservative transient stability results.

11. The steady-state model for the induction motor should not be used to model the motor when performing transient stability studies.

6.2 SCOPE FOR FUTURE RESEARCH

More research work is still needed to investigate the following :

1. The effects of induction motor characteristics on the system dynamic stability.

2. The dynamic aspect of voltage stability. A software program should be developed.

3. The relationship between multiple loadflow solutions and voltage collapse.

4. The relationship between the eigenvalues of system state matrix "A" and the determinant of the Jacobian matrix [J].

APPENDIX 1: NINEBUS BENCHMARK NETWORK PARAMETERS

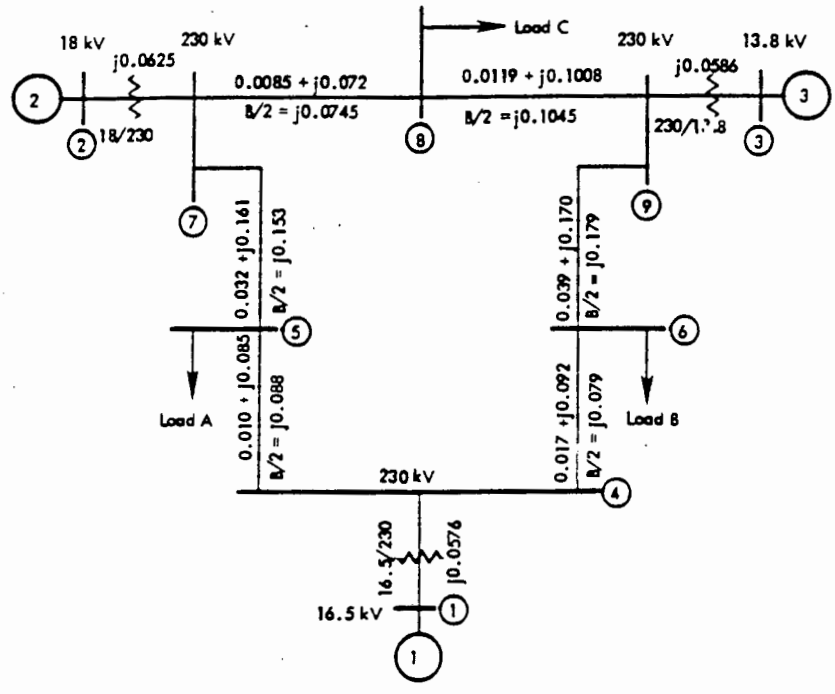

Figure A1.1 :
Impedance diagram; all impedances are in pu on 100 MVA base

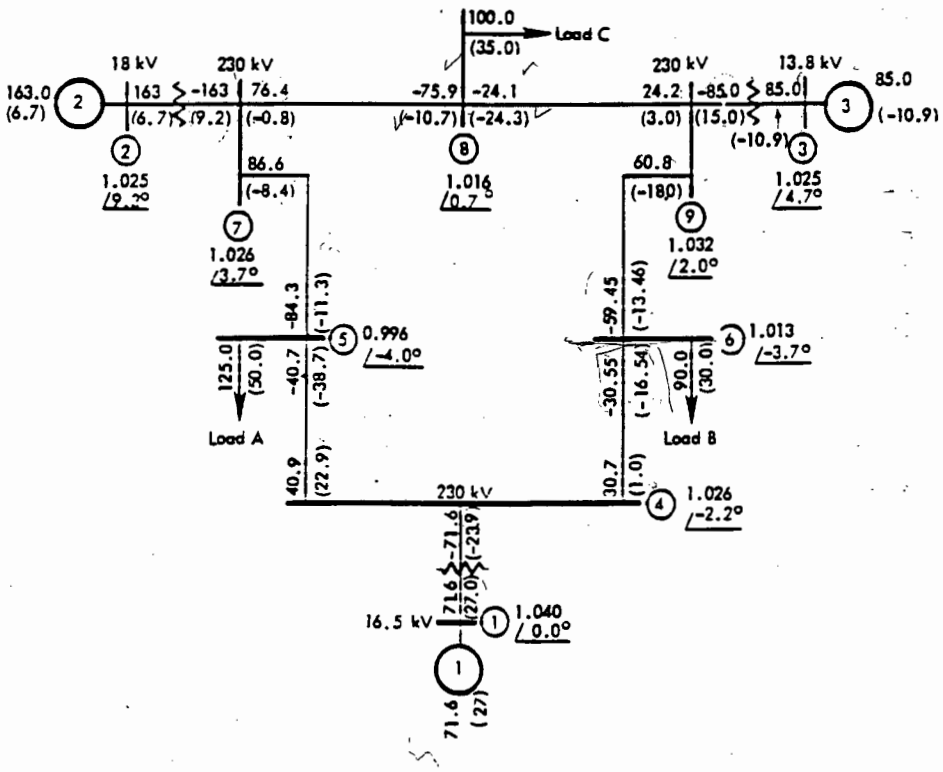

Figure A1.2 :
Prefault loadflow solution for ninebus system;
flows are in MW and MVAR

Table A1.1 : Generator data

Generator	1	2	3
Inertia H	6.396	3.302	2.3828
Speed damping D	0.00	0.00	0.00
X_d	1.581	1.651	1.680
X_q	1.531	1.59	1.610
X'_d	0.380	0.232	0.232
X'_q	0.955	0.380	0.320
X''_d	0.252	0.171	0.171
X''_q	0.248	0.171	0.171
X_l	0.291	0.102	0.095
T'_{d0}	5.390	5.9	5.890
T'_{q0}	1.500	0.535	0.600
T''_{d0}	0.053	0.033	0.034
T''_{q0}	0.135	0.078	0.080
S(1.0)	0.0905	0.105	0.121
S(1.2)	0.345	0.477	0.610

APPENDIX 2 : MATHEMATICAL EXPRESSIONS FOR INDUCTION MOTORS

A2.1 INDUCTION MOTOR MODELS

Before developing the induction motor models, it is imperative to understand the following concepts which will be used when developing these models.

(a) The transformation from a-b-c system to d-q axes system.
(b) The theory of neglecting the stator transients.
(c) The accuracy of the reduced order model
These three concepts are discussed below separately.

A2.1.1 The transformation from a-b-c to d-q axes

In this section reference frames will be employed to show that the DC circuit theory may be used to determine the performance of induction machines. This method offers a rigorous means of analyzing electrical transients due to applied voltage of any periodic form.

Consider a two pole,three-phase symmetrical induction machine in figure A2.1. The stator and rotor are connected as a three-wire system.

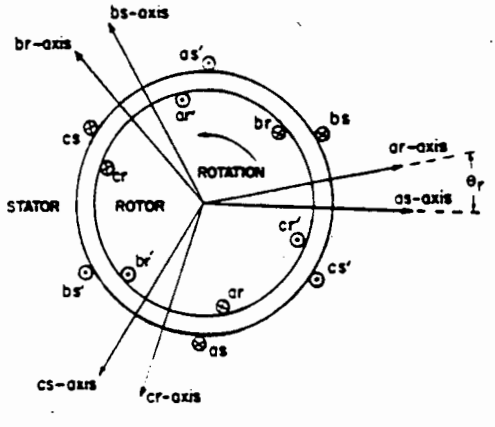

figure A2.1
Two pole, three-phase, symmetrical induction machine

The flux-linkage equations can be written [56] as follows:

$$\begin{bmatrix} \psi_{as} \\ \psi_{bs} \\ \psi_{cs} \\ \psi_{ar} \\ \psi_{br} \\ \psi_{cr} \end{bmatrix} = \begin{bmatrix} L_{ss} & 0 & 0 \\ 0 & L_{ss} & 0 \\ 0 & 0 & L_{ss} \\ L_{sr}\cos\theta_r & L_{sr}\cos(\theta_r-2\pi/3) & L_{sr}\cos(\theta_r+2\pi/3) \\ L_{sr}\cos(\theta_r+2\pi/3) & L_{sr}\cos\theta_r & L_{sr}\cos(\theta_r-2\pi/3) \\ L_{sr}\cos(\theta_r-2\pi/3) & L_{sr}\cos(\theta_r+2\pi/3) & L_{sr}\cos\theta_r \end{bmatrix}$$

$$\begin{bmatrix} L_{sr}\cos\theta_r & L_{sr}\cos(\theta_r+2\pi/3) & L_{sr}\cos(\theta_r-2\pi/3) \\ L_{sr}\cos(\theta_r-2\pi/3) & L_{sr}\cos\theta_r & L_{sr}\cos(\theta_r+2\pi/3) \\ L_{sr}\cos(\theta_r+2\pi/3) & L_{sr}\cos(\theta_r-2\pi/3) & L_{sr}\cos(\theta_r+2\pi/3) \\ L & 0 & 0 \\ 0 & L & 0 \\ 0 & 0 & L \end{bmatrix} \begin{bmatrix} i_{as} \\ i_{bs} \\ i_{cs} \\ i_{ar} \\ i_{br} \\ i_{cr} \end{bmatrix}$$

.....(A2.1)

where $L_{ss} = L_s - L_{sm}$ is the stator phases mutual coupling

$L_{rr} = L_r - L_{rm}$ is the rotor phases mutual coupling

The mutual inductances between stator phases and between rotor phases vary sinusoidally with the rotor phase displacement. This will cause the time-varying coefficients to appear in the voltage equations. This feature is undesirable and can be eliminated by transforming the rotor and stator voltages to a common frame of reference.

In common cases, the induction motor analysis is performed in a synchronous reference frame or in a stationary reference frame. It is convenient however, to develop the equations in an arbitrary frame of reference and from these to obtain equations

in a specific reference frame. Figure A2.2 below shows the axis of two-pole, three-phase symmetrical induction machine with the orthogonal set (d,q axis) rotating at an arbitrary angular velocity ω included.

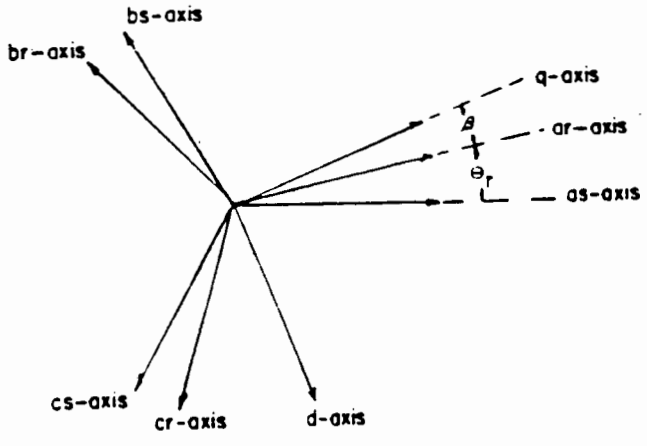

figure A2.2
Axis of two-pole, three-phase symmetrical machine

The transformation equation to direct and quadrature axes are written as follows:

(i) Stator transformation

$$f_{qs} = 2/3 \left[f_{as}\cos\theta + f_{bs}\cos(\theta - 2\pi/3) + f_{cs}\cos(\theta + 2\pi/3) \right]$$

$$f_{ds} = 2/3 \left[f_{as}\sin\theta + f_{bs}\sin(\theta - 2\pi/3) + f_{cs}\sin(\theta + 2\pi/3) \right]$$

$$f_{0s} = 1/3 \left[f_{as} + f_{bs} + f_{cs} \right] \qquad \text{.....(A2.2)}$$

(ii) Rotor transformation

$$f_{qr} = 2/3 \left[f_{ar}\cos\beta + f_{br}\cos(\beta-2\pi/3) + f_{cr}\cos(\beta+2\pi/3) \right]$$

$$f_{dr} = 2/3 \left[f_{ar}\sin\beta + f_{br}\sin(\beta-2\pi/3) + f_{cr}\sin(\beta+2\pi/3) \right]$$

$$f_{0r} = 1/3 \left[f_{ar} + f_{br} + f_{cr} \right] \qquad \text{.....(A2.3)}$$

where $\beta = \theta - \theta_r$

In these expressions f can represent either voltage, current or flux linkages. The transformation equations are valid regardless of the of the form of the voltages and currents in the stator and the rotor. For balanced conditions, the third equation in both the stator and rotor transformations above becomes unnecessary because three voltages or currents would be defined by any two.

The induction motor equations will be derived later in this section by using these transformations.

A2.1.2 The justificationfor neglecting the stator transients

Various simplified methods of predicting the dynamic behavior of induction machines have been investigated [18],[19],[27]. Neglecting the stator transients reduces the order of the model and still provides a fairly accurate representation of the dynamic behavior of the induction motor as compared to the complete model [28],[29]. Some insight is needed however, to determine the effect of neglecting the stator transients on the reduced order model.

The principal effect of the stator transients is to introduce a DC-offset in the armature currents and flux linkages as a result of magnitude changes in stator voltages.When a short circuit occurs at or near the load, the voltage magnitude will change rapidly and considerably. The stator currents expressing this condition (assuming no losses) contains three components: a

fundamental frequency component, a DC component and a double-frequency component expressed as [30]:

$$i_a = \sqrt{2}\frac{E}{X''}\cos(\omega t + \alpha_0) - \frac{E}{\sqrt{2}}\left(\frac{1}{X'_d} + \frac{1}{X_q}\right)\cos\alpha_0$$

$$- \frac{E}{\sqrt{2}}\left(\frac{1}{X'_d} - \frac{1}{X_q}\right)\cos(2\omega t + \alpha_0) \qquad \text{.....(A2.4)}$$

An inherent assumption in the above equation is that the current does not pass through zero at the instant of the short circuit, otherwise there would be no DC component. To neglect the stator transients, the time-varying stator fluxes in the direct and quadrature axes are set to zero. The above equation could be simplified and is only represented by the fundamental frequency component as:

$$i_a = \sqrt{2}\,\frac{E}{X''}\cdot\cos(\omega t - \alpha_0) \qquad \text{.....(A2.5)}$$

This action reduces the order of the machine model as will be shown in the following sections.

A2.1.3 Accuracy of the reduced order model

Various papers stress the importance of evaluating the accuracy of the reduced induction motor models [28],[30],[31] and [32]. This evaluation is necessary in order to determine if the reduced order model would be acceptable as a close approximate of the higher order models.

It has been documented [30] that when neglecting the stator transients, the resulting reduced order model would be accurate for large induction motors (greater than 100kW) but inaccurate for small motors (less than 50kW). The modal analysis method was used to compare these results.

The modal analysis method uses the state space equations to determine the eigenvalues of the induction motor's "A" matrix. These eigenvalues define the different modes of the motor.The induction motor can be divided into three distinct modes: the stator mode,the rotor mode and the speed mode. There is a cross-coupling of the stator variables in these modes.

In the stator mode, the contribution of the stator flux linkages is higher than those of the rotor flux linkages and the speed, hence the name 'stator mode'. Similarly, in the rotor mode,the contribution of the rotor flux-linkages is greater than those of the stator flux-linkages and speed, hence the name 'rotor mode'. More detailed evaluation of the reduced order models can be carried out by using Selective Modal Analysis or SMA [30],[33].

Selective Modal Analysis is a comprehensive framework for accurate, efficient and physically-based modelling and analysis of selected portions of the structure and behavior of linear time invariant dynamic systems. With SMA the part of the model that we are interested in is singled out in a direct manner and the remainder of the model is equivalenced [16] in such a way as to leave the selected part intact.

Krause in [29] analyzes different-sized machines ranging from 3 hp to 6000 hp. (Note that the horsepower units hp are retained in this section for analysis of this reference). The eigenvalues of the reduced order models for machines that are rated above 100 hp are very close to the corresponding full models. In this case it would suffice to use the reduced order models.For small machines (less than 50 hp) however there is a large error between the full and reduced order models. Thus for small machines the stator transients should not be neglected in stability studies.

Hamdan in [30] shows how to overcome this problem by introducing compensating factors for the reduced order models. These compensation factors would 'adjust' the eigenvalues of small

machine's reduced order models to be approximately equal to the eigenvalues of the full model, while leaving the reduced ordermodel for large machines relatively unchanged. Selective Modal Analysis is used because it allows the straightforward weighting of the effects of the neglected state variables and the determination of the compensation factors for small sized motors. The method of introducing compensation factors for the reduced order models is not the subject of this study and will not be discussed any further. The next section will discuss the various induction motor models used for stability studies.

A2.2 DOUBLE-CAGE INDUCTION MOTOR

Industrial power system loads consist mainly of large induction motors. These motors are equipped with a double-cage or deep-bar rotor in order to have high starting torque and low starting current to enable direct starting. This section will develop the models for a double-cage induction machine.The following section will develop models for the single-cage induction machine.

A2.2.1 FULL 7^{th}-ORDER MODEL

The full-order model of the double-cage induction motor can be represented on a synchronous rotating reference as follows:

$$\begin{aligned} V_s &= r_s i_s + j\omega\psi_s + \dot{\psi}_s \\ 0 &= r_r i_r + js\omega\psi_r + \dot{\psi}_r \\ 0 &= r_R i_R + js\omega\psi_R + \dot{\psi}_R \end{aligned} \qquad \text{.....(A2.6)}$$

where the voltage, currents and flux-linkages are time-dependent, complex variables and related to the real variables by

$$f = f_d - jf_q \qquad \text{.....(A2.7)}$$

with f representing voltage, current or flux-linkage and d,q the

real and quadrature axes respectively. These equations are based on the same assumptions as used in the theory of electrical machines [24].

Employing the per-unit system with equal per-unit mutual inductance between the three windings on each axis [12], the inductance matrix [L] in

$$[\psi] = [L][i] \qquad \text{.....(A2.8)}$$

is written as

$$[L] = \begin{bmatrix} L_m + L_s & L_m & L_m \\ L_m & L_m + L_r & L_m \\ L_m & L_m & L_m + L_R \end{bmatrix} \qquad \text{.....(A2.9)}$$

where L_s, L_r, L_R are the self-inductances of the stator, inner rotor and outer rotor windings respectively and L_m is the mutual coupling (assumed equal) between these windings. Making [i] the subject of the formula in (A2.8)

$$[i] = [L]^{-1}\,[\psi] \qquad \text{.....(A2.10)}$$

with

$$[L]^{-1} = (1/l) * \begin{bmatrix} l_{11} & -L_R L_m & -L_r L_m \\ -L_R L_m & l_{22} & -L_s L_m \\ -L_r L_m & -L_s L_m & l_{33} \end{bmatrix} \qquad \text{.(A2.11)}$$

where

$$\begin{aligned} l_{11} &= L_r L_R + L_r L_m + L_R L_m \\ l_{22} &= L_s L_R + L_s L_m + L_R L_m \\ l_{33} &= L_s L_r + L_s L_m + L_r L_m \\ l &= L_s L_r L_R + L_s L_r L_m + L_s L_R L_m + L_r L_R L_m \end{aligned} \qquad \text{..... (A2.12)}$$

The state-variable form can be obtained by substituting (A2.10) in (A2.6). Note that the fluxes are chosen as state variables instead of currents. Since the flux does not change instanteneously, a larger time step can be chosen to obtain the same accuracy, thus saving on computation time.

$$
\begin{aligned}
\dot{\psi}_s &= -[(r_s l_{11}/l) + j\omega]\psi_s + (r_s L_R L_m/l)\psi_r + (r_s L_r L_m/l)\psi_R + v \\
\dot{\psi}_r &= (r_r L_R L_m/l)\psi_s - [(r_r l_{22}/l) + js\omega]\psi_r + (r_r L_s L_m/l)\psi_R \qquad \ldots(A2.13) \\
\dot{\psi}_R &= (r_R L_r L_m/l)\psi_s + (r_R L_s L_m/l)\psi_r - [(r_R l_{33}/l) + js\omega]\psi_R
\end{aligned}
$$

The equations for the mechanical motion in per-unit is given by

$$\dot{s} = -(1/2H\omega)\ (t_e - t_l) \qquad (A2.14)$$

where $t_e = Im\{\psi_s^* i_s\}$ and s is the slip

For digital simulation, the complex variables in (A2.13) and (A2.14) are resolved into the d, q axes as expressed by (A2.7) resulting in:

$$
\begin{aligned}
\dot{\psi}_{sd} &= -(r_s l_{11}/l)\psi_{sd} - \omega\psi_{sq} + (r_s L_R L_m/l)\psi_{rd} + (r_s L_r L_m/l)\psi_{Rd} + v_d \\
\dot{\psi}_{sq} &= \omega\psi_{sd} - (r_s l_{11}/l)\psi_{sq} + (r_s L_R L_m/l)\psi_{rq} + (r_s L_r L_m/l)\psi_{Rq} + v_q \\
\dot{\psi}_{rd} &= (r_r L_R L_m/l)\psi_{sq} - (r_r l_{22}/l)\psi_{rd} - s\omega\psi_{rq} + (r_r L_s L_m/l)\psi_{Rd} \\
\dot{\psi}_{rq} &= (r_r L_R L_m/l)\psi_{sq} + s\omega\psi_{rd} - (r_r l_{22}/l)\psi_{rq} + (r_r L_s L_m/l)\psi_{Rq} \\
\dot{\psi}_{Rd} &= (r_R L_r L_m/l)\psi_{sd} + (r_R L_s L_m/l)\psi_{rd} - (r_R l_{33}/l)\psi_{Rd} - s\omega\psi_{Rq} \\
\dot{\psi}_{Rq} &= (r_R L_r L_m/l)\psi_{sq} + (r_R L_s L_m/l)\psi_{rq} + s\omega\psi_{Rd} - (r_R l_{33}/l)\psi_{Rq} \\
\dot{s} &= -(1/2H\omega)\ [(L_R L_m/l)\psi_{sd}\psi_{rq} + (L_R L_m/l)\psi_{sq}\psi_{rd} + (L_r L_m/l)\psi_{sd}\psi_{Rq} - \\
&\quad (L_r L_m/l)\psi_{sq}\psi_{Rd} - t_l] \qquad \ldots\ldots\ldots\ldots\ldots\ldots(A2.15)
\end{aligned}
$$

A2.2.2 REDUCED 5th-ORDER MODEL

The outer cage of an induction motor is usually designed so that there is a high starting torque and low starting current. This is accomplished by making the resistance and leakage reactance of the starting (outer) cage r_R, L_R higher and lower respectively than the corresponding parameters of the running (inner) cage r_r, L_r resulting in $r_R >> r_r$ and $L_R << L_r$.

Comparing the time constants $T_r = L_r/r_r$ and $T_R = L_R/r_R$ we note that $T_R << T_r$ and that the transients associated with the outer cage are much faster than those with the inner cage. Neglecting these fast transients, by setting $\dot{\psi}_R = 0$ in (A2.13), we obtain a reduced 5th order model described by equations (A2.19).

Setting $\dot{\psi}_R = 0$ in (A2.13) we obtain

$$\psi_R = \frac{(L_r L_m/l_{33})\,(1-js')\psi_s \;(L_s L_m/l_{33})\,(1-js')\psi_r}{1 + s'^2} \qquad .....(A2.16)$$

where $\quad s' = (\omega l/r_R l_{33})\, s$

Substituting (A2.15) in the first two equations of (A2.13) we get the reduced form of the machine model:

$$\begin{aligned}
\dot{\psi}_s &= (R_{11} + jL_{11})\psi_s + (R_{12} + jL_{12})\psi_r + v \\
\dot{\psi}_r &= (R_{21} + jL_{21})\psi_s + (R_{22} + jL_{22})\psi_r \qquad .....(A2.17)
\end{aligned}$$

$$\dot{s}' = -(1/2H\omega)\,[(\omega l/r_s r_R l_{33})\; Im\{(R_{12} - jL_{12})\psi_s \psi_r^*\} - (\omega l L_r/r_s r_R L_s l_{33}) L_{12} |\psi_s|^2 - t_l']$$

with

$$R_{11} = -(r_s l_{11}/l) + (r_s L_r^2 L_m^2/l\, l_{33})/(1 + s'^2)$$
$$R_{22} = -(r_r l_{22}/l) + (r_r L_s^2 L_m^2/l\, l_{33})/(1 + s'^2)$$

$$
\begin{aligned}
R_{12} &= -(r_s L_R L_m/l) + (r_s L_s L_r L_m^2/ll_{33})/(1 + s'^2) \\
R_{21} &= (r_r/r_s)\, R_{12} \\
L_{11} &= -\omega - (r_s L_r^2 L_m^2/ll_{33})/(1 + s'^2) \\
L_{22} &= -(r_R l_{33}/l)s' - r_r L_s^2 L_m^2/ll_{33})s'/(1 + s'^2) \\
L_{12} &= -(r_s L_s L_r L_m^2/ll_{33})s'/(1 + s'^2) \\
L_{21} &= (r_r/r_s)\, L_{12} \\
t_l' &= (\omega l/r_R l_{33})\, t_l
\end{aligned}
\qquad \text{.....(A2.18)}
$$

Expressing (A2.17) in real direct and quadrature axes by using (A2.7) we obtain the state space formulation used in digital simulations:

$$
\begin{aligned}
\dot{\psi}_{sd} &= R_{11}\psi_{sd} + L_{11}\psi_{sq} + R_{12}\psi_{rd} + L_{12}\psi_{rq} + v_d \\
\dot{\psi}_{sq} &= -L_{11}\psi_{sd} + R_{11}\psi_{sq} + L_{12}\psi_{rd} + R_{12}\psi_{rq} + v_q \\
\dot{\psi}_{rd} &= R_{21}\psi_{sd} + L_{21}\psi_{sq} + R_{22}\psi_{2d} + L_{22}\psi_{rq} \\
\dot{\psi}_{rq} &= -L_{21}\psi_{sd} + R_{21}\psi_{sq} + L_{22}\psi_{rd} + R_{22}\psi_{rq}
\end{aligned}
\qquad \text{.....(A2.19)}
$$

$$
\begin{aligned}
\dot{s}' = -(1/2H\omega)\, [\; & (\omega l/r_s r_R l_{33}) R_{12}(\psi_{sd}\psi_{rq} - \psi_{sq}\psi_{rd}) - \\
& (\omega l/r_s r_R l_{33}) L_{12}(\psi_{sd}\psi_{rd} + \psi_{sq}\psi_{rq}) - \\
& (\omega l L_r/r_s r_R L_s l_{33}) L_{12}(\psi_{sd}^2 - \psi_{sq}^2) - t_l' \;]
\end{aligned}
$$

A2.2.3 REDUCED 3rd-ORDER MODEL

This model is obtained by neglecting the stator transients in (A2.17). This is equivalent to setting the time derivative of ψ_s to zero. The theory of neglecting stator transients was discussed in the preceding section.

The first equation of (4.17) with $\dot{\psi} = 0$ can be expressed in d and q axes as

$$\psi_{sd} = [1/(R_{11}^2 + L_{11}^2)]\,[-(R_{11}R_{12} + L_{11}L_{12})\psi_{rd} - (R_{11}L_{12} - R_{12}L_{11})\psi_{rq} - R_{11}v_d + L_{11}v_q]$$

$$\psi_{sq} = [1/(R_{11}^2 + L_{11}^2)]\,[-(R_{11}L_{12} - R_{12}L_{11})\psi_{rd} - (R_{11}R_{12} + L_{11}L_{12})\psi_{rq} - L_{11}v_d - R_{11}v_q] \qquad \text{.....(A2.20)}$$

The 3rd-order model can now be obtained by replacing the last three equations of (A2.17) with (A2.20). This is the lowest order model for double-cage induction motors.

A2.3 SINGLE-CAGE INDUCTION MOTOR

Single-cage induction motor models are usually applicable to small and medium induction motors (less than 50 kw). Large induction motors can however be equivalenced to a single-cage rotor that will have the same performance characteristics to system parameter changes. The full fifth-order and reduced third-order models for a single-cage induction motor models will now be developed.

A2.3.1 FULL 5TH-ORDER MODEL

The voltage equations for the rotor and stator can be written, on a synchronously rotating reference frame, as follows:

$$v_s = r_s i_s + j\omega\psi_s + \dot{\psi}_s$$
$$0 = r_r i_r + j\omega\psi_r + \dot{\psi}_r \qquad \text{.....(A2.21)}$$

where the subscripts s and r denote the rotor and stator circuits respectively.

To represent (A2.21) in terms of flux linkages in order to aid computational stability [28],[29] and noting that

$$[i] = [L]^{-1} [\psi]$$

where

$$[L] = 1/\ l * \begin{bmatrix} l_r + l_m & -l_m \\ -l_m & l_s + l_m \end{bmatrix}$$

we obtain the following equations:

$$\dot{\psi}_s = -[\ (r_s l_{11}/l) + j\omega\ ]\psi_s - L_m/l\ \psi_r + v_s$$
$$\dot{\psi}_r = (r_r L_m/l)\psi_s + (\ l_{22}/l - js\omega\ )\psi_r \qquad \text{.....(A2.22)}$$

where $l_{11} = L_r + L_m$
$l_{22} = L_s + L_m$
$l = L_s L_r + L_s L_m + L_r L_m$

The equation of mechanical motion is given by (4.14) as

$$\dot{s} = -1/(2H\omega)\ (\ t_e - t_l) \qquad \text{.....(A2.23)}$$

By using (A2.7), equations (A2.22) can be expressed in real and quadrature axis as

$$\dot{\psi}_{sd} = -(r_s l_{11}/l)\psi_{sd} + \omega\psi_{sq} - L_m/l\ \psi_{rd} + v_d$$

$$\dot{\psi}_{sq} = \omega\psi_{sd} + (r_s l_{11}/l)\psi_{sq} + L_m/l\ \psi_{rq} - v_q$$

$$\dot{\psi}_{rd} = (r_r L_m/l)\psi_{sd} + l_{22}/l\ \psi_{rd} - s\omega\psi_{rq}$$

$$\dot{\psi}_{rq} = -(r_r L_m/l)\psi_{sq} - s\omega\psi_{rd} - (l_{22}/l)\ \psi_{rq} \qquad \text{.....(A2.24)}$$

$$\dot{s} = -1/(2H\omega)\ [\ (L_m/l)\psi_{sd}\psi_{rq} + (L_m/l)\psi_{sq}\psi_{rd} - t_l]$$

Equations (A2.24) represents the full 5th-order model for a single-cage induction machine. Although this model has the same order as the reduced 5th-order model for the double-cage motor, it is apparent that their structures are quite different.

A2.32 REDUCED 3RD-ORDER MODEL

The reduced third-order model can be obtained by neglecting the stator transients in (A2.22). This is achieved by making $\dot{\psi}_s = 0$ in the first equation of (A2.22) resulting in

$$\psi_s = \frac{-(L_m/l)\psi_r + v_s}{r_s l_{11}/l + j\omega} \qquad \text{.....(A2.25)}$$

Substituting (A2.25) in the second equation of (A2.22) and resolving directly into direct and quadrature axes we obtain the reduced third-order model as:

$$\dot{\psi}_{rd} = [(-L_m/l)M - (l_{22}/L_r)]\psi_{rd} + [(\omega L_m/r_s l_{11})M - s\omega\ ]\psi_{rq} + Mv_d$$

$$\dot{\psi}_{rq} = [(\omega L_m/r_s l_{11})M - s\omega]\psi_{rd} + [(L_m/l)M + (l_{22}/L_r)]\psi_{rq} + Mv_q$$

$$\text{.....(A2.26)}$$

where $$M = \frac{r_r L_m/r_s l_{11}}{r_s l_{11}/l + j\omega}$$

The equation for mechanical motion can be obtained by replacing ψ_{sq} and ψ_{sd} in (A2.24) by

$$\psi_{sd} = \frac{-L_m r_{s11}}{l^2}\psi_{rd} + \frac{\omega L_m}{l}\psi_{rq}$$

$$\psi_{sq} = \frac{-\omega L_m}{l}\psi_{rd} - \frac{L_m r_{s11}}{l^2}\psi_{rq}$$

A2.3 LINEARIZED INDUCTION MOTOR MODELS

It is customary to use a linearized machine model in power system dynamic studies so that linear system analysis can be conveniently applied. Non-linear models are linearized around an operating point with the assumption that the variables have small deviations from the operating point.

This section will focus on linearizing the non-linear model of the double-cage induction motor. The process of linearization could be directly applied to the fifth and the third-order machine models. However, the coefficients of the resulting equations would have complicated algebraic expressions. A simpler approach is to linearize the full seventh-order model and to use this model to obtain the linearized versions of the fifth and third-order models. This process can be done as follows:

Let the seventh-order linearized model $[\dot{\mathbf{x}}] = [\mathbf{A}][\mathbf{x}] + [\mathbf{B}][\mathbf{u}]$ be partitioned into two sections with one section representing the variables to be ignored and the other section the variable to be retained. The partitioned linear model will be

$$\begin{bmatrix} \dot{x}_1 \\ \dot{x}_2 \end{bmatrix} = \begin{bmatrix} A_{11} & A_{12} \\ A_{21} & A_{22} \end{bmatrix} \begin{bmatrix} x_1 \\ x_2 \end{bmatrix} + \begin{bmatrix} B_{11} & B_{12} \\ B_{21} & B_{22} \end{bmatrix} \begin{bmatrix} u_1 \\ u_2 \end{bmatrix} \quad \text{.....(A2.27)}$$

where $[x_2]$ represents the variables whose transients are to be neglected and $[x_1]$ the remaining variables. Thus for the fifth-order model $[x_2]$ represents the starting cage flux linkages and or the third-order model the stator flux-linkages would be included.

Setting $\dot{x}_2 = 0$ and eliminating x_2 results in a lower order model

$$[\dot{x}_1] = [A]^*[x_1] + [u]^* \quad \text{.....(A2.28)}$$

where $[A]^* = [A_{11}] - [A_{12}][A]^{-1}[A_{21}]$

$[u]^* = [u_1] - [A_{12}][A_{22}][u_2]$

The non-linear equations of the double-cage induction motor (A2.10) can now be expressed in the state space form (A2.27) as

$$\begin{bmatrix} \dot{x}_1 \\ \dot{x}_2 \end{bmatrix} = \begin{bmatrix} A_{11} & A_{12} \\ A_{21} & A_{22} \end{bmatrix} \begin{bmatrix} x_1 \\ x_2 \end{bmatrix} + \begin{bmatrix} B_{11} & B_{12} \\ B_{21} & B_{22} \end{bmatrix} \begin{bmatrix} u_1 \\ u_2 \end{bmatrix} \quad \text{...(A2.29)}$$

where

$$[x_1] = \begin{bmatrix} \Delta\psi_{sd} \\ \Delta\psi_{sq} \\ \Delta\psi_{rd} \\ \Delta\psi_{rq} \end{bmatrix} \qquad [\dot{x}_1] = \begin{bmatrix} \dot{\psi}_{sd} \\ \dot{\psi}_{sq} \\ \dot{\psi}_{rd} \\ \dot{\psi}_{rq} \end{bmatrix}$$

$$[x_2] = \begin{bmatrix} \Delta\psi_{Rd} \\ \Delta\psi_{Rq} \\ \Delta\tau_1 \end{bmatrix} \qquad [\dot{x}_2] = \begin{bmatrix} \dot{\psi}_{Rd} \\ \dot{\psi}_{Rq} \\ \dot{s} \end{bmatrix}$$

$$[A_{11}] = \frac{1}{l}\begin{bmatrix} -r_s l_{11} & -\omega l & r_s L_R L_m & 0 \\ \omega l & -r_s l_{11} & 0 & r_s L_R L_m \\ 0 & r_r L_R L_m & -r_r l_{22} & -s\omega l \\ 0 & r_r L_R L_m & s\omega l & -r_r l_{22} \end{bmatrix}$$

$$[A_{12}] = -\frac{1}{l}\begin{bmatrix} r_s L_r L_m & 0 & 0 \\ 0 & r_s L_r L_m & 0 \\ r_s L_r L_m & 0 & 0 \\ 0 & r_r L_s L_m & 0 \end{bmatrix}$$

$$[A_{21}] = \frac{1}{l}\begin{bmatrix} r_R L_r L_m & 0 & r_R L_s L_m & 0 \\ 0 & r_R L_r L_m & 0 & r_R L_s L_m \\ -\left(\frac{L_R L_m \psi_{rq_0} + L_r L_m \psi_{Rq_0}}{2H\omega}\right) & -\left(\frac{L_R L_m \psi_{rd_0} + L_r L_m \psi_{Rd_0}}{2H\omega}\right) & 0 & 0 \end{bmatrix}$$

$$[A_{22}] = \frac{1}{l}\begin{bmatrix} -r_R l_{33} & -s\omega l & 0 \\ s\omega l & -r_R l_{33} & 0 \\ 0 & 0 & l/2H\omega \end{bmatrix}$$

APPENDIX 3 : MATHEMATICAL MODELS FOR POWER SYSTEM LOADS

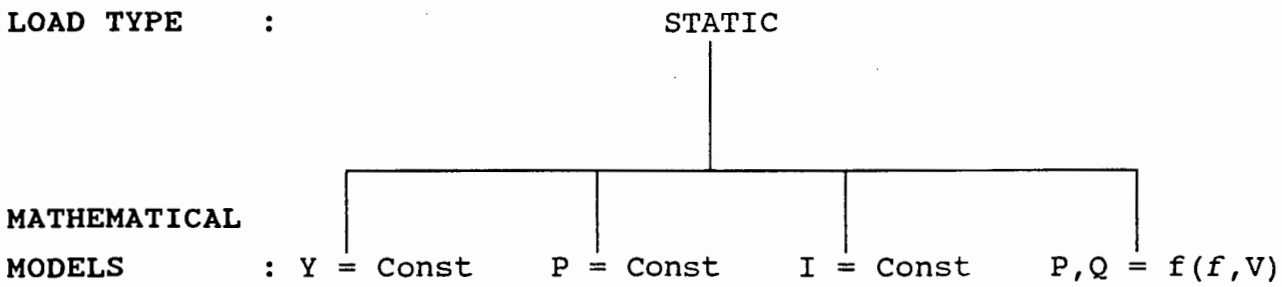

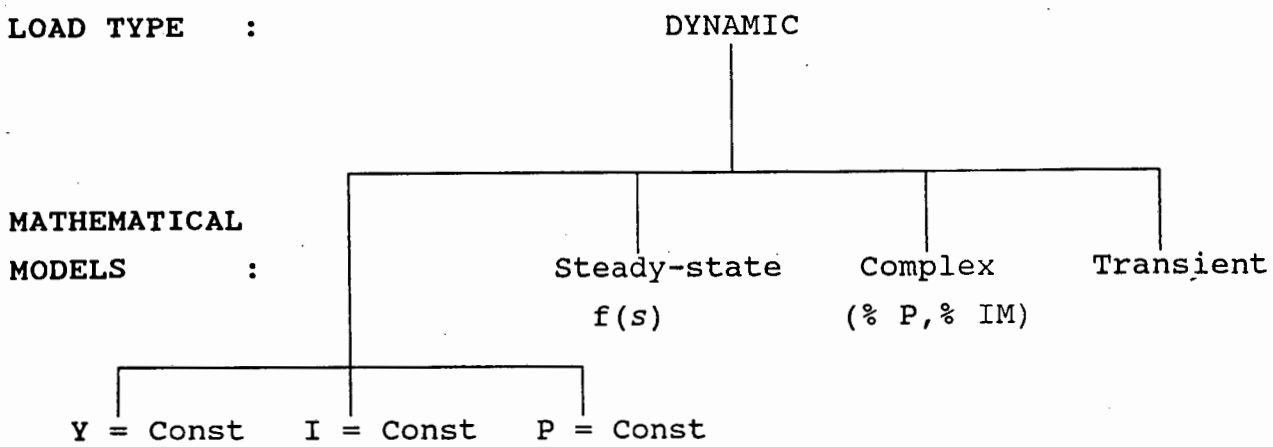

APPENDIX 4 : INDUCTION MOTOR PARAMETERS

The parameters for the 15.3 MVA induction motor are as follows :

Transient	Steady-state
$X = 4.777$	$R_1 = 0.00293$
$X' = 0.237$	$X_1 = 0.107$
$X'' = 0.170$	$X_m = 4.67$
$T' = 0.765$	$R_2 = 0.020$
$T'' = 0.011$	$X_2 = 0.064$
$X_l = 0.170$	$R_3 = 0.020$
$H = 4.5$	$X_3 = 0.070$
$S(1.0) = 0.139$	
$S(1.2) = 0.436$	

All parameters are given on the motor base (15.3 MVA).

LIST OF REFERENCES

[1] M.A Pai, Energy function analysis for power system stability, (Boston/Dordrecht/London : Kluwer Academic Publishers, 1989)

[2] EPRI,Modeling for power system simulation, Volume 2 : Modeling concepts, EPRI EL-3318, Vol2, Final report, Dec 1983

[3] IEEE Task Force on definitions and procedures, "Current usage and suggested practices in power system stability simulations for synchronous machines", IEEE Transactions on Energy Conversion, Vol. EC-1, No.1, March 1986, pp.77-92

[4] P.L Dandeno, " Development of generator models for stability analysis particularly for turbogenerators: An historical perspective ", IEEE Symposium on Synchronous machine modeling, 1983 Winter meeting, pp.1-4

[5] G.G. Richards, O.T. Tan "Simplified Models For Induction Machine Transients Under Balanced and Unbalanced Conditions" IEEE Trans. on Industry Applications, Vol. IA-17, No.1, Jan/Feb 1981, pp.15-21

[6] N.A. Khalil, O.T. Tan, I.U. Baran, "Reduced Order Models For Induction Motors" IEEE Trans. on Power Apparatus and Systems, Vol. PAS-101, No. 9, September 1982, pp.3135-3140

[7] B. Habibula, Y. Yu, "Physicallly Realizable Wide Power Range Optimal Controllers For Power Systems", IEEE Trans. Vol PAS-93, 1974, pp.1498-1506

[8] P.L Dandeno, P.Kundur, " Stability performance of 555 MVA Turboalternators - Digital comparisons with system operating tests", IEEE Trans. on PAS, Vol 93, No.3 May/June 1974, pp.767 - 776

[9] P.L. Dandeno, P. Kundur and R.P. Schulz, "Recent Trends and Progress in Synchronous machine Modeling in the Electric Utility Industry" Proceedings IEEE, Vol 62, No.7, pp 941-950, July 1974

[10] P.L. Dandeno, R.L. Hauth and R.P Schulz, "Effect of Synchronous Machine Modelling in Large Scale Stability Studies", IEEE Trans. on Power Apparatus and Systems, Vol. PAS-92, pp 574-582,March/April 1973.

[11] M. Kemal Ïnan "Modal Analysis of Synchronous Machine Dynamics", IEEE Trans. on Circuits and Systems, Vol. CAS-29, No. 10, October 1982, pp.688-699

[12] A.A. Fouad, V. Vittal, et. al., "Direct Transient Stability Assessment with Excitation Control", IEEE Trans. on Power Systems, Vol. 4, No. 1, February 1989, pp.75-82

[13] P. Anderson, A.A Fouad, Power System Stability and Control, Iowa State University Press, Ames, 1977.

[14] P M Anderson, "Analysis of faulted power system",Iowa State University Press, Imes, IA, 1973.

[15] Stagg and El-Abiad,Computer methods in Power System Analysis, McGraw-Hill, 1968.

[16] S B Crary, Power System stability, vol 2 , New York;Wiley 1947

[17] M H Kent et. al, "Dynamic modelling of loads in stability studies", IEEE Trans. on PAS, Vol PAS-88, No.5, may 1969 pp.756-763.

[18] W W Price et. al., "Load modelling for power flow and transient stability computer studies", IEEE Power Engineering Society, PES Winter meeting, New Orleans, Louisiana, Feb. 1-6, 1987, Paper No. 87 WM 080-5.

[19] M.Y Akhtar, "Frequency-dependent dynamic representation of induction motor loads", Proc. IEE Vol 115, No.6 pp.802-812 June 1968.

[20] IEEE Committee Report, "System Load Dynamics-Simulation Effects and Determination of Load Constants", IEEE Trans on PAS Vol PAS-92, pp 600-609, March/April 1973.

[21] C. Concordia and S. Ihara "Load representation in power system stability studies", IEEE Trans. on Power apparatus and Systems, vol PAS-101, no.4, pp.969-977 April 1982.

[22] M.M.Abdel Hakim "Dynamic single-unit representation of induction motor groups", IEEE Trans. on Power Apparatus and Systems, vol PAS-95 no.1, pp.155-165, Jan/Feb 1976.

[23] F Illeceto, A Capasso, "Dynamic Equivalents of Asynchronous motor loads in system stability studies" IEEE Trans. on PAS, Vol PAS-93, pp.1650-1659, Sept/Oct 1974.

[24] T. Ohyama, A Watanabe, K Nishimura and S Tsuruta "Voltage dependence of composite loads in Power Systems", IEEE Trans. on PAS, Vol PAS-104, No.1, pp.3064-3073 Nov 1985.

[25] W W Price, K A Wirgau et. al, "Load modelling for Power flow and transient stability computer studies", IEEE/PES 1987 Winter Meeting 87 WM 080-5.

[26] G J Rogers, J D Manno and R T H Alden, "An aggregate induction motor model for industrial plants", IEEE Trans. on PAS, vol PAS-103, No.4, pp.683-690, April 1984.

[27] D.S. Brereton, D.G. Lewis and C.C Young "Representation of induction motor loads during power system stability studies", AIEE Trans. Vol 76, Pt. III pp.451-460, 1957.

[28] P C Krause et al, "The theory of neglecting stator transients", IEEE Trans. on PAS, Vol PAS-98 No.1, pp.141-148, Jan/Feb 1979.

[29] N Gunaratnam," The effects of neglecting stator transients in induction machine modelling", IEEE Trans. on PAS, Vol PAS-99, No.6 pp.2050-2059, Nov/Dec 1980.

[30] H M A Hamdan, "An improved reduced order model for induction machines" Electric Machines and Power Systems Vol 17, pp.283-293, 1989.

[31] N A Khalil, O T Tan and I U Baran, "Reduced order models for double-cage induction motors", IEEE Trans. on PAS vol PAS-101, No.9 pp.3135-3140, Sept. 1982.

[32] K P R Sastry and R E Burridge, "Investigation of a reduced order model for induction machine dynamic dynamic studies", IEEE Trans on PAS vol PAS-95, No.3, pp.962-969, May/June 1976.

[33] J L Sancha, I L Perez-Arriaga, "Selective Modal Analysis of power system oscillatory instability", IEEE Trans. on Power Systems vol 3, No.2 pp.429-438, May 1988.

[34] T C Skvarenina, P C Krause, "Accuracy of a reduced order model of induction machines in dynamic stability studies", IEEE Trans. on PAS, Vol PAS-98, No.4, pp.1192-1197,

[35] M. Chan, R. Gutman, B.M Pasternack, "Understanding voltage collapse in bulk transmission systems", ibid pp 3: 34-85

[36] J. Zaborszky, "Some basic issues in voltage stability and viability ", EPRI EL-6183 Proceedings: Bulk Power System Voltage Phenomena - Voltage stability and Security, January 1989, 1.11 pp 1-60.

[37] C.C Lin, "Characteristics of a voltage collapse mechanism due to the effects of On-load tap changers", Proceedings 1986 IEEE International Symposium on Circuits and Systems, vol.3, pp 1028 - 1030.

[38] J. Medanic, M Ilic-Spong, J. Christensen, "Discrete models of slow voltage dynamics for under load tap-changing transformer coordination", Paper 86 SM 345-6 presented at the 1986 IEEE PES Summer Meeting, Mexico City, Mexico, July 1986.

[39] C. Barbier and J. Barret, "An analysis of phenomena of voltage collapse on a transmission system", Revue Generale de L'Electricite Special issue, July 1980, Paris,France, pp 3 - 21.

[40] Y. Sekine, A. Yokoyama, " Dynamic stability analysis taking into account load flow multisolutions and load characteristics," 8th PSCC, Helsinki, 19-24 August 1984, pp 976 - 982.

[41] C. Rajagopalan , M A Pai, "An integrated approach to dynamic and static voltage stability", Proceedings of the 1989 American Control Conference, Pittsburgh, USA, vol 2, 21-23 June 1989, pp 1231 - 1236.

[42] R.J Thomas, Hsiao-Dong Chiang, "On dynamic voltage instabilities in Electric Power Systems", EPRI EL-6183 Proceedings: Bulk power system voltage phenomena - voltage stability and security, January 1989, pp 2575 - 2595.

[43] M.Z El-Sadek and F.N Abdelbarr, " Effects of induction motor load in provoking transient voltage instabilities in power systems ", Electric power systems research, vol 17, 1989, pp.119-127.

[44] V.I Idelchik, V.I Tarasov, "Experimental investigations of existence, non-uniqueness and convergence of solutions of power flow problem equations in power systems", 4th PSCC, Grenoble, 1972.

[45] Y. Tamura, H. Mori, S. Iwamoto, "Relationship between voltage instability and multiple load flow solutions in electric power systems", IEEE Trans. on Power Applications and Systems, vol PAS-102. no.5, May 1983, pp 1115 - 1125.

[46] Y. Sekine and A. Yokoyama, " Multisolutions for load flow problem of power system and their physical stability ", 7th PSCC, Lausanne, 12 - 17 July 1981, pp 819-826.

[47] Y. Sekine and A. Yokoyama, " Dynamic stability analysis taking into account load flow multisolutions and load characteristics ", 8th PSCC, Helsinki, 19 - 24 August 1984, pp.976 - 982.

[48] C.L De Marco and A.R Bergen, " A security measure for random load disturbance in non-linear power system models ", IEEE Trans. on circuits and systems, Vol.CAS-34, No.12, December 1987, pp.1546-1557.

[49] H.G Kwatny, A.K Pasrija and L.Y Bahar, " Static Bifurcations in Electric power networks: Loss of steady-state stability and voltage collapse ", IEEE Trans. on circuits and systems, Vol.CAS-33, No.10, October 1986, pp.981 - 991.

[50] P. Kessel and H. Glavitsch, " Estimating the voltage stability of a power system ", IEEE Trans. on power delivery, Vol.PWRD-1, No.3, July 1986, pp.346-354

[51] C. Barbier and J. Barret, " An analysis of phenomena of voltage collapse on a transmission system ", Revue Generale de L'Electricite, Tome 89, no.10, October 1980, pp.3 - 21.

[52] C. Lemaitre, J.P Paul, Y. Harmand and Y.S Zhao, " An indicator of the risk of voltage profile instability for real-time control applications ", IEEE Trans. on power systems, Vol.5, No.1, February 1990, pp.154 - 161.

[53] Fitzgerald et. al, Electric Machinery, Fourth edition, Mcgraw Hill, pp.371-379, 1985

[54] Venikov A, Transient phenomena in electric power systems, Pergamon Press, pp.40-57, 1964.

[55] E. Handschin, et al, " Electric load modeling : Analysis, identification and validation ", Proceedings of the 9th PSCC, Cascais, Portugal, Sept. 1987, pp.549-555.

[56] P.C Krause, " Method of multiple reference frames applied to the analyses of symmetrical induction machinery ", IEEE Trans. Vol. PAS-87, No.1, Jan 1968, pp.218-227.

Consider a synchronous machine swinging with respect to an infinite bus. The swing equation for the machine is given by

$$\frac{2H}{\omega_r}\frac{d^2\delta}{dt^2} + D\frac{d\delta}{dt} = P_m - P_e = P_a \quad \ldots\ldots\ldots\ldots (1.5)$$

The damping factor D in the above equation is usually set to zero when using the equal area criterion.

Equation 1.5 can be rewritten in the form given below :

$$\frac{d^2\delta}{dt^2} = \frac{\omega_r}{2H} P_a \quad \ldots\ldots\ldots\ldots\ldots\ldots (1.6)$$

Equation 1.6 can be manipulated by integration to obtain the relative speed as follows :

$$\frac{d\delta}{dt} = \sqrt{\frac{\omega_r}{H}\int_{\delta_o}^{\delta_1} P_a \, d\delta} \quad \ldots\ldots (1.7)$$

For stability to be retained, the speed of the machines must be the same. Thus

$$\frac{d\delta}{dt} = 0 \quad \text{or} \quad \int_{\delta_o}^{\delta_1} P_a \, d\delta = 0 \quad \ldots\ldots\ldots\ldots (1.8)$$

Since $P_a = P_m - P_e$, $\int_{\delta_o}^{\delta_1} \left(P_m - P_e\right) = 0.$

This integral may be interpreted as the area between the curves of P_m versus δ and P_e versus δ. Figure 1.3 below show these curves, for a change in load. Figure 1.4 shows the curves for a change in the transfer reactance between the machine and the infinite bus due to a fault.